7-22-2012

Fabrication and Characterization of Multifunctional Chitosan Microspheres and Their Incorporation Into Composite Scaffolds for Enhanced Bone Regeneration

Benjamin Taylor Reves

FABRICATION AND CHARACTERIZATION OF MULTIFUNCTIONAL CHITOSAN MICROSPHERES AND THEIR INCORPORATION INTO COMPOSITE SCAFFOLDS FOR ENHANCED BONE REGENERATION

by

Benjamin Taylor Reves

A Dissertation

Submitted in Partial Fulfillment of the

Requirements for the Degree of

Doctor of Philosophy

Major: Biomedical Engineering

The University of Memphis

August 2012

DEDICATION

This dissertation is dedicated to my parents. I am very thankful for all of the love and support they have given me- not just the past few years, but my entire life. For that, I am eternally grateful.

ACKNOWLEDGEMENTS

I would like to thank my advisor, Dr. Warren O. Haggard, for sharing his wisdom and experience with me. I am also grateful to all of my committee members for their excellent advice and guidance. To my labmates and fellow BAM members, thank you for the stimulating discussions and many suggestions you imparted. I am especially grateful to Dr. Amber Jennings and Jared Cooper for their willingness to assist me throughout this journey.

ABSTRACT

Reves, Benjamin Taylor. Ph.D. The University of Memphis. August 2012. Fabrication and Characterization of Multifunctional Chitosan Microspheres and Their Incorporation Into Composite Scaffolds for Enhanced Bone Regeneration. Major Professor: Warren O. Haggard, Ph.D.

Insufficient fracture healing affects hundreds of thousands of people every year in the United States, resulting in devastating economic and social impacts. To treat these severe fractures, our laboratory has developed chitosan-nano-hydroxyapatite microspheres and scaffolds. The purpose of this research was to improve these scaffolds by increasing their degradation rate to allow better bone ingrowth and to increase and extend the elution of bone morphogenetic protein-2 (BMP-2) from the constructs. We hypothesized that a composite approach combining chitosan and carboxymethylchitosan microspheres would result in scaffolds with improved degradation and elution properties while maintaining good cytocompatibility and sufficient mechanical properties.

The scaffold constructs are prepared by fusing chitosan microspheres together using an acid wash to make the beads adherent. This approach promotes flexibility by allowing multiple microsphere types to be incorporated into the scaffolds. Chitosan microspheres with 80% degree of deacetylation were selected as the first component of the composite scaffolds. These microspheres demonstrated good mechanical properties (compressive modulus of 1.6 ± 0.3 MPa) and excellent cytocompatibility.

The second bead type was optimized for degradation and drug delivery. The carboxymethylation of chitosan microspheres was performed using monochloroacetic acid. The carboxymethylchitosan microspheres were crosslinked using two different approaches: amine-amine crosslinking using genipin (Gen-X CMCS beads) and amide bond formation using carbodiimide chemistry (X-CMCS). The Gen-X CMCS beads

displayed poor degradation and elution properties; whereas, the X-CMCS beads displayed extensive degradation (82.7 ± 1.2%) and extended elution of BMP-2 for at least forty-five days. Composite X-CMCS/CS scaffolds were prepared and demonstrated improved degradation and drug delivery compared to CS-only scaffolds while maintaining sufficient mechanical characteristics and cytocompatibility.

This research demonstrated the advantages of using a composite approach and supported our hypothesis. By optimizing each bead type for a specific purpose, the overall properties of the scaffolds were improved. The combination of CS and X-CMCS microspheres resulted in composite scaffolds that demonstrated excellent potential for enhancing bone regeneration in severe fractures.

PREFACE

The economic and social costs of insufficient fracture healing are enormous. Roughly, $6.4 billion is spent each year in the United States to correct non-unions and delayed healing in patients with severe fractures. The purpose of this research was to fabricate and characterize an enhanced bone regenerative scaffold. The main body of this dissertation contains the following manuscripts which have been published or will be submitted for publication:

Chapter 2: Osteoinductivity Assessment of BMP-2 Loaded Composite Chitosan-Nano-Hydroxyapatite Scaffolds in a Rat Muscle Pouch. Published in *Materials*. 2011; 4: 1360-1374.

Chapter 3: Preparation and Functional Assessment of Composite Chitosan-Nano-Hydroxyapatite Scaffolds for Bone Regeneration. Published in *Journal of Functional Biomaterials*. 2012; 3: 114-130.

Chapter 4: Fabrication and Characterization of Crosslinked Carboxymethylchitosan Microspheres and Their Incorporation Into Composite Scaffolds for Enhanced Bone Regeneration. Planned submission to *Journal of Biomedical Materials Research Part B: Applied Biomaterials* (July 2012).

TABLE OF CONTENTS

LIST OF TABLES

LIST OF FIGURES

Chapter 1 Introduction

1. Problem Statement

Of the approximate 8 million bone fractures that occur in the United States each year, 5-10% of them will result in delayed healing or non-union [1, 2]. The economic and social impacts of insufficient fracture healing are devastating, and a non-union can cost upwards of $16,000/patient to correct [3]. Although autografts and allografts are commonly used to treat severe fractures, they have a number of drawbacks [4-8]. For these reasons, much research has focused on the development of bone tissue scaffolds. These constructs provide a temporary matrix to which osteoblasts can attach and proliferate, resulting in the formation of new bone [9, 10]. These scaffolds must meet a number of requirements including the following: 1) appropriate surface chemistry to favor cellular attachment, differentiation, and proliferation; 2) controlled degradability so that tissue will gradually replace the scaffold; 3) adequate mechanical properties that match the intended site of implantation; 4) interconnected porosity that promotes tissue integration and vascularization; and 5) easy to manufacture, sterilize, and implant [1, 11]. Previously, our laboratories have developed chitosan-nano-hydroxyapatite scaffolds that meet many of these requirements and have shown potential as a delivery device for the local release of bone morphogenetic protein-2 (BMP-2) [12-14]. Although our technology has shown promising results in vitro and in vivo, these scaffolds have demonstrated slower degradation than desired and a less than optimal release profile of BMP-2 [12, 14]. The goal of this project is to enhance the bone regenerative scaffolds by improving their degradation and BMP-2 release profiles while maintaining their good cytocompatibility and mechanical properties.

2. Background

2.1. Fracture Healing

Roughly eight million bone fractures occur in the United States each year. Due to the tremendous capacity of bone to heal itself, only 5-10% of these injuries will result in delayed healing or non-union [1, 2]. These severe fractures are often caused by high-impact forces such as motor vehicle accidents, gunshot wounds, crush injuries, or explosions. This type of injury leads to fractures in which the vasculature around the site is severely damaged and the bone is fragmented into multiple pieces or even an entire section of bone is missing [15-17].

Fracture healing occurs in three phases: early inflammatory stage, repair stage, and late remodeling stage [15, 18, 19]. A hematoma is formed shortly after a fracture occurs. Due to prostaglandin and growth factor release, a number of cell types migrate to the fracture site including inflammatory cells, fibroblasts, and mesenchymal stem cells. As vascularization improves, bone repair can proceed. A soft callus forms first which is then replaced by a hard callus of woven bone. In the final stage of fracture healing, the unorganized woven bone is remodeled into structured tissue with normal bone architecture [15, 18, 19].

A number of growth factors play roles in the bone healing cascade. These proteins include BMP-2, transforming growth factor-beta, fibroblast growth factor, platelet-derived growth factor, and vascular endothelial growth factor [18, 20]. BMP-2 is very important in bone repair, and it has even been shown that initiation of fracture healing will not occur in the absence of endogenous BMP-2 [21]. BMP-2 is present in all three

stages of fracture healing, and it promotes chemotaxis of stem cells to the fracture site, angiogenesis, and the differentiation of stem cells into osteoblasts [20, 22-26].

2.2. Current Treatment Strategies

Bone grafts are often used to aid healing of severe fractures, and autograft procedures are the current gold standard treatment. An autograft is obtained from a different location on the patient's body, such as the iliac crest of the hip. Drawbacks for autograft procedures include surgical site infection, difficulty shaping the graft to fit the defect, requirements of additional surgical procedures, extended recovery times, and donor site morbidity [4, 5, 7, 8]. An allograft is a graft retrieved from a different person, typically a cadaver. Allografts have demonstrated variable efficacy and are associated with immunologic concerns [1, 5, 6]. Demineralized bone matrix (DBM) is prepared by removing the inorganic portion of bone, leaving behind the non-mineralized matrix and associated proteins. DBM products have demonstrated considerable variability in efficacy and are unreliable [27, 28].

For these reasons, much research has focused on the development of bone graft substitutes. These constructs must meet a number of requirements as previously described. Many technologies meet some of the needed characteristics, but very few meet all of them. For instance, scaffolds composed of strong materials like polycaprolactone and polyurethane have good mechanical strength but degrade very slowly [29, 30]. Collagen sponges and alginate, agarose, and hyaluronic acid hydrogels are degradable, but have compressive moduli orders of magnitude less than that of trabecular bone [31-34]. The brittle nature and poor fatigue resistance of many bioceramics, such as calcium phosphates and bioactive glasses, limits their usefulness in treating large bone defects

[35, 36]. Popular degradable polyesters, including polyglycolide and polylactide, have undesirable acidic degradation byproducts that can negatively impact bone repair [10, 37].

Many bone graft substitutes are also used as local drug delivery devices for growth factors and/or antibiotics [9, 20, 38, 39]. Release of BMP-2 from bone scaffolds has received much attention, due to the growth factor's importance in the bone healing cascade. Some success has been achieved clinically, but the full potential of BMP-2 in augmenting fracture repair has not been realized. The main hindrance thus far has been the inability to provide sustained delivery of physiologically relevant levels of BMP-2 [7, 9, 37, 40-42]. Many of the currently available BMP-2 delivery materials demonstrate a burst release, and as much as 80% of growth factor activity is lost after forty-eight hours post-implantation [43]. Excessive amounts of costly BMP-2 are loaded initially due to BMP-2's very short half-life of 7-16 minutes in vivo [9, 41, 44-46]. These supraphysiological levels of growth factor released within the first few hours after surgery do not aid healing and can cause adverse side effects, such as ectopic bone formation, soft tissue swelling, and bone cysts [10, 45-49]. Indeed, a number of studies have shown that the extended delivery of BMP-2 throughout the bone healing cascade is more effective that a large initial burst release of BMP-2 [40, 45, 46, 50-52]. By delivering BMP-2 more efficiently, less total BMP-2 would be required, and the number of complications and health care costs associated with augmentation of fracture repair may potentially be decreased [7, 46].

2.3. Previous Work

Our laboratory has developed chitosan-nano-hydroxyapatite microspheres and scaffolds to enhance healing in severe fractures [12-14]. The chitosan-nano-hydroxyapatite microspheres are prepared using a co-precipitation method. Porous scaffolds are then fabricated by washing the beads in 1% acetic acid for approximately ten seconds. The acid slightly dissolves the outermost portions of the microspheres and makes them adherent. Chitosan is natural carbohydrate co-polymer containing glucosamine and N-acetyl-D-glucosamine units. Chitosan has biocompatible, osteoconductive, mucoadhesive, and enhanced would healing capabilities and has been used in numerous biomedical applications including orthopaedic tissue engineering [11, 53-58]. Hydroxyapatite is a crystalline calcium phosphate and is the main inorganic component of bone [59]. Hydroxyapatite has been incorporated into implants and scaffolds to enhance the response of osteoblasts [60-66].

Our chitosan-nano-hydroxyapatite scaffolds have shown good potential for use in bone regenerative applications. Chesnutt et al. demonstrated the cytocompatibility of our scaffolds with human fetal osteoblast cells, and the scaffolds were found to be osteoconductive in vivo in a rat calvarial defect [12, 13]. Reves et al. demonstrated the feasibility of using the composite as a drug delivery device for elution of BMP-2 [14]. Although the technology showed great promise in augmenting fracture healing, areas for improvement were noted. The microspheres and scaffolds demonstrated slow degradation in vitro and in vivo. Chesnutt et al. measured less than three percent degradation of the chitosan-nano-hydroxyapatite scaffolds in a 500μg/mL lysozyme solution [12-14]. The goal of bone regeneration is for new bone to completely replace the temporary matrix

over time. If the scaffolds do not degrade in a timely manner, limited tissue ingrowth will occur and fracture healing will be impaired [9, 67, 68]. Also, a significant burst effect release of BMP-2 from the chitosan scaffolds was observed [14]. As previously discussed, an extended elution of BMP-2 is desired over a large burst release.

2.4. Carboxymethylchitosan

Chitosan is a versatile material containing a number of hydroxyl and amine groups that allow for numerous modification strategies [11, 55, 56]. One such strategy is the carboxymethylation of chitosan using monochloroacetic acid [69-72]. Since carboxymethylchitosan (CMCS) is water-soluble, it is often crosslinked to form hydrogels. CMCS contains both amine and carboxyl groups, and 1-ethyl-3-(3-dimethylaminopropyl) carbodiimide (EDC) can be used to crosslink CMCS by forming amide bonds [70, 72-75]. Genipin, a natural amine-amine crosslinker derived from the Gardenia plant, has been used to crosslink chitosan and CMCS. Genipin is of interest for use in biomedical applications, since it has demonstrated excellent cytocompatibility compared to other commonly used crosslinkers such as glutaraldehyde [76-80]. Most research using EDC or genipin to crosslink CMCS has been performed in solution or on highly porous constructs. The feasibility of using these chemicals to crosslink dense CMCS microspheres has not been investigated.

Carboxymethylchitosan (CMCS) films and gels have demonstrated good biocompatibility [70-72, 81-83]. In addition, CMCS constructs have increased degradation compared to their chitosan counterparts. Wang et al. measured a 70% reduction in the mass of CMCS tubes compared to only 4.3% for chitosan tubes [70, 72]. Thus, the carboxymethylation of chitosan microspheres is expected to increase their

degradability. The addition of a carboxyl group to the chitosan beads may also improve their BMP-2 elution profile. The isoelectric point of BMP-2 is approximately 9.0, which means that BMP-2 will have a net-positive charge at neutral pH [4, 84, 85]. The presence of a negatively-charged carboxyl group may promote interaction between BMP-2 and CMCS leading to a more extended elution. The inclusion of CMCS microspheres into chitosan scaffolds is expected to improve the degradation and BMP-2 delivery properties of the constructs.

3. Hypothesis

Chitosan scaffolds with beads prepared using a single microsphere fabrication method are not expected to meet all the characteristics required of a bone graft substitute. We believe a better strategy is to incorporate multiple bead types into the scaffolds, and each bead type in the construct should be optimized for a particular purpose. Specifically, we hypothesized that composite scaffolds composed of CMCS and chitosan microspheres would result in constructs with increased degradation and extended BMP-2 release compared to chitosan-only scaffolds, while maintaining good biocompatibility and sufficient mechanical properties.

The goal of this research was to develop an improved bone regenerative scaffold, and this dissertation is organized in the following manner. The second chapter describes an in vivo osteoinductivity study in which the ability of BMP-2 loaded chitosan-nano-hydroxyapatite scaffolds to form bone in a rat muscle pouch was determined. The results of this investigation demonstrated the need for enhancement of our scaffold technology. At this point, a multi-bead scaffold was envisioned. The third chapter describes the

optimization of the chitosan bead component of the scaffolds. The fabrication and incorporation of CMCS beads into composite scaffolds is described in the fourth chapter.

Chapter 2 Osteoinductivity Assessment of BMP-2 Loaded Composite Chitosan-Nano-Hydroxyapatite Scaffolds in a Rat Muscle Pouch

1. Introduction

Of the approximate eight million bone fractures that occur in the United States each year, 5-10% of these fractures will result in delayed healing or non-union [1]. The current gold standard for augmenting healing in these troublesome fractures is the use of autografts. However, autografts suffer from a number of drawbacks including surgical site infection, difficulty shaping the graft to fit the defect, donor site morbidity, and limited graft material [2-4]. Allografts are not as effective as autografts and transmission of disease from the donor remains a concern [3-5]. Demineralized bone matrix displays extremely varying rates of effectiveness [6,7]. For these reasons, much current research has focused on the development of bone regeneration scaffolds that can be used as bone graft substitutes. These scaffolds are designed to provide a matrix to which osteoblasts can attach and proliferate. Ideally, the scaffolds will provide mechanical strength initially and then degrade as new bone is deposited [8,9]. Our laboratories have developed composite chitosan-nano-hydroxyapatite scaffolds to enhance fracture healing [10-12].

After cellulose, the most abundant biopolymer is chitin. Chitin is found in the exoskeletons of crustaceans and insects [13,14]. The deacetylated derivative of chitin is known as chitosan, and chitosan is a carbohydrate copolymer composed of glucosamine and N-acetyl-D-glucosamine units joined by β-1,4 glycosidic bonds. If the copolymer contains more than 50% glucosamine units, it is referred to as chitosan; whereas, it is still called chitin if it retains more than 50% N-acetyl-D-glucosamine monomers [15,16]. Chitosan has a number of properties including biocompatibility, biodegradability, mucoadhesiveness, and wound healing capabilities that make it useful as a biomaterial.

Chitosan is very versatile and can be prepared as films, gels, sponges, beads, fibers and other forms and has been used in various applications including wound healing, drug delivery, and bone tissue engineering [14-20].

Ideally, scaffolds used for bone regeneration need mechanical strength [8]. The pores of the scaffold must remain open to allow tissue ingrowth into the interior of the scaffolds and to maintain good nutrient/waste exchange [21,22]. Our composite scaffolds incorporate the strength and hardness of hydroxyapatite with the toughness and flexibility of chitosan. Hydroxyapatite is the main inorganic component of bone and has been used in coatings to improve osteoblast response to implants [9,14,23-26]. In addition, our labs have demonstrated the enhanced bone regenerative capacity of composite scaffolds over chitosan-only scaffolds [10,11].

To further increase the bone regenerative properties of graft substitutes, the scaffolds can also serve as a carrier for the local delivery of growth factors [21,27,28]. Bone morphogenetic protein-2, BMP-2, has been widely investigated for augmenting fracture healing due to its pleiotropic nature. BMP-2 recruits stem cells to the fracture site, promotes angiogenesis, and causes differentiation of the stem cells into osteoblasts [27,29-33]. We have previously shown that increased BMP-2 loading can be achieved using composite scaffolds instead of chitosan-only scaffolds. We also demonstrated that even further BMP-2 loading can be achieved using lyophilization (freeze-drying) to increase the surface area of the scaffolds [12].

The objective of this investigation was to evaluate the osteoinductivity of BMP-2 loaded composite chitosan-nano-hydroxyapatite scaffolds in a rat muscle pouch model. The murine muscle pouch model is a well-established model for determining the

osteoinductivity of materials [34-36]. We hypothesized that the lyophilized composite scaffolds would induce the most bone formation due to enhanced BMP-2 loading.

2. Results and Discussion

Porous composite scaffolds were successfully prepared by fusing chitosan-nano-hydroxyapatite beads together using an acid wash (Figure 1). The initial porosity of the non-lyophilized and lyophilized scaffolds were 35.8 ± 2.1% and 53.6 ± 3.6%, respectively [12]. Thus, the lyophilized scaffolds are slightly more porous than the non-lyophilized scaffolds. It has been suggested that a minimum porosity of thirty percent is required for bone regeneration [37]. In addition, the 100–800 micron pore diameters of the composite scaffolds are suitable for bone regeneration [10], since pores of at least one hundred microns are required for osteogenesis [9].

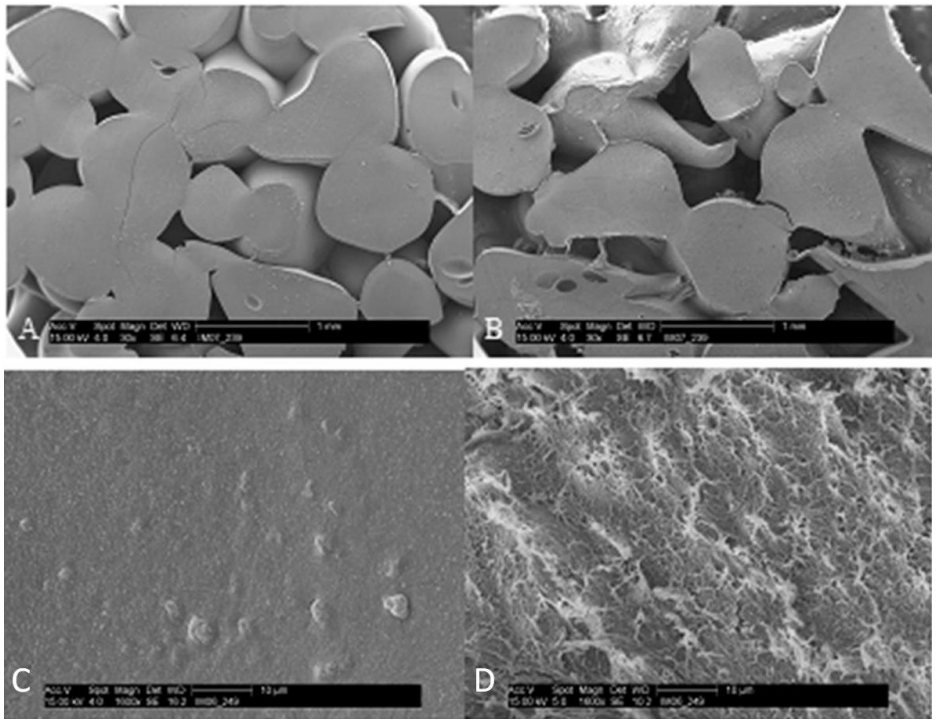

Figure 1. Scanning electron micrograph (SEM) images of composite scaffolds and microspheres. A) Non-lyophilized composite scaffold, 30×. B) Lyophilized composite scaffold, 30x. C) Surface of non-lyophilized composite microsphere, 1600×. D) Surface of lyophilized composite microsphere, 1600x. Note the slightly increased porosity of the lyophilized scaffolds. The surface of the lyophilized microsphere is considerably rougher than the surface of the non-lyophilized microsphere.

Following implantation into rat muscle pouches for one month, the osteoinductive potential of the composite scaffolds was determined. Using BIOQUANT OSTEO II imaging software, the amount of residual implant material, osteoid, and new bone as a percent of total implant area were quantified (Table 1). The remaining space in the implant area was occupied by fibrous or muscle tissue.

Table 1. Composite scaffold performance. N/A: Not applicable; a: Bone and marrow.

Scaffold Type	Scaffold (%)	Osteoid (%)	Bone (%)
Lyophilized (no rhBMP-2)	65.2 ± 3.7	8.8 ± 2.6	1.8 ± 0.8
Lyophilized with rhBMP-2	59.2 ± 6.1	10.4 ± 1.2	1.2 ± 0.3
Non-lyophilized with rhBMP-2	71.8 ± 3.0	7.7 ± 2.4	1.0 ± 0.7
Collagen Sponge with rhBMP-2	N/A	N/A	94.0 ± 4.4[a]

As seen in Table 1 and displayed in Figure 2, the majority of the implant space was still occupied by scaffold material after one month. Recall that the initial porosities of non-lyophilized and lyophilized scaffolds were 35.8 ± 2.1% and 53.6 ± 3.6%, respectively [12]. Thus, no degradation was observed, and the scaffolds actually appeared to increase in mass slightly during this experiment. This slight increase may be due to histological artifacts. Also, the amount of remaining chitosan was determined by evaluating thin slices through the scaffold; whereas, the initial porosity was determined using slices through the entire scaffold obtained by Micro-CT. Using the same 92.3% degree of deacetylation (DDA) chitosan, Chesnutt *et al*. observed no measurable degradation during a two-week *in vitro* degradation study and very minimal degradation during a 12-week rat calvarial defect model [10,11].

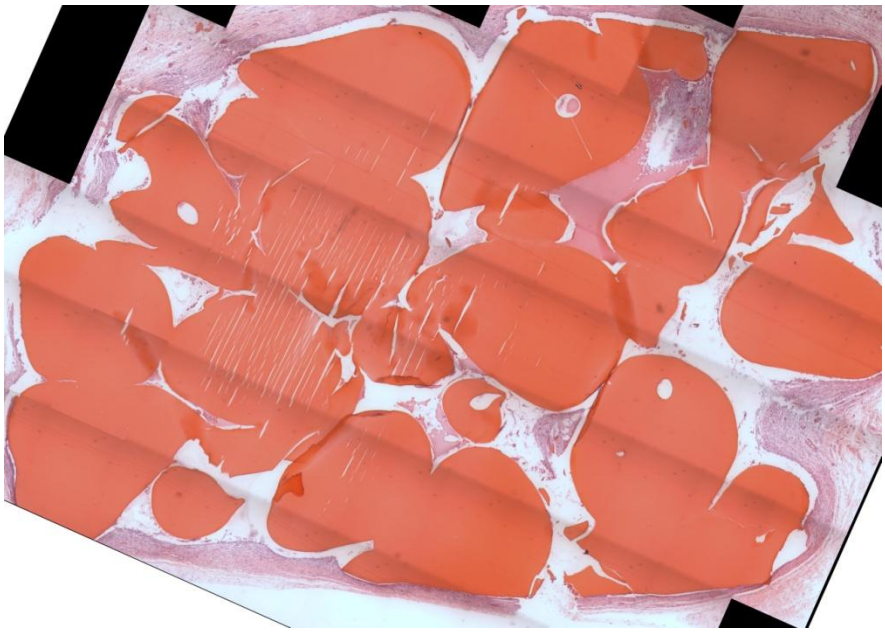

Figure 2. Light microscope image of representative histology section, H&E stain. The bright red objects are residual scaffold material. Note that most of the implant space is still occupied by scaffold material. Some histological artifacts are present in this particular section. Scaffold type was non-lyophilized with rhBMP-2.

As previously discussed, controlled degradation is an important characteristic of bone regenerative scaffolds. If the scaffolds do not degrade in a timely manner, extensive new bone formation will be prevented due to lack of space [21,38,39]. The 92.3% DDA chitosan used in this study was chosen due to its good mechanical properties; however, chitosan with a lower DDA has been shown to degrade considerably faster [18,40]. As DDA decreases, so does the crystallinity of the chitosan. This lower crystallinity allows lysozyme, the main enzyme responsible for chitosan degradation *in vivo*, easier access to the glycosidic bonds between the monomers [18,41]. Other potential methods for increasing scaffold degradation include using a lower molecular weight chitosan, decreasing the weight percent of chitosan, and using other solvent acids.

The composite chitosan-nano-hydroxyapatite scaffolds appeared to be very biocompatible. No adverse tissue reactions were observed. A small amount of new bone was seen in the implant area for all three groups (Figures 3, 4, and 5).

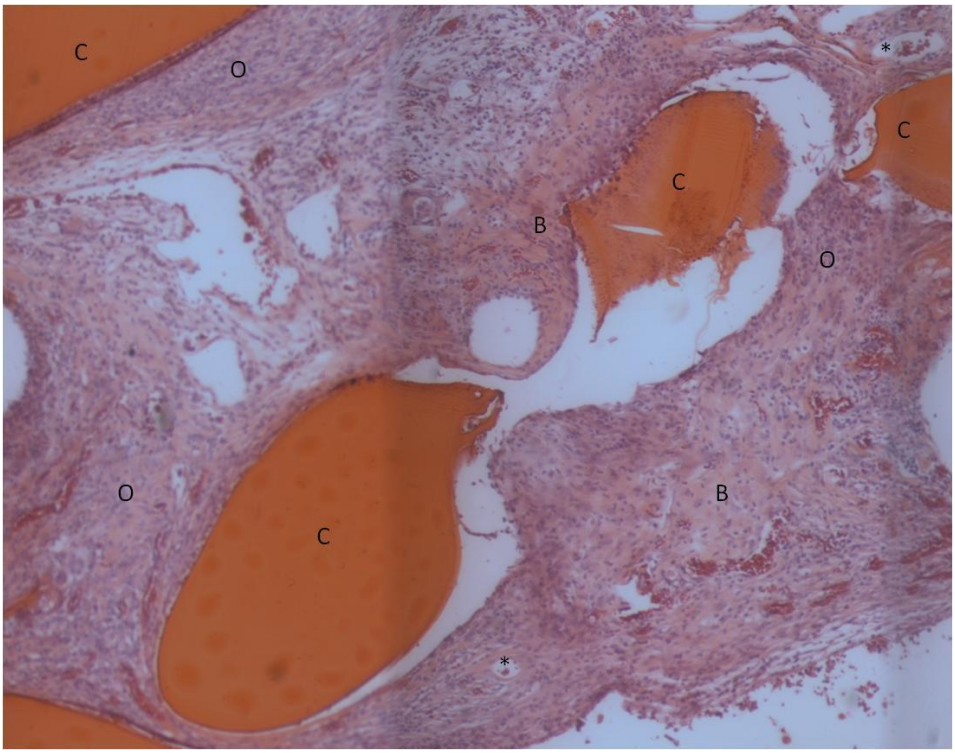

Figure 3. Light microscope image of lyophilized scaffold without rhBMP-2, H&E stain. The bright red objects are residual scaffold material. New bone tissue near and adjacent to the scaffold is present. An extensive amount of osteoid material which is in the process of becoming mineralized is also evident. Some capillaries with red blood cells in their interior can be seen. C: residual chitosan, B: bone, O: osteoid, *: capillaries.

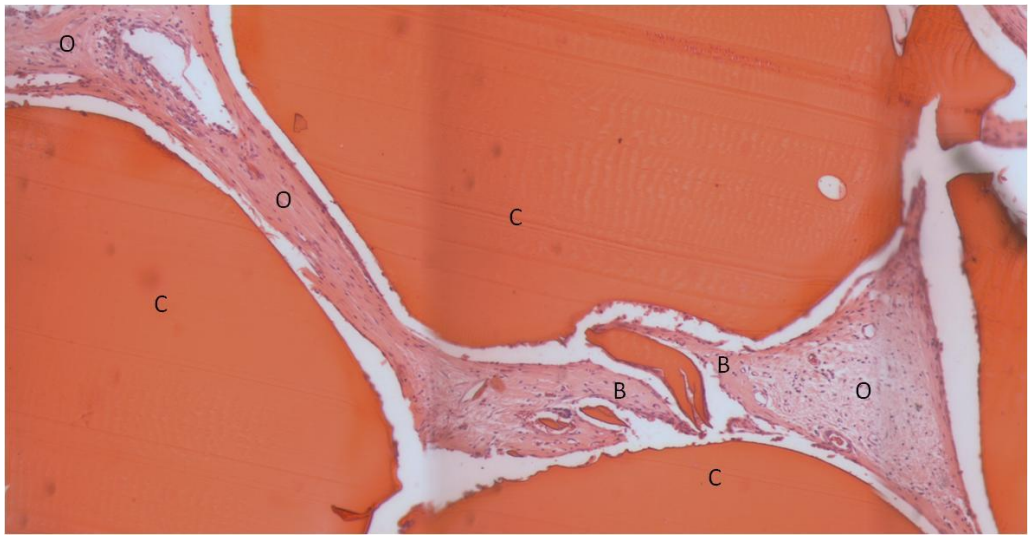

Figure 4. Light microscope image of lyophilized scaffold with rhBMP-2, H&E stain. The bright red objects are residual scaffold material. Some bone has formed in the pores of the scaffold. The remaining tissue appears to be osteoid material in the process of becoming mineralized. C: residual chitosan, B: bone, O: osteoid.

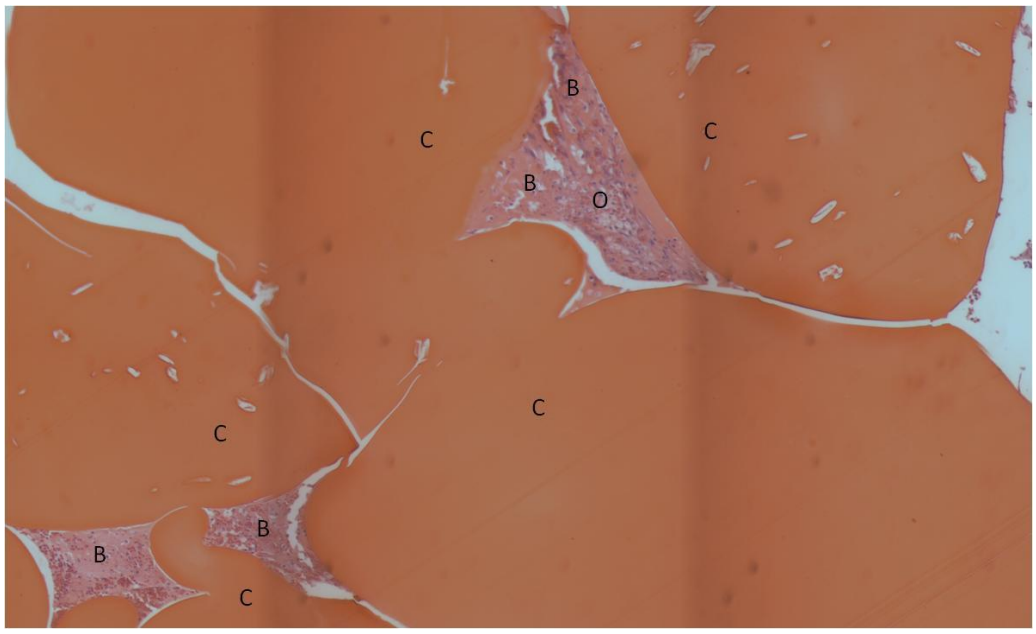

Figure 5. Light microscope image of non-lyophilized scaffold with rhBMP-2, H&E stain. The bright red objects are residual scaffold material. Bone and osteoid are occupying the pores of the scaffold. C: residual chitosan, B: bone, O: osteoid.

The amount of new bone was not statistically different between the groups ($p = 0.16$). It was somewhat surprising that new bone was found in the lyophilized scaffolds without BMP-2. Both chitosan [14,15,21] and hydroxyapatite [4,35,42] are considered to be osteoconductive, meaning that they are able to support the attachment and proliferation of bone cells but do not have the ability to cause stem cells to differentiate into osteoblasts. Furthermore, various composite chitosan-hydroxyapatite preparations have been shown to be osteoconductive [43-46]. However, some *in vitro* and *in vivo* data claiming hydroxyapatite to be osteoinductive does exist. Lin *et al*. demonstrated the ability of porous hydroxyapatite to induce expression of genes for alkaline phosphatase, osteocalcin, and Type I collagen in uncommitted pluripotent C3H10T1/2 mouse stem cells [47]. Porous nanohydroxyapatite/polyamide 66 scaffolds were found to be osteoinductive in New Zealand white rabbit muscle pouches by Xu *et al*. [48]. Hydroxyapatite has also been shown to be osteoinductive in large animals. Ripamonti *et al*. have demonstrated the ability of hydroxyapatite disks derived from coral and hydroxyapatite disks prepared using a solid-state reaction to be osteoinductive when implanted intramuscularly in baboons [49,50]. A number properties including topography, surface energy, surface area, and crystallinity of hydroxyapatite and other calcium phosphate materials are crucial in determining their osteoconductive and osteoinductive potentials [25,51-54]. In this study, the scaffolds appear to have the right combination of these surface chemistry and microarchitecture properties to impart some degree of osteoinductivity. It should also be noted that in the current experimental design, each rat received two scaffolds (one in each bilateral pouch); thus, it is possible that BMP-2 was able to diffuse from one implant site to another. However, proteolytic

enzymes are expected to quickly degrade any diffusing BMP-2, and the half-life of BMP-2 is 7-16 minutes [55]. Thus, we believe the presence of new bone in the scaffold group without BMP-2 is an indication that our composite scaffolds are very suitable for bone regeneration. It is also very promising that new bone was observed in direct contact with the composite scaffolds.

While the amount of new bone observed for the composite scaffolds was low, more mineralized tissue might have been observed if a later timepoint had been used. However, considerable amounts of osteoid were observed for the three experimental groups. Thus, significant regions of unmineralized matrix which were expected to be later mineralized and converted to bone were observed. Since the composite scaffolds did not degrade and occupied a large portion of the implant area, the amount of new bone and osteoid were normalized to the amount of space available for tissue formation by calculating the bone tissue index (BTI) using the following equation:

$$BTI = \frac{(Bone + Osteoid)}{(100 - Scaffold)} \times 100\% \quad (1)$$

Thus, the BTI is an indicator of how much of the open pore space in the implant area was filled in with new bone or was in the process of being converted to bone after one month. Table 2 displays the BTI for the experimental groups.

Table 2. Bone Tissue Index (BTI) values for composite scaffolds.

Scaffold Type	Bone Tissue Index (%)
Lyophilized (no rhBMP-2)	30.6 ± 8.5
Lyophilized with rhBMP-2	28.8 ± 5.4
Air-dried with rhBMP-2	30.5 ± 5.7

The values of the BTIs for all three groups were approximately thirty percent and were not statistically different ($p = 0.90$). This degree of bone and osteoid formation is comparable to that observed in studies with other non-degrading porous implant materials. Baril *et al*. observed 20–25% bone ingrowth after six weeks into the pores of titanium implants with approximately 50% porosity [56]. Only 11.4 ± 2.4 and 10.5 ± 1.8% of bone ingrowth as a percent of void space after twelve weeks was observed by Willie *et al*. in titanium foam implants with porosities of 74.4 and 79.0%, respectively [57]. Following implantation of hydroxyapatite implants with 50% porosity into the femoral condyles of rabbits, Wang *et al*. observed 2.54 ± 0.59% bone ingrowth (as a percent of total defect area) after three weeks [58]. This value is similar to the bone ingrowth observed after four weeks in our chitosan-nano-hydroxyapatite scaffolds. However, Wang *et al.* found no bone in the interior region of their implants; whereas, new bone was found in the interior region of our scaffolds directly adjacent to composite beads. After three weeks of implantation in rat tibial defects, Zreiqat *et al*. observed approximately 25% bone ingrowth into pores of ceramic Hardystonite (77.5% porosity) and Sr-Hardystonite (78% porosity) [59]. Thus, we believe that our composite chitosan-nano-hydroxyapatite scaffolds have similar or potentially improved osteogenic capacity compared to the discussed biomaterials.

The experimental group containing lyophilized scaffolds with BMP-2 was expected to perform the best in this study due to increased BMP-2 loading. However, our hypothesis was not confirmed. The lack of degradation by the scaffolds may have reduced the effectiveness of BMP-2 delivery, since there was little space for new bone to be deposited. Also, the success of BMP-2 delivery depends upon the release profile of the

specific carrier [60-62]. Although there is some debate over what type of delivery profile is optimal for promoting osteogenesis, evidence suggests that a small to moderate burst release followed by sustained release of BMP-2 may be most effective [63-65]. *In vitro* characterization of BMP-2 elution from the composite scaffolds revealed a large burst release in which the majority of the growth factor was released within the first few days [12]. Perhaps more new bone would have been seen in the BMP-2 groups if a more optimal release profile occurred. We believe that the 36μg of BMP-2 per implant used in this study was an appropriate amount. Levels as low as 1.0 μg [60] to as high as 150 μg [66] of BMP-2 have been used successfully in similar murine ectopic bone models. Engstrand *et al.* observed greatly increased bone volume when 50 μg of BMP-2 was delivered compared to 10 μg [61]. An amount of 20μg of BMP-2 maintained ectopic bone formation better than 10, 5, or 2.5 μg in a study by Lee *et al*. [67].

Somewhat surprisingly, the increased total porosity of the lyophilized scaffolds did not result in increased new bone formation compared to non-lyophilized scaffolds. The non-lyophilized scaffolds did have the lowest value for amount of new bone (Table 1), but this value was not statistically significant. The differences in porosity between the non-lyophilized and lyophilized scaffolds (35.8 ± 2.1 and 53.6 ± 3.6, respectively) may not have been enough to considerably alter bone tissue formation. Although only a small amount of new bone was observed in this study, our composite scaffolds were able to promote and sustain ectopic bone growth. Furthermore, bone was found in the interior of the scaffolds and in direct contact with the scaffolds. We believe that our technology can be modified to produce scaffolds with a

faster degradation rate and that these scaffolds will be able to support extensive bone formation.

The BMP-2 loaded absorbable collagen sponge used as a positive control in this study completely degraded after one month and the implant area was filled in with bone and adipose tissue. Bone or adipose tissue (indicative of marrow formation) filled in 94.0 ± 4.4% of the implant area. No adverse tissue response to the material was observed (Figure 6).

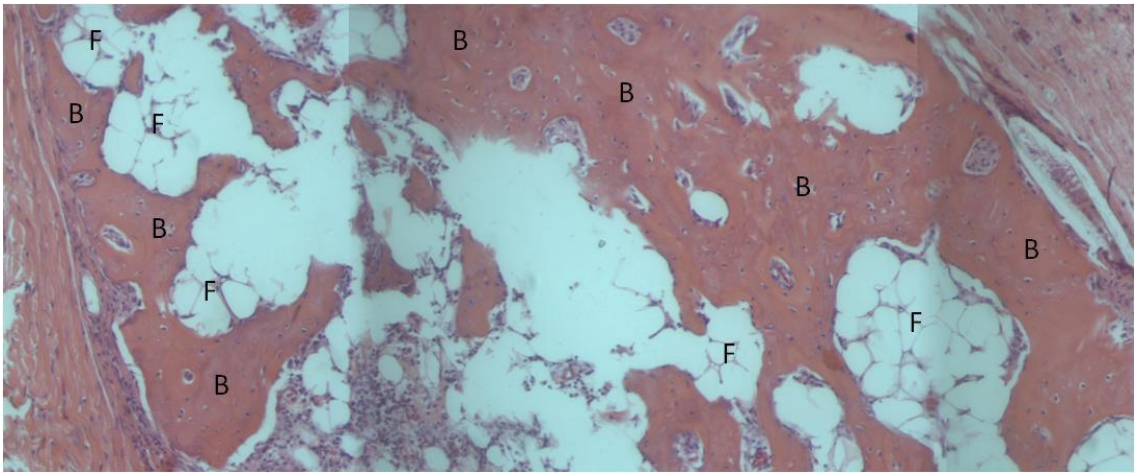

Figure 6. Light microscope image of absorbable collagen sponge, H&E stain. The collagen sponge has completely resorbed and is being replaced with bone. Fat globules indicative of marrow formation can also be seen. B: bone, F: fat globules.

The BMP-2 loaded absorbable sponge promoted extensive osteogenesis as expected. This sponge is used clinically to promote interbody spinal fusion and in the treatment of open tibial fractures. Although the sponge degrades quickly to allow extensive new bone formation, the collagen sponge cannot provide mechanical support to the fracture site and must be used in conjunction with hardware to prevent collapse of the defect [68].

3. Experimental Section

3.1. Composite Microsphere and Scaffold Fabrication

Composite microspheres and scaffolds were prepared as previously described [12]. Firstly, microspheres were fabricated using a co-precipitation method. A solution containing 3.57 weight percent (wt. %) chitosan (92.3% DDA; $M_v = 4.66 \times 10^5$ g/mole; Vanson, Redmond, WA), 0.1M $CaCl_2$, and 0.06 M NaH_2PO_4 (Ca:P ratio = 1.67) was prepared in 2 wt. % acetic acid. A precipitation solution (pH = 13) containing 20 wt. % NaOH, 30 wt. % methanol, and 50 wt. % water was prepared. Using a syringe pump, the chitosan solution was added dropwise through 21G needles into the precipitation solution, and spherical microspheres immediately formed. The composite microspheres were allowed to wash in the precipitation solution for 24 h to allow crystalline hydroxyapatite to form. The microspheres were then washed in deionized (DI) water until a neutral pH (<7.5) was achieved.

Porous composite scaffolds were formed by adhering the microspheres together. The microspheres were briefly rinsed in 1 wt. % acetic acid and packed into 13mm-diameter plastic tubes to dry. Once the scaffolds had completely dried, they were rehydrated in DI water and cut into cylinders with an approximate height of 4mm and diameter of 5.75 mm. Some of the scaffolds were allowed to dry again; whereas, some of the rehydrated scaffolds were placed in a freezer at −20 °C and subsequently lyophilized in a 2.5 L Labconco freeze-dryer. All scaffolds were sterilized using 25 kGy gamma irradiation.

3.2. Scaffold Preparation for Surgery

The following groups (n = 6) were prepared for implantation into rat muscle pouches: A) lyophilized scaffolds without rhBMP-2, B) lyophilized scaffolds with

rhBMP-2 (Genetics Institute, Cambridge, MA), C) non-lyophilized scaffolds with rhBMP-2, and D) absorbable collagen sponge (Medtronic, Inc., Memphis, TN) with rhBMP-2. The collagen sponge was aseptically cut into pieces 1 cm. × 1 cm. A 9.0μg/mL solution of rhBMP-2 was prepared in sterile water. An amount of 4 mL of rhBMP-2 solution was added to Groups B, C, and D for 48 h in sterile glass vials. After 48 h, the loading solution was aspirated and the scaffolds were stored in the glass vials at 4 °C until the surgeries.

3.3. Animal Surgeries

All procedures described were approved by the Institutional Animal Care and Use Committee at the University of Memphis (Protocol #0639) and conform to the laws and regulations of the United States. Upon arrival, twelve three-to-four month-old male Sprague Dawley rats were allowed to acclimate for one week. For surgery, rats were anesthetized with a subcutaneous injection of telazol. The back of each rat was shaved and scrubbed with betadine. A single 1.5 cm incision was made through the skin on each side of the midline. In each incision, a 1 cm pouch was created in the latissimus dorsi muscle using blunt dissection. A single randomized test specimen was implanted in each muscle pouch. Following implantation, the muscle and skin incisions were closed with 4-0 Vicryl sutures.

The rats were sacrificed after one month. The implants and surrounding tissue were excised and stored in 10% formalin. Following decalcified histological processing, three sections of each sample were stained with hematoxylin and eosin. Using the BIOQUANT OSTEO II v.8.10.20 imaging system, the total implant area in each section was identified. Sections were analyzed for amount of residual implant material, new

bone, and osteoid as a percent of total implant area. One-way analysis of variance (ANOVA) was performed to determine statistical significance between groups with $p < 0.05$ considered significant.

4. Conclusions

The ability of composite chitosan-nano-hydroxyapatite scaffolds to promote ectopic bone formation in a rat muscle pouch was demonstrated. Interestingly, both BMP-2 loaded scaffolds and scaffolds without BMP-2 were also able to promote osteogenesis. Increased bone formation due to local BMP-2 delivery was not observed, possibly due to the lack of degradation exhibited by the scaffolds. Also, the large burst effect release of BMP-2 from the composite scaffolds may not have been the optimal elution profile to promote ectopic bone growth. Although new bone formation in the total implant area was minimal (less than 2%), roughly thirty percent of the void space of the composite scaffolds contained bone or osteoid after one month. An absorbable collagen sponge loaded with BMP-2 used as a positive control completely degraded after one month, and $94.0 \pm 4.4\%$ of the implant area contained new bone or marrow.

Acknowledgements

The authors would like to thank Medtronic, Inc. for donation of an absorbable collagen sponge and Jeffrey Hollinger for his generous donation of rhBMP-2. Also, we would like to thank Karyl Buddington, D.V.M. and the University of Memphis animal care facilities. The authors are grateful to Patti Lott and the Center for Metabolic Bone Disease at the University of Alabama at Birmingham for their expertise in histological processing.

References

1. Dawson, J.I.; Oreffo, R.O. Bridging the regeneration gap: Stem cells, biomaterials and clinical translation in bone tissue engineering. *Arch Biochem. Biophys.* **2008**, *473*, 124-131.

2. Griffin, M.; Iqbal, S.A.; Bayat, A. Exploring the application of mesenchymal stem cells in bone repair and regeneration. *J. Bone Jt. Surg. Br.* **2011**, *93*, 427-434.

3. Khan, Y.; Yaszemski, M.J.; Mikos, A.G.; Laurencin, C.T. Tissue engineering of bone: Material and matrix considerations. *J. Bone Jt. Surg. Am.* **2008**, *90*, 36-42.

4. Nandi, S.K.; Roy, S.; Mukherjee, P.; Kundu, B.; De, D.K.; Basu, D. Orthopaedic applications of bone graft & graft substitutes: A review. *Indian J. Med. Res.* **2010**, *132*, 15-30.

5. Kretlow, J.D.; Mikos, A.G. Review: Mineralization of synthetic polymer scaffolds for bone tissue engineering. *Tissue Eng.* **2007**, *13*, 927-938.

6. Bae, H.; Zhao, L.; Zhu, D.; Kanim, L.E.; Wang, J.C.; Delamarter, R.B. Variability across ten production lots of a single demineralized bone matrix product. *J. Bone Jt. Surg. Am.* **2010**, *92*, 427-435.

7. Kinney, R.C.; Ziran, B.H.; Hirshorn, K.; Schlatterer, D.; Ganey, T. Demineralized bone matrix for fracture healing: Fact or fiction? *J. Orthop. Trauma* **2010**, *24*, S52-S55.

8. Logeart-Avramoglou, D.; Anagnostou, F.; Bizios, R.; Petite, H. Engineering bone: Challenges and obstacles. *J. Cell. Mol. Med.* **2005**, *9*, 72-84.

9. Karageorgiou, V.; Kaplan, D. Porosity of 3D biomaterial scaffolds and osteogenesis. *Biomaterials* **2005**, *26*, 5474-5491.

10. Chesnutt, B.M.; Viano, A.M.; Yuan, Y.; Yang, Y.; Guda, T.; Appleford, M.R.; Ong, J.L.; Haggard, W.O.; Bumgardner, J.D. Design and characterization of a novel chitosan/nanocrystalline calcium phosphate composite scaffold for bone regeneration. *J. Biomed. Mater. Res. Part A* **2009**, *88*, 491-502.

11. Chesnutt, B.M.; Yuan, Y.; Buddington, K.; Haggard, W.O.; Bumgardner, J.D. Composite chitosan/nano-hydroxyapatite scaffolds induce osteocalcin production by osteoblasts *in vitro* and support bone formation *in vivo*. *Tissue Eng. Part A* **2009**, *15*, 2571-2579.

12. Reves, B.T.; Bumgardner, J.D.; Cole, J.A.; Yang, Y.; Haggard, W.O. Lyophilization to improve drug delivery for chitosan-calcium phosphate bone scaffold construct: A preliminary investigation. *J. Biomed. Mater. Res., Part B* **2009**, *90*, 1-10.

13. Chen, J.K.; Shen, C.R.; Liu, C.L. N-acetylglucosamine: Production and applications. *Mar. Drugs* **2010**, *8*, 2493-2516.

14. Venkatesan, J.; Kim, S.K. Chitosan composites for bone tissue engineering—An overview. *Mar. Drugs* **2010**, *8*, 2252-2266.

15. Di Martino, A.; Sittinger, M.; Risbud, M.V. Chitosan: A versatile biopolymer for orthopaedic tissue-engineering. *Biomaterials* **2005**, *26*, 5983-5990.

16. Kim, I.Y.; Seo, S.J.; Moon, H.S.; Yoo, M.K.; Park, I.Y.; Kim, B.C.; Cho, C.S. Chitosan and its derivatives for tissue engineering applications. *Biotechnol. Adv.* **2008**, *26*, 1-21.

17. Swetha, M.; Sahithi, K.; Moorthi, A.; Srinivasan, N.; Ramasamy, K.; Selvamurugan, N. Biocomposites containing natural polymers and hydroxyapatite for bone tissue engineering. *Int. J. Biol. Macromol.* **2010**, *47*, 1-4.

18. Shi, C.; Zhu, Y.; Ran, X.; Wang, M.; Su, Y.; Cheng, T. Therapeutic potential of chitosan and its derivatives in regenerative medicine. *J. Surg. Res.* **2006**, *133*, 185-192.

19. Jayakumar, R.; Menon, D.; Manzoor, K.; Nair, S.V.; Tamura, H. Biomedical applications of chitin and chitosan based nanomaterials-A short review. *Carbohydr. Polym.* **2010**, *82*, 227-232.

20. Peter, M.; Ganesh, N.; Selvamurugan, N.; Nair, S.V.; Furuike, T.; Tamura, H.; Jayakumar, R. Preparation and characterization of chitosan-gelatin/nanohydroxyapatite composite scaffolds for tissue engineering applications. *Carbohydr. Polym.* **2010**, *80*, 687-694.

21. Jiang, T.; Kumbar, S.G.; Nair, L.S.; Laurencin, C.T. Biologically active chitosan systems for tissue engineering and regenerative medicine. *Curr. Top. Med. Chem.* **2008**, *8*, 354-364.

22. Jones, A.C.; Arns, C.H.; Hutmacher, D.W.; Milthorpe, B.K.; Sheppard, A.P.; Knackstedt, M.A. The correlation of pore morphology, interconnectivity and physical properties of 3D ceramic scaffolds with bone ingrowth. *Biomaterials* **2009**, *30*, 1440-1451.

23. Hermida, J.C.; Bergula, A.; Dimaano, F.; Hawkins, M.; Colwell, C.W., Jr.; D'Lima, D.D. An *in vivo* evaluation of bone response to three implant surfaces using a rabbit intramedullary rod model. *J. Orthop. Surg. Res.* **2010**, *5*, 57:1-57:8.

24. Coelho, P.G.; Freire, J.N.; Granato, R.; Marin, C.; Bonfante, E.A.; Gil, J.N.; Chuang, S.K.; Suzuki, M. Bone mineral apposition rates at early implantation times around differently prepared titanium surfaces: A study in beagle dogs. *Int. J. Oral Maxillofac. Implant.* **2011**, *26*, 63-69.

25. Xiong, J.; Li, Y.; Hodgson, P.D.; Wen, C. *In vitro* osteoblast-like cell proliferation on nano-hydroxyapatite coatings with different morphologies on a titanium-niobium shape memory alloy. *J. Biomed. Mater. Res., Part A* **2010**, *95*, 766–773.

26. Thian, E.S.; Huang, J.; Ahmad, Z.; Edirisinghe, M.J.; Jayasinghe, S.N.; Ireland, D.C.; Brooks, R.A.; Rushton, N.; Best, S.M.; Bonfield, W. Influence of nanohydroxyapatite patterns deposited by electrohydrodynamic spraying on osteoblast response. *J. Biomed. Mater. Res. Part A* **2008**, *85*, 188-194.

27. Lieberman, J.R.; Daluiski, A.; Einhorn, T.A. The role of growth factors in the repair of bone. Biology and clinical applications. *J. Bone Jt. Surg. Am.* **2002**, *84-A*, 1032-1044.

28. Devescovi, V.; Leonardi, E.; Ciapetti, G.; Cenni, E. Growth factors in bone repair. *Chir. Organi Mov.* **2008**, *92*, 161-168.

29. Reddi, A.H. Bone morphogenetic proteins: From basic science to clinical applications. *J. Bone Jt. Surg. Am.* **2001**, *83-A*, S1-S6.

30. Ai-Aql, Z.S.; Alagl, A.S.; Graves, D.T.; Gerstenfeld, L.C.; Einhorn, T.A. Molecular mechanisms controlling bone formation during fracture healing and distraction osteogenesis. *J. Dent. Res.* **2008**, *87*, 107-118.

31. Fiedler, J.; Roderer, G.; Gunther, K.P.; Brenner, R.E. BMP-2, BMP-4, and PDGF-bb stimulate chemotactic migration of primary human mesenchymal progenitor cells. *J. Cell. Biochem.* **2002**, *87*, 305-312.

32. Huang, Z.; Nelson, E.R.; Smith, R.L.; Goodman, S.B. The sequential expression profiles of growth factors from osteoprogenitors to osteoblasts *in vitro*. *Tissue Eng.* **2007**, *13*, 2311-2320.

33. Zhang, F.; Qiu, T.; Wu, X.; Wan, C.; Shi, W.; Wang, Y.; Chen, J.G.; Wan, M.; Clemens, T.L.; Cao, X. Sustained BMP signaling in osteoblasts stimulates bone formation by promoting angiogenesis and osteoblast differentiation. *J. Bone Miner. Res.* **2009**, *24*, 1224-1233.

34. Katz, J.M.; Nataraj, C.; Jaw, R.; Deigl, E.; Bursac, P. Demineralized bone matrix as an osteoinductive biomaterial and *in vitro* predictors of its biological potential. *J. Biomed. Mater. Res. Part B* **2009**, *89*, 127-134.

35. Lee, J.H.; Lee, K.M.; Baek, H.R.; Jang, S.J.; Ryu, H.S. Combined effects of porous hydroxyapatite and demineralized bone matrix on bone induction: *In vitro* and *in vivo* study using a nude rat model. *Biomed. Mater.* **2011**, *6*, 015008.

36. Qiu, Q.Q.; Liu, X.H.; Connor, J. Effects of e-beam radiation, storage, and hydration on osteoinductivity of DBM/AM composite. *J. Biomed. Mater. Res. Part B* **2009**, *91*, 401-408.

37. Borden, M.; Attawia, M.; Khan, Y.; Laurencin, C.T. Tissue engineered microsphere-based matrices for bone repair: Design and evaluation. *Biomaterials* **2002**, *23*, 551-559.

38. Alsberg, E.; Kong, H.J.; Hirano, Y.; Smith, M.K.; Albeiruti, A.; Mooney, D.J. Regulating bone formation via controlled scaffold degradation. *J. Dent. Res.* **2003**, *82*, 903-908.

39. Oest, M.E.; Dupont, K.M.; Kong, H.J.; Mooney, D.J.; Guldberg, R.E. Quantitative assessment of scaffold and growth factor-mediated repair of critically sized bone defects. *J. Orthop. Res.* **2007**, *25*, 941-950.

40. Ren, D.W.; Yi, H.F.; Wang, W.; Ma, X.J. The enzymatic degradation and swelling properties of chitosan matrices with different degrees of N-acetylation. *Carbohydr. Res.* **2005**, *340*, 2403-2410.

41. Madihally, S.V.; Matthew, H.W. Porous chitosan scaffolds for tissue engineering. *Biomaterials* **1999**, *20*, 1133-1142.

42. Habibovic, P.; Kruyt, M.C.; Juhl, M.V.; Clyens, S.; Martinetti, R.; Dolcini, L.; Theilgaard, N.; van Blitterswijk, C.A. Comparative *in vivo* study of six hydroxyapatite-based bone graft substitutes. *J. Orthop. Res.* **2008**, *26*, 1363-1370.

43. Danilchenko, S.N.; Kalinkevich, O.V.; Pogorelov, M.V.; Kalinkevich, A.N.; Sklyar, A.M.; Kalinichenko, T.G.; Ilyashenko, V.Y.; Starikov, V.V.; Bumeyster, V.I.; Sikora, V.Z.; *et al.* Characterization and *in vivo* evaluation of chitosan-hydroxyapatite bone scaffolds made by one step coprecipitation method. *J. Biomed. Mater. Res. Part A* **2011**, *96*, 639-647.

44. Thein-Han, W.W.; Misra, R.D. Biomimetic chitosan-nanohydroxyapatite composite scaffolds for bone tissue engineering. *Acta Biomater.* **2009**, *5*, 1182-1197.

45. Venugopal, J.R.; Giri Dev, V.R.; Senthilram, T.; Sathiskumar, D.; Gupta, D.; Ramakrishna, S. Osteoblast mineralization with composite nanofibrous substrate for bone tissue regeneration. *Cell Biol. Int.* **2011**, *35*, 73-80.

46. Kong, L.; Ao, Q.; Wang, A.; Gong, K.; Wang, X.; Lu, G.; Gong, Y.; Zhao, N.; Zhang, X. Preparation and characterization of a multilayer biomimetic scaffold for bone tissue engineering. *J. Biomater. Appl.* **2007**, *22*, 223-239.

47. Lin, L.; Chow, K.L.; Leng, Y. Study of hydroxyapatite osteoinductivity with an osteogenic differentiation of mesenchymal stem cells. *J. Biomed. Mater. Res. Part A* **2009**, *89*, 326-335.

48. Xu, Q.; Lu, H.; Zhang, J.; Lu, G.; Deng, Z.; Mo, A. Tissue engineering scaffold material of porous nanohydroxyapatite/polyamide 66. *Int. J. Nanomed.* **2010**, *5*, 331–335.

49. Magan, A.; Ripamonti, U. Geometry of porous hydroxyapatite implants influences osteogenesis in baboons (Papio ursinus). *J. Craniofacial Surg.* **1996**, *7*, 71-78.

50. Ripamonti, U.; Richter, P.W.; Thomas, M.E. Self-inducing shape memory geometric cues embedded within smart hydroxyapatite-based biomimetic matrices. *Plast. Reconstr. Surg.* **2007**, *120*, 1796-1807.

51. Lee, Y.T.; Yu, B.Y.; Shao, H.J.; Chang, C.H.; Sun, Y.M.; Liu, H.C.; Hou, S.M.; Young, T.H. Effects of the surface characteristics of nano-crystalline and micro-particle calcium phosphate/chitosan composite films on the behavior of human mesenchymal stem cells *in vitro*. *J. Biomater. Sci., Polym. Ed.* **2010.**

52. Habibovic, P.; Sees, T.M.; van den Doel, M.A.; van Blitterswijk, C.A.; de Groot, K. Osteoinduction by biomaterials—Physicochemical and structural influences. *J. Biomed. Mater. Res., Part A* **2006**, *77*, 747-762.

53. Bjerre, L.; Bunger, C.; Baatrup, A.; Kassem, M.; Mygind, T. Flow perfusion culture of human mesenchymal stem cells on coralline hydroxyapatite scaffolds with various pore sizes. *J. Biomed. Mater. Res. Part A* **2011**, *97*, 251-263.

54. Ruhe, P.Q.; Hedberg-Dirk, E.L.; Padron, N.T.; Spauwen, P.H.; Jansen, J.A.; Mikos, A.G. Porous poly(DL-lactic-co-glycolic acid)/calcium phosphate cement composite for reconstruction of bone defects. *Tissue Eng.* **2006**, *12*, 789-800.

55. Balmayor, E.R.; Feichtinger, G.A.; Azevedo, H.S.; van Griensven, M.; Reis, R.L. Starch-poly-epsilon-caprolactone microparticles reduce the needed amount of BMP-2. *Clin. Orthop. Relat. Res.* **2009**, *467*, 3138-3148.

56. Baril, E.; Lefebvre, L.P.; Hacking, S.A. Direct visualization and quantification of bone growth into porous titanium implants using micro computed tomography. *J. Mater. Sci. Mater. Med.* **2011**, *22*, 1321-1332.

57. Willie, B.M.; Yang, X.; Kelly, N.H.; Merkow, J.; Gagne, S.; Ware, R.; Wright, T.M.; Bostrom, M.P. Osseointegration into a novel titanium foam implant in the distal femur of a rabbit. *J. Biomed. Mater. Res. Part B* **2010**, *92*, 479-488.

58. Wang, W.; Itoh, S.; Tanaka, Y.; Nagai, A.; Yamashita, K. Comparison of enhancement of bone ingrowth into hydroxyapatite ceramics with highly and poorly interconnected pores by electrical polarization. *Acta Biomater.* **2009**, *5*, 3132-3140.

59. Zreiqat, H.; Ramaswamy, Y.; Wu, C.; Paschalidis, A.; Lu, Z.; James, B.; Birke, O.; McDonald, M.; Little, D.; Dunstan, C.R. The incorporation of strontium and zinc into a calcium-silicon ceramic for bone tissue engineering. *Biomaterials* **2010**, *31*, 3175-3184.

60. Boerckel, J.D.; Kolambkar, Y.M.; Dupont, K.M.; Uhrig, B.A.; Phelps, E.A.; Stevens, H.Y.; Garcia, A.J.; Guldberg, R.E. Effects of protein dose and delivery system on BMP-mediated bone regeneration. *Biomaterials* **2011**, *32*, 5241-5251.

61. Engstrand, T.; Veltheim, R.; Arnander, C.; Docherty-Skogh, A.C.; Westermark, A.; Ohlsson, C.; Adolfsson, L.; Larm, O. A novel biodegradable delivery system for bone morphogenetic protein-2. *Plast. Reconstr. Surg.* **2008**, *121*, 1920-1928.

62. Takita, H.; Vehof, J.W.; Jansen, J.A.; Yamamoto, M.; Tabata, Y.; Tamura, M.; Kuboki, Y. Carrier dependent cell differentiation of bone morphogenetic protein-2 induced osteogenesis and chondrogenesis during the early implantation stage in rats. *J. Biomed. Mater. Res., Part A* **2004**, *71*, 181-189.

63. Brown, K.V.; Li, B.; Guda, T.; Perrien, D.S.; Guelcher, S.A.; Wenke, J.C. Improving bone formation in a rat femur segmental defect by controlling bone morphogenetic protein-2 release. *Tissue Eng. Part A* **2011**, *17*, 1735-1746.

64. Maeda, H.; Sano, A.; Fujioka, K. Controlled release of rhBMP-2 from collagen minipellet and the relationship between release profile and ectopic bone formation. *Int. J. Pharm.* **2004**, *275*, 109-122.

65. Srouji, S.; Ben-David, D.; Lotan, R.; Livne, E.; Avrahami, R.; Zussman, E. Slow-release human recombinant bone morphogenetic protein-2 embedded within electrospun scaffolds for regeneration of bone defect: *In vitro* and *in vivo* evaluation. *Tissue Eng. Part A* **2011**, *17*, 269-277.

66. Luca, L.; Rougemont, A.L.; Walpoth, B.H.; Gurny, R.; Jordan, O. The effects of carrier nature and pH on rhBMP-2-induced ectopic bone formation. *J. Controlled Release* **2010**, *147*, 38-44.

67. Lee, J.H.; Kim, C.S.; Choi, K.H.; Jung, U.W.; Yun, J.H.; Choi, S.H.; Cho, K.S. The induction of bone formation in rat calvarial defects and subcutaneous tissues by recombinant human BMP-2, produced in Escherichia coli. *Biomaterials* **2010**, *31*, 3512-3519.

68. McKay, W.F.; Peckham, S.M.; Badura, J.M. A comprehensive clinical review of recombinant human bone morphogenetic protein-2 (INFUSE Bone Graft). *Int. Orthop.* **2007**, *31*, 729-734.

Chapter 3 Preparation and Functional Assessment of Composite Chitosan-Nano-Hydroxyapatite Scaffolds for Bone Regeneration

1. Introduction

Approximately, five to ten percent of bone fractures will result in delayed healing or non-union [1]. In Europe, insufficient bone healing results in socioeconomic losses of around 14.7 billion euros each year [2]. Although autografts and allografts are commonly used to treat these troublesome fractures, a number of drawbacks with these procedures have generated interest in the development of bone graft substitutes [3-6]. These bone graft substitutes are designed to provide a favorable matrix to which osteoblasts can attach, proliferate, and subsequently produce new bone. These materials are also expected to provide some mechanical support and stability to the fracture site until osteogenesis occurs. In addition, these bone scaffolds should degrade in a timely manner so that new bone can completely fill the defect site [7-10]. Many of these scaffolds also serve as drug delivery vehicles for the local release of growth factors to further augment fracture healing [2, 11, 12].

Our laboratory group has previously developed chitosan-nano-hydroxyapatite scaffolds for use in bone regeneration [13-15]. The scaffolds are prepared by fusing composite microspheres together to form porous scaffolds. Chitosan is a carbohydrate co-polymer containing glucosamine and N-acetyl-D-glucosamine monomers[16, 17]. Chitosan displays a number of properties including biocompatibility, degradability, mucoadhesiveness, and an ability to promote wound healing that have led to the development of chitosan sponges, films, gels, beads, etc. for use in various biomedical applications [16-20]. Hydroxyapatite is the main inorganic component of bone and has been used to improve osseointegration of implants and in bone graft substitutes [20-23].

We have previously demonstrated the potential of these composite chitosan-nano-hydroxyapatite scaffolds to serve as bone graft substitutes both *in vitro* and *in vivo* [13-15]. Although the scaffolds are very biocompatible and we have observed new bone in direct contact with the scaffolds *in vivo*, more extensive new bone formation appears to be prevented due to slow degradation of the scaffolds [13, 14]. We believe that the osteogenic capacity of the scaffolds can be further enhanced by improving the degradation profile of the scaffolds.

An important parameter of chitosan is degree of deacetylation (DDA), which is defined as the ratio of deacetylated glucosamine units to the total number of monomers [16, 17]. DDA has an effect on a number of chitosan properties, including crystallinity, degradation, and mechanical strength. Since the lower number of acetyl residues allow for tighter packing of the polymer chains, high DDA chitosan will be more crystalline than lower DDA chitosan (if all other parameters are equal) [19, 24, 25]. High DDA chitosan materials are more rigid and stronger than low DDA chitosan materials [26, 27], but degrade more slowly [24, 27-30]. In previous studies, composite scaffolds were prepared using 92.3% DDA chitosan [13-15]. This high DDA was chosen due to its good mechanical properties. Using lower DDA chitosan to fabricate composite scaffolds may result in increased degradation.

Our laboratory group has also demonstrated that increased surface area can be obtained by freeze-drying (lyophilization) [15]. Increased surface area may promote degradation by exposing more of the surface of the scaffolds to lysozyme and by increasing fluid uptake. Chitosan is soluble in weak organic acids due to protonation of the amine group on the glucosamine residues, and the pK_a is approximately 6.5 [31].

Washing composite microspheres in a mildly acidic solution before fusing them into scaffolds was identified as another potential method to increase scaffold degradation. Lower DDA chitosan, lyophilization, and a mild acid wash were evaluated for increased degradation of composite scaffolds.

Although the main goal of this research is to improve the degradation profile of the scaffolds to allow more extensive bone ingrowth, the other characteristics required of bone scaffolds should still be met. The scaffolds need sufficient mechanical properties to provide space maintenance at the fracture site and to prevent collapse of the scaffold pores [8]. Maintaining porosity is vital so that cells can migrate to the interior of the scaffold and so that proper nutrient/waste exchange can occur throughout the scaffold [7, 32, 33]. The scaffolds must provide a favorable surface for osteoblast attachment and proliferation [8]. Chitosan-nano-hydroxyapatite composite scaffolds had previously been shown to have both superior mechanical properties and induce more favorable cellular responses compared to plain chitosan scaffolds [13, 14]. The addition of more hydroxyapatite to the composite scaffolds could possibly improve the properties of the scaffolds even more. In this research, fabrication parameters including chitosan DDA, microsphere drying method, hydroxyapatite content, and the use of a mild acid wash were investigated to fabricate composite chitosan-nano-hydroxyapatite scaffolds with improved properties for bone regeneration.

2. Experimental Section

2.1. Phase I: Effects of DDA and Drying Method

In Phase I of this research, the effects of DDA and drying method were evaluated. Air-dried (A/D) and freeze-dried (F/D) 61% and 80% DDA scaffolds were prepared (Figure 1).

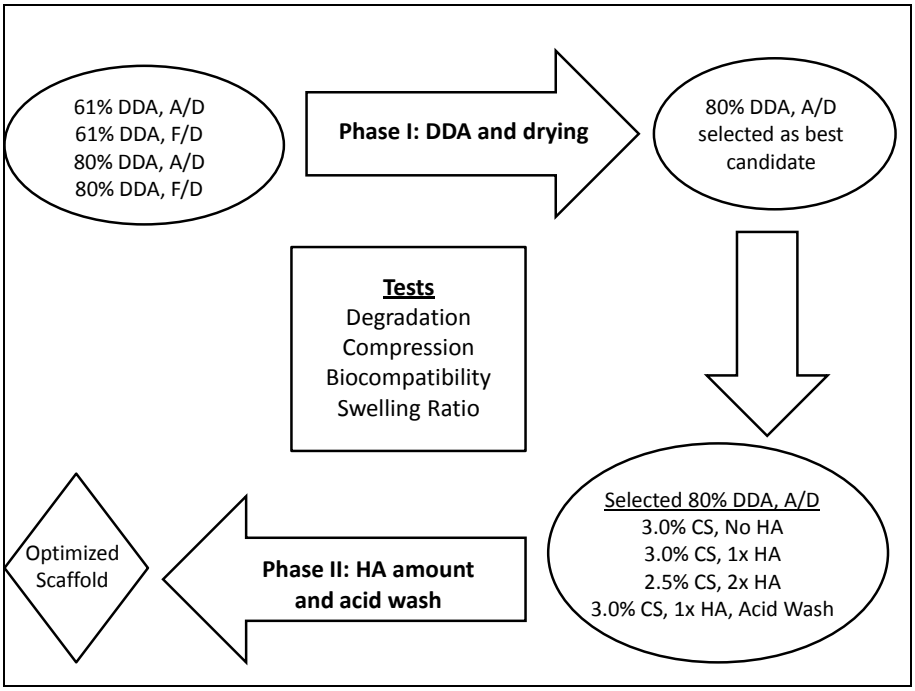

Figure 1. Experimental design used for scaffold characterization. Degradation of air-dried and freeze-dried 61% and 80% DDA microspheres was also determined. All groups underwent SEM analysis. A/D: air-dried; F/D: freeze-dried; CS: chitosan; HA: hydroxyapatite.

2.1.1. Microsphere Fabrication

Composite chitosan-nano-hydroxyapatite microspheres were prepared using a co-precipitation method as previously described [13, 15]. Briefly, solutions containing 61% DDA (MW = 220 kDa) or 80% DDA (MW = 260 kDa) chitosan (Primex, Siglufjordur,

Iceland), 0.1M $CaCl_2$, and 0.06M NaH_2PO_4 (referred to as 1x HA, Ca:P ratio = 1.67) were prepared in 2 volume percent (vol. %) acetic acid (Table 1).

Table 1. Chitosan solutions used to make composite beads. Note: Dissolved in 200 mL of 2 vol. % acetic acid. CS: Chitosan, HA: Hydroxyapatite.

Microsphere Type	Chitosan (g)	$CaCl_2 \bullet 2H_20$ (g)	$NaH_2PO_4 \bullet H_20$ (g)
61% DDA: 3.5% CS, 1x HA	7.00	2.94	1.66
80% DDA: 3.0% CS, 1x HA	6.00	2.94	1.66

A precipitation solution (pH = 13) containing 20 weight percent (wt. %) NaOH, 30 wt. % methanol, and 50 wt. % water was prepared. Using a syringe pump, the chitosan solution was added dropwise through 16G needles into the precipitation solution, and microspheres immediately formed. The microspheres were stirred in the precipitation solution for 24 hours to allow crystalline hydroxyapatite to form. The microspheres were then washed in deionized (DI) water until a neutral pH (<7.5) was achieved.

Microspheres were either air-dried (A/D) or freeze-dried (F/D). Air-drying was performed by placing neutralized beads in plastic weigh boats and drying them in a chemical fume hood at room temperature. Freeze-drying was performed by placing neutralized (still hydrated) beads in plastic weigh boats and pre-freezing at −20 °C in a laboratory freezer for two hours. The beads were then freeze-dried in a 2.5L Labconco lyophilizer for 48 hours.

2.1.2. Scaffold Fabrication

Porous scaffolds were prepared by fusing dried microspheres together. The microspheres were rinsed in 1wt. % acetic acid for approximately ten seconds in a ceramic sieve. Excess acid was removed using a vacuum. This very brief acid wash

gently dissolves the outer layer of the beads and makes them adherent. Using a laboratory spatula, the microspheres were then placed in 12mm diameter polystyrene tubes to form cylindrical scaffolds. Only very slight pressure was applied to the microspheres with the spatula as they were placed in the polystyrene tubes. After approximately one minute, the scaffolds were removed from the molds and allowed to air-dry. Following rehydration, the scaffolds can be cut into any height as desired.

2.2. Phase II: Effects of Hydroxyapatite Content and MES Acid Wash

2.2.1 Microsphere and Scaffold Fabrication

Based on the data obtained in Phase I, air-dried 80% DDA scaffolds were determined to be good candidates for bone regeneration. In Phase II, the following groups of air-dried 80% DDA beads/scaffolds were prepared to determine the effect of hydroxyapatite content and a mild acid wash: 3.0% CS, No HA; 3.0%, 1x HA; 2.5% CS, 2x HA; and 3.0% CS, 1x HA, acid wash. As seen in Table 2, No HA refers to solutions containing only chitosan, and 2x HA denotes solutions with 0.2M $CaCl_2$ and 0.12M NaH_2PO_4 (Ca:P ratio = 1.67).

Table 2. Chitosan solutions used to make air-dried 80% DDA beads. Note: Dissolved in 200 mL of 2 vol. % acetic acid. CS: Chitosan, HA: Hydroxyapatite. *Also prepared using MES acid wash.

Microsphere Type	**Chitosan (g)**	**$CaCl_2 \bullet 2H_20$ (g)**	**$NaH_2PO_4 \bullet H_20$ (g)**
3.0% CS, No HA	6.00	0.00	0.00
3.0% CS, 1x HA*	6.00	2.94	1.66
2.5% CS, 2x HA	5.00	5.88	3.31

In Phase II, all of the microspheres were air-dried. Scaffolds were prepared by the method previously described.

2.2.2. MES Acid Wash

Some of the 3.0% CS, 1x HA beads underwent a mild acid wash before being air-dried (Table 2). A 40 mM 2-(N-morphilino)ethanesulfonic acid (MES) solution was prepared, and the pH was raised to 6.1 using concentrated NaOH. Neutralized microspheres (80% DDA, 3.0% CS, 1x HA) were added to the MES solution. The microspheres were allowed to wash for ten minutes, and the pH was maintained at 6.1 by adding additional MES powder. The microspheres were removed, washed in DI water, washed in 70% and 95% ethanol, and placed in a chemical fume hood to dry. After completely drying, the microspheres were then washed in 1x phosphate buffered saline for thirty minutes and allowed to completely air-dry again. Scaffolds were prepared by the method previously described.

2.3. Characterization

2.3.1. Scanning Electron Microscopy

Scanning electron micrograph (SEM) images of composite microspheres and scaffolds were obtained using a Philips XL30 environmental microscope. Samples were coated with 30nm of Au/Pd before imaging to make them conductive. Microsphere size and surface topography were evaluated using SEM images.

2.3.2. Microsphere and Scaffold Degradation

Immediately prior to starting the degradation study, microsphere samples were placed in a convection oven at 50 °C to mitigate the effects of ambient humidity. After one hour, the microspheres were removed from the convection oven and weighed. An amount of 4mL of degradation solution containing 100 μg/mL lysozyme (MP Biomedicals, Cat. No. 100834) + antibiotics/antimycotic (1 unit/mL penicillin, 1 μg/mL

streptomycin, and 0.25 μg/mL amphotericin B) in DI water was added to each sample. Lysozyme is the main enzyme responsible for chitosan degradation *in vivo* [29, 34]. The samples were placed in an incubator at 37 °C, and the degradation solution was refreshed every three days. After one month, the microspheres were allowed to air-dry and were then heated in a convection oven at 50 °C for one hour. The microspheres were weighed and the percent weight change was determined using the following equation:

$$(\text{Initial weight} - \text{final weight})/(\text{Initial weight}) \times 100 \quad (1)$$

Scaffold degradation was performed in the same manner as microsphere degradation. Scaffolds were completely submerged in 6 mL of 100 μg/mL lysozyme + antibiotics/antimycotic. After one month, the percent weight change was measured.

2.3.3. Compression Testing

The compressive moduli of scaffolds were determined using an Instron load frame (Model # 33R 4465). Since the scaffolds will become hydrated after implantation, they were rehydrated in DI water. 61% DDA scaffolds were rehydrated for four hours. The interior beads of 80% DDA scaffolds were not completely hydrated after four hours, so these scaffolds were rehydrated for eight hours. The diameter of the scaffolds varied depending on the microsphere type, and the rehydrated scaffolds were sectioned so that the height:diameter ratio was maintained at approximately 1.5. The scaffolds were then compressed at a strain rate of 0.1 min^{-1} until 50% strain was achieved. The compressive modulus was determined using the initial linear portion of the stress-strain curve.

2.3.4. Swelling Ratio

The swelling ratio of scaffolds was determined. Pre-weighed scaffolds were placed in 10 mL of deionized water and put in an incubator at 37 °C. After 24 hours, the scaffolds were removed and pat-dried to remove any excess moisture on the surface. The scaffolds were re-weighed and the swelling ratio was determined using the following equation:

$$(\text{Final weight} - \text{Initial weight}) / (\text{Initial weight}) \times 100 \quad (2)$$

2.3.5. Biocompatibility

The biocompatibility of each microsphere type was evaluated using osteoblast-like SAOS-2 cells. Cells in McCoy's 5A media supplemented with 15% fetal bovine serum and antibiotics/antimycotic were seeded at a density of 2.2×10^5 cells/sample onto microspheres in Transwell inserts in 24-well plates. The cells were incubated at 37 °C with 5% CO_2. After allowing cells to attach for three hours, the inserts were transferred to empty wells, and cell attachment was evaluated using the CellTiter-Glo assay (Promega). A standard curve relating luminescence output from the assay to cell number was constructed by seeding cells at a known concentration. The remaining samples were returned to the incubator after media refreshment, and cell numbers were determined on Day 2 and Day 5.

2.4. Statistical Analysis

Mean ± standard deviations are presented. One-factor ANOVA with Bonferroni post-test was performed to determine statistical differences, with $p < 0.05$ considered

significant. Two-factor ANOVA with Bonferroni post-test was used to analyze the biocompatibility data.

3. Results

3.1. SEM Images

Processing parameters were found to have an effect on microsphere properties (Figures 2 and 3). Air-dried microspheres are smaller and spherical compared to freeze-dried microspheres which are larger and somewhat teardrop-shaped. Air-dried 61% DDA beads have a very smooth surface; whereas, some cracks and surface roughness are visible on air-dried 80% beads. Larger scale surface features are visible on both 61% and 80% DDA freeze-dried microspheres. When the amount of hydroxyapatite was increased, the surface of the air-dried 80% DDA beads became considerably rougher. The MES acid wash altered the shape of the beads. The edges of the acid-washed beads appeared rounded due to slight dissolution; interestingly, the surface of these beads was considerably smoother than that of 80% DDA beads which had not undergone the acid wash. For all bead types, porous scaffolds were successfully prepared by fusing microspheres together.

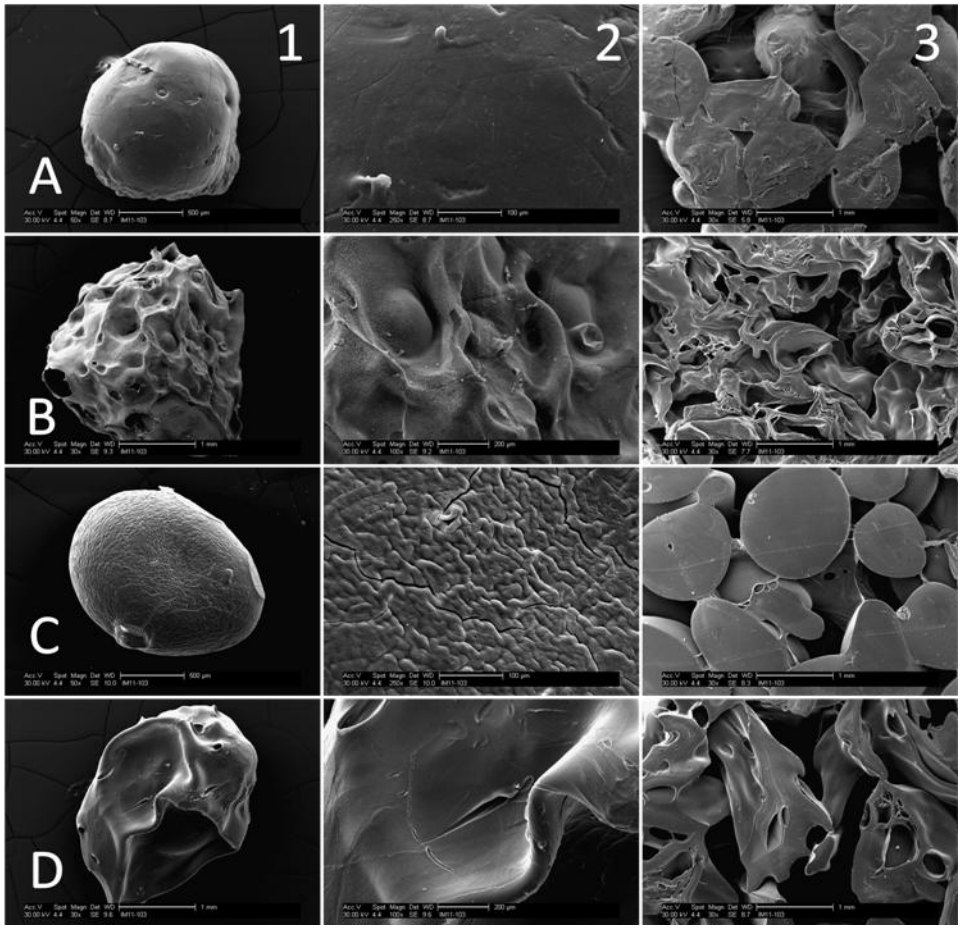

Figure 2. SEM micrographs of air-dried (A/D) and freeze-dried (F/D) 61% and 80% DDA microspheres and scaffolds. **A**: 61% DDA, 3.5% CS, 1x HA, A/D; **B**: 61% DDA, 3.5% CS, 1x HA, F/D; **C**: 80% DDA, 3.0% CS, 1x HA, A/D; **D**: 80% DDA, 3.0% CS, 1x HA, F/D. **1**: Microsphere at low magnification- 50x (A,C) and 30x (B,D); **2**: Microsphere at high magnification- 250x (A,C) and 100x (B,D); **3**- Scaffolds at 30x magnification.

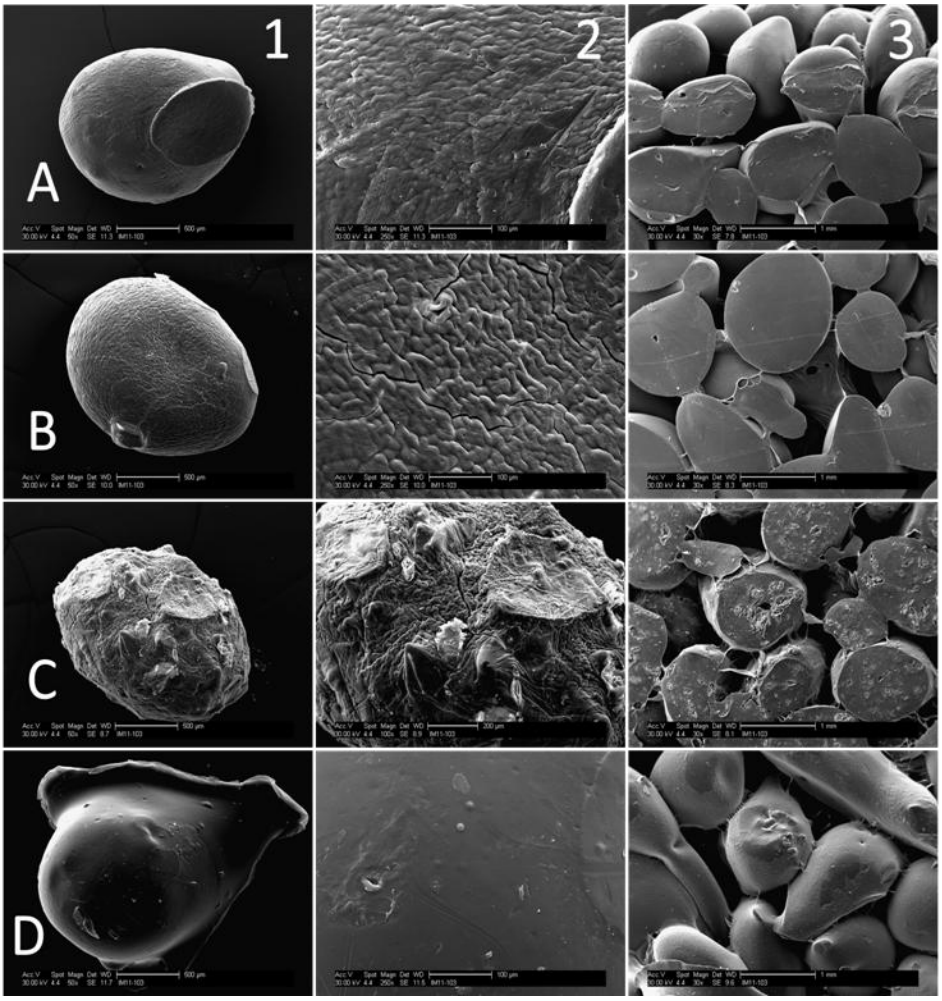

Figure 3. SEM micrographs of air-dried 80% DDA microspheres and scaffolds. **A**: 3.0% CS, No HA; **B**: 3.0% CS, 1x HA; **C**: 2.5% CS, 2x HA; **D**: 3.0% CS, 1x HA, MES acid wash. **1**: Microsphere at low magnification- 50x; **2**: Microsphere at high magnification- 250x (A,B,D) and 100x (C); **3**: Scaffolds at 30x magnification.

3.2. Microsphere Degradation

As seen in Figure 4, 61% DDA microspheres were found to degrade approximately five times faster than 80% DDA microspheres. Freeze-drying minimally increased the degradation of 61% DDA beads ($p < 0.001$) but did not increase the degradation of 80% DDA beads ($p = 0.70$).

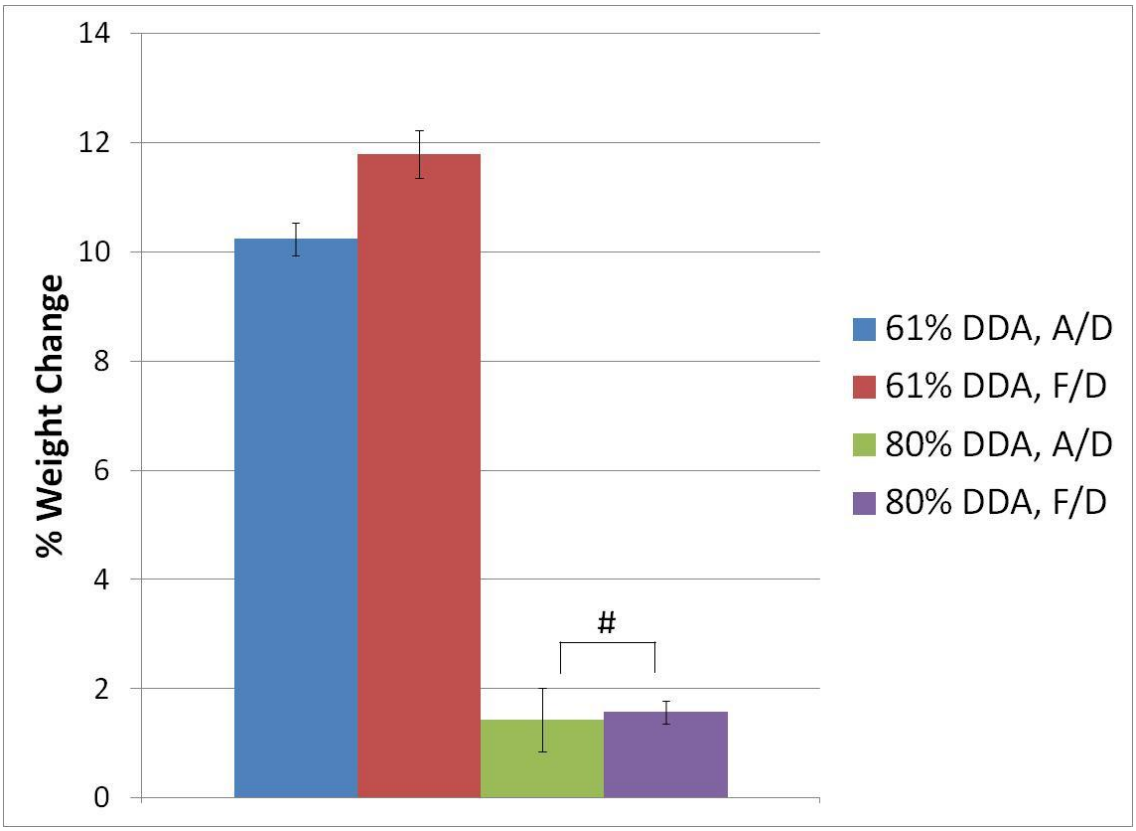

Figure 4. Degradation of 61% DDA and 80% DDA microspheres. 61% DDA microspheres are 3.5% CS, 1x HA. 80% DDA microspheres are 3.0% CS, 1x HA. Statistical differences existed between all groups except 80% DDA air-dried and 80% DDA freeze-dried beads. # represents no statistical difference. N = 3.

3.3. Phase I: Effects of DDA and Drying Method

Overall, the degradation rate of scaffolds was much lower than that of microspheres (Table 3). Freeze-dried 61% DDA scaffolds had the highest degradation with 3.5 ± 0.5% weight change after one month, which was statistically different from all of the other groups ($p < 0.001$). The degradation rates of the other three scaffold groups were statistically similar.

Table 3. Degradation, compression testing, and swelling ratio of composite scaffolds. [a]: Statistically different from all other groups. [b]: Statistically different from all other groups.

Scaffold Type	Degradation (% wt. change) (N = 4)	Compressive Modulus (MPa) (N = 3)	Swelling Ratio (%) (N = 4)
61% DDA, A/D	1.4 ± 0.5	0.67 ± 0.06	148.3 ± 11.7 [b]
61% DDA, F/D	3.5 ± 0.5 [a]	0.12 ± 0.01	267.1 ± 15.3 [b]
80% DDA, A/D	1.3 ± 0.1	3.79 ± 0.51 [a]	88.5 ± 1.9 [b]
80% DDA, F/D	0.8 ± 0.3	0.81 ± 0.14	116.5 ± 6.9 [b]

Scaffolds composed of air-dried 80% DDA microspheres had the largest compressive modulus (Table 3), which was statistically different from all of the other groups ($p < 0.001$). None of the scaffolds fractured during compression testing. The 61% DDA scaffolds had higher swelling ratios than the 80% DDA scaffolds, and freeze-drying increased the swelling ratio (Table 2). Statistical differences in swelling ratio existed between all of the groups.

Both air-dried and freeze-dried 61% and 80% DDA microspheres were found to be biocompatible (Figure 5). Cell numbers increased at each timepoint. The only statistically significant difference between the bead types was between 61% DDA freeze-dried beads and 80% DDA air-dried beads on Day 5 ($p < 0.001$).

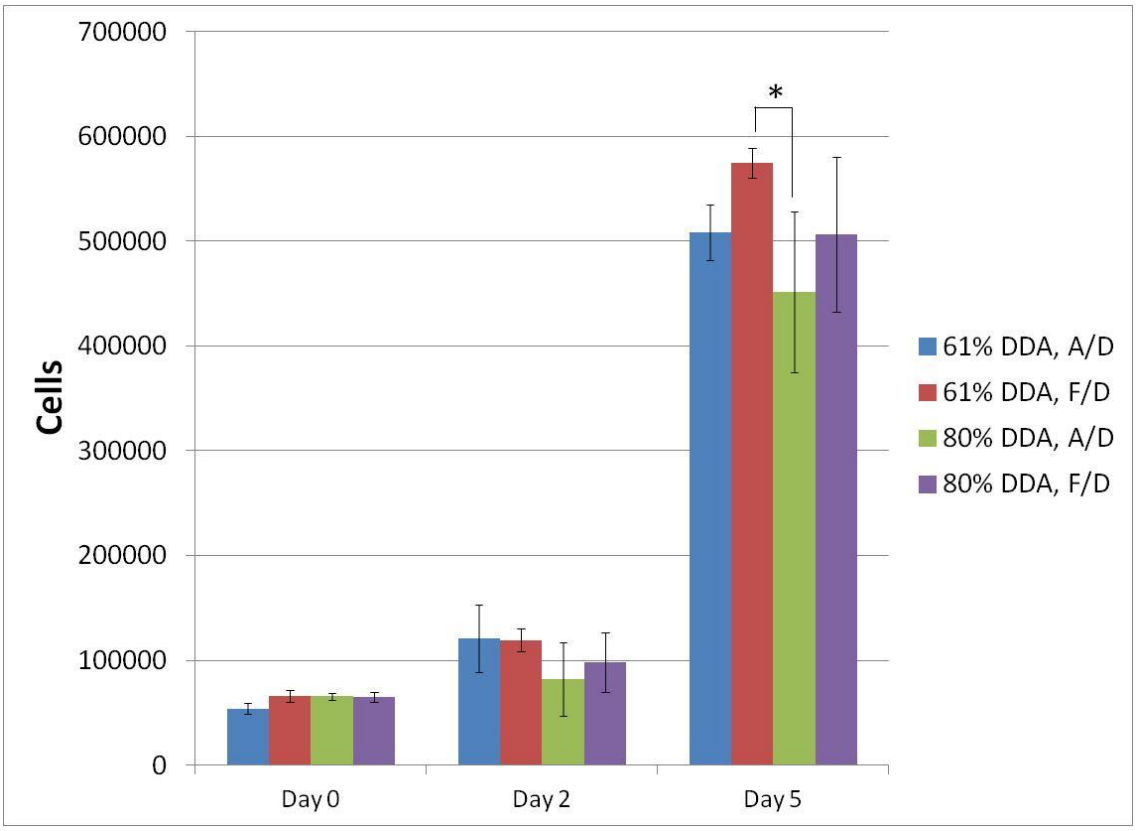

Figure 5. Biocompatibility of composite microspheres using SAOS-2 cells. * represents statistical significance. N = 4.

3.4. Phase II: Effects of Hydroxyapatite Content and MES Acid Wash

Since all of the scaffold groups displayed similar biocompatibility and degradation characteristics in Phase I, compression testing was used to select a candidate for additional studies. Due to their considerably higher compressive modulus of 3.79 ± 0.51 MPa (Table 3), air-dried 80% DDA scaffolds with 3.0% CS, 1x HA were selected as the most promising formulation for further enhancement. In Phase II, the effects of hydroxyapatite content and an MES wash on air-dried 80% DDA scaffolds were determined.

Scaffolds composed of 3.0% CS, 1x HA were found to still have the highest compressive modulus of all groups tested (Figure 6). However, this value was not significantly different from scaffolds prepared with 2.5% CS, 2x HA, which had a value of 3.04 ± 0.58 MPa ($p = 0.535$). A decrease in the compressive modulus to 1.57 ± 0.32 MPa was observed in the scaffolds prepared without hydroxyapatite ($p<0.001$). The compressive moduli of 3.0% CS, 1x HA scaffolds which had undergone the mild acid wash was significantly reduced to 1.76 ± 0.35 MPa ($p < 0.001$).

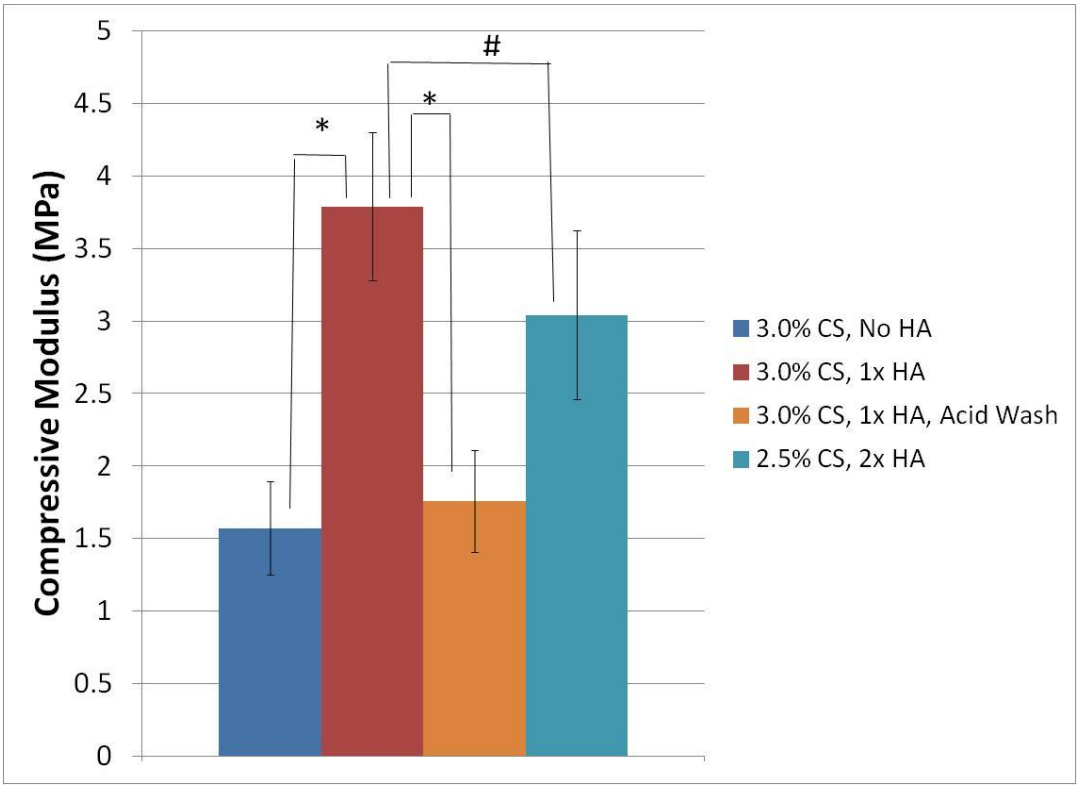

Figure 6. Compressive moduli of air-dried 80% DDA scaffolds. Scaffolds were compressed at a strain rate of 0.1 min-1 until 50% strain was achieved. None of the scaffolds fractured during testing. The compressive moduli were calculated from the initial linear portion of the stress-strain curve. * represents statistical significance. # represents no statistical difference. N = 3.

Scaffolds undergoing the acid wash were found to have a degradation of 4.4 ± 0.4% after one month (Table 4), which was significantly higher than all of the other groups ($p < 0.001$). The acid wash increased the swelling ratio of the scaffolds. Increasing the hydroxyapatite content was found to decrease the swelling ratio.

Table 4. Degradation and swelling ratio of 80% DDA scaffolds. [a]: statistically different from all other groups. [b]: statistically different from all other groups.

Scaffold Type	Degradation (% wt. change) (N = 4)	Swelling Ratio (%) (N = 4)
3.0% CS, No HA	−0.3 ± 0.4 [a]	159.1 ± 1.9 [b]
3.0% CS, 1x HA	1.3 ± 0.1	88.5 ± 1.9 [b]
2.5% CS, 2x HA	1.7 ± 0.2	66.1 ± 0.9 [b]
3.0% CS, 1x HA, Acid Wash	4.4 ± 0.4 [a]	180.4 ± 3.3 [b]

All of the 80% DDA microsphere variations were found to be biocompatible (Figure 7). No differences in attachment were found on Day 0. On Day 2, all of the groups had statistically similar number of cells compared to Day 0, except for the No HA group which had significantly more cells ($p = 0.009$). The No HA group had significantly more cells than the 2x HA group ($p = 0.001$) and acid wash group ($p = 0.010$) on Day 2. By Day 5, cell numbers had increased for all bead types compared to previous timepoints. The No HA group had the most cells compared to the other groups, and the other three groups were not statistically different.

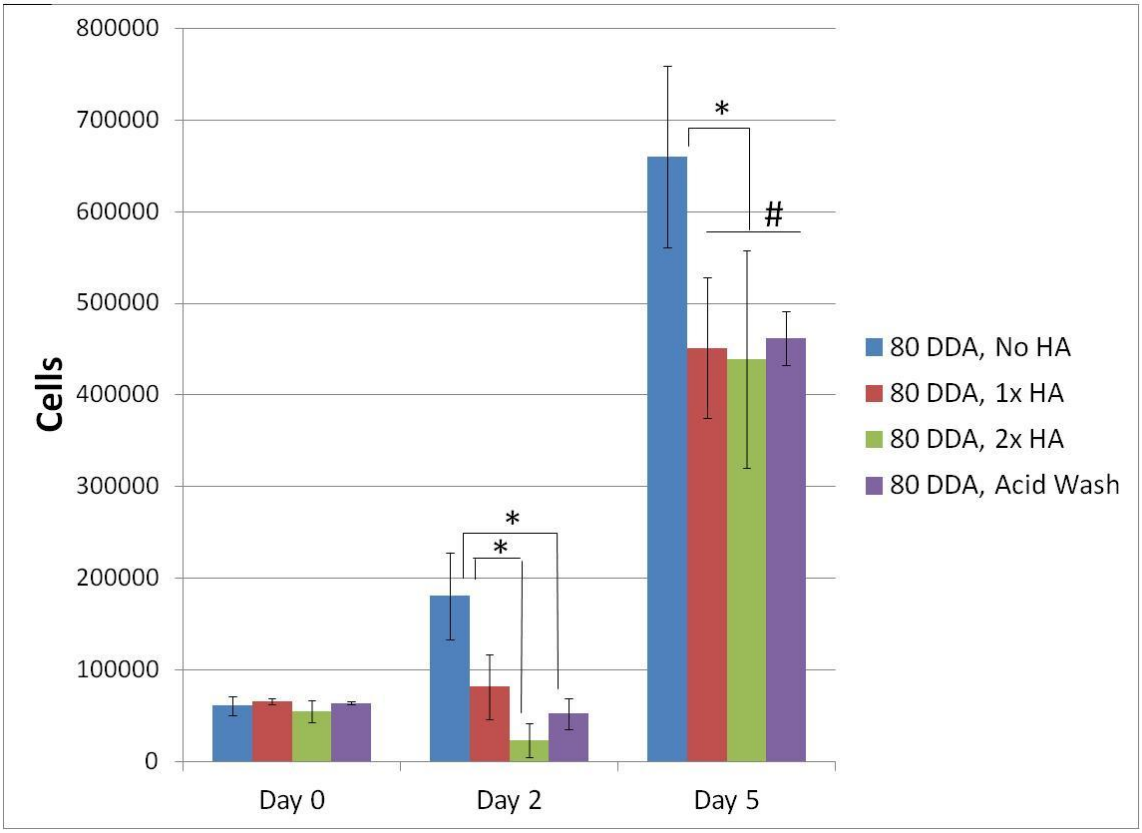

Figure 7. Biocompatibility of 80% DDA microspheres using SAOS-2 cells. * represents statistical significance. # represents no statistical difference. N = 4.

4. Discussion

Composite chitosan-nano-hydroxyapatite microspheres were successfully prepared using a co-precipitation method. SEM analysis revealed that fabrication parameters had an effect on bead characteristics including size, shape, and surface roughness. In addition, porous composite scaffolds composed of fused microspheres were successfully fabricated. The degradation, mechanical, biocompatibility, and swelling ratio properties of the modified microspheres and scaffolds were evaluated to determine the best formulation for bone regeneration.

4.1. Phase I: Effects of DDA and Drying Method

Interestingly, the concentration of chitosan that can be used to fabricate beads successfully is within a narrow range. When the chitosan solution is dripped into the precipitating solution, the chitosan solution cannot be too thick or too thin. If the chitosan solution is too thick, long strands or very teardrop-shaped beads instead of spherical microparticles will precipitate. In contrast, if the chitosan solution is too thin, small fragments of chitosan will precipitate instead of microspheres. In these studies, 61% DDA beads could only be prepared using a 3.5% chitosan solution due to the reasons discussed above. When 80% DDA beads were prepared, a 3.5% chitosan solution produced very elongated particles. However, spherical 80% DDA beads could be fabricated when 3.0% and 2.5% chitosan solutions were used.

The increased degradation of 61% DDA microspheres compared to 80% DDA microspheres was expected. Chitosan films, beads, and sponges have been shown to degrade faster when prepared with lower DDA [24, 27-30]. Lim *et al.* observed the weight half-lives of 52.6%, 56.1%, and 62.4% DDA chitosan beads to be 9.8, 27.3, and 56 days compared to weight half-lives of over 84 days for 71.7, 81.7, and 93.5% DDA beads [29]. The fabrication method for preparation of these beads was not disclosed. There is some debate about why high DDA chitosan degrades more slowly. Some researchers have suggested that the crystalline nature of high DDA chitosan prevents lysozyme from easily accessing the glycosidic bonds between the polymer chains, resulting in slower degradation [19, 25]. Others researchers have suggested that the binding site of lysozyme requires a certain number of acetylated residues to be present for lysozyme to be able to degrade chitosan [28, 30].

Since freeze-drying was previously shown to increase the surface area of microspheres over 200× [15] and freeze-drying increased the swelling ratio, it is somewhat surprising that freeze-drying only increased the degradation of 61% DDA beads by less than two percent. Furthermore, scaffolds were observed to degrade more slowly than microspheres. The freeze-dried 61% DDA scaffolds degraded the fastest but only exhibited 3.5 ± 0.5% weight change over one month. Presumably, these differences in degradation between beads and scaffolds are a surface area issue.

Mechanical properties are an important consideration for bone regeneration constructs, and air-dried 80% DDA scaffolds were found to have the highest compressive modulus. This is most likely due to their higher crystallinity and lower swelling ratio. It should be noted that even though the 61% DDA scaffolds were rehydrated for only four hours, they had lower compressive moduli than the 80% DDA scaffolds which had been rehydrated for eight hours. Other researchers have also observed increased compressive strength and modulus when using higher DDAs [26, 27]. The 3.79 ± 0.51 MPa compressive moduli of the air-dried 80% DDA scaffolds is considerably higher than the approximately 10 kPa or less moduli reported for many chitosan scaffold preparations [10, 35, 36]. Furthermore, air-dried 80% DDA scaffolds had the best handleability. Handleability refers to the ease with which we believe a surgeon could grab, manipulate, and place the scaffold into a bone defect. For these reasons, we felt that air-dried 80% DDA scaffolds held the most promise as bone tissue scaffolds of the formulations tested, and the next phase of the investigation focused on further improving the air-dried 80% DDA scaffolds.

4.2. Phase II: Effects of Hydroxyapatite Content and MES Acid Wash

Other researchers have also observed that the addition of nano-hydroxyapatite decreases the swelling ratio [10, 37] and increases the compressive moduli and strength of chitosan scaffolds [10, 38]. However, addition of too much hydroxyapatite may have negative effects. In the current study, the compressive modulus of air-dried 80% DDA scaffolds with 3.0% CS, 1x HA (3.79 ± 0.51 MPa) was higher than that of both 3.0% CS, No HA (1.57 ± 0.32 MPa) and 3.0% CS, 2x HA (2.51 ± 0.16 MPa, data not shown) scaffolds. Similar to our results, Zhang *et al.* observed that increasing the hydroxyapatite content of chitosan-nano-hydroxyapatite scaffolds improved compressive strength to a point, but further increases in hydroxyapatite content decreased the compressive strength [38]. In addition to altering structure at a molecular level, too much hydroxyapatite may prevent the beads from being able to be fused together as soundly, resulting in poorer mechanical properties. In fact, beads containing 4x HA could not even be fused together into scaffolds (data not shown). Somewhat surprisingly, the compressive modulus of scaffolds made with 2.5% CS, 2x HA beads was not significantly different from that of 3.0% CS, 1x HA. For this reason, air-dried 80% DDA scaffolds were prepared with 2.5% CS, 2x HA instead of 3.0% CS, 2x HA during Phase II of the experiments.

In this study, plain 80% DDA microspheres without hydroxyapatite promoted increased proliferation of SAOS-2 cells compared to composite microspheres with hydroxyapatite. This result was unexpected, since we previously observed greater cell proliferation on composite scaffolds compared to plain scaffolds [13, 14]. These previous investigations were performed using human fetal osteoblast cells and human embryonic

palatal mesenchymal stem cells. The SAOS-2 cells used in the current study may respond differently to hydroxyapatite than the other cell types.

The MES acid wash was found to increase degradation of air-dried 80% DDA scaffolds to 4.4 ± 0.4%. During the acid wash, the beads appeared to shrink slightly and felt slightly "sticky"- suggesting mild dissolution. The degradation rate of acid-washed scaffolds could potentially be increased even further by using a lower pH or increasing the wash time. When compared to freeze-dried 61% DDA scaffolds, the 80% DDA acid-washed scaffolds had both higher degradation and compressive modulus.

Depending on the intended application, the properties of the chitosan-nano-hydroxyapatite microspheres can be altered by changing the fabrication parameters as demonstrated in this research. For application in bone tissue engineering, using a combination of bead types to prepare scaffolds may be a promising approach. A combination of fast-degrading 61% DDA freeze-dried beads or acid-washed beads could be used in conjunction with slower-degrading but mechanically stronger 80% air-dried beads. The fast-degrading beads could deliver a growth factor such as BMP-2 and then degrade, increasing the available space for tissue ingrowth. The slower-degrading beads would provide mechanical stability at the fracture site until new bone had developed and then be resorbed more slowly. The ratio of beads types could be altered to give an optimized scaffold for an intended musculoskeletal application.

5. Conclusions

Microspheres with 61% DDA had over 10% degradation after one month compared to less than 2% for 80% DDA microspheres, and freeze-drying minimally increased the degradation of 61% DDA microspheres. Scaffold degradation was found to

be lower than microsphere degradation. The 3.8 ± 0.5 MPa compressive modulus of air-dried 80% DDA scaffolds made them good potential candidates for bone regeneration. Increases in hydroxyapatite content did not increase the compressive modulus of the 80% air-dried scaffolds. A brief acid wash in an MES solution increased the degradation of air-dried 80% DDA scaffolds. All of the composite microspheres tested demonstrated good biocompatibility with SAOS-2 osteoblast-like cells. This study demonstrated the ability to modify the functional properties of composite chitosan-nano-hydroxyapatite scaffolds by altering the DDA, drying method, hydroxyapatite content, and using an MES wash.

References

1. Dawson, J. I.; Oreffo, R. O., Bridging the regeneration gap: stem cells, biomaterials and clinical translation in bone tissue engineering. *Arch Biochem Biophys* **2008,** *473*, 124-131.

2. Schmidmaier, G.; Schwabe, P.; Strobel, C.; Wildemann, B., Carrier systems and application of growth factors in orthopaedics. *Injury* **2008,** *39 Suppl 2*, S37-43.

3. Griffin, M.; Iqbal, S. A.; Bayat, A., Exploring the application of mesenchymal stem cells in bone repair and regeneration. *J Bone Joint Surg Br* **2011,** *93*, 427-434.

4. Khan, Y.; Yaszemski, M. J.; Mikos, A. G.; Laurencin, C. T., Tissue engineering of bone: material and matrix considerations. *J Bone Joint Surg Am* **2008,** *90 Suppl 1*, 36-42.

5. Kretlow, J. D.; Mikos, A. G., Review: mineralization of synthetic polymer scaffolds for bone tissue engineering. *Tissue Eng* **2007,** *13*, 927-938.

6. Nandi, S. K.; Roy, S.; Mukherjee, P.; Kundu, B.; De, D. K.; Basu, D., Orthopaedic applications of bone graft & graft substitutes: a review. *Indian J Med Res* **2010,** *132*, 15-30.

7. Karageorgiou, V.; Kaplan, D., Porosity of 3D biomaterial scaffolds and osteogenesis. *Biomaterials* **2005,** *26*, 5474-5491.

8. Logeart-Avramoglou, D.; Anagnostou, F.; Bizios, R.; Petite, H., Engineering bone: challenges and obstacles. *J Cell Mol Med* **2005,** *9*, 72-84.

9. Muzzarelli, C.; Muzzarelli, R. A., Natural and artificial chitosan-inorganic composites. *J Inorg Biochem* **2002,** *92*, 89-94.

10. Thein-Han, W. W.; Misra, R. D., Biomimetic chitosan-nanohydroxyapatite composite scaffolds for bone tissue engineering. *Acta Biomater* **2009,** *5*, 1182-1197.

11. Kempen, D. H.; Creemers, L. B.; Alblas, J.; Lu, L.; Verbout, A. J.; Yaszemski, M. J.; Dhert, W. J., Growth factor interactions in bone regeneration. *Tissue Eng Part B Rev* **2010,** *16*, 551-566.

12. Lieberman, J. R.; Daluiski, A.; Einhorn, T. A., The role of growth factors in the repair of bone. Biology and clinical applications. *J Bone Joint Surg Am* **2002,** *84-A*, 1032-1044.

13. Chesnutt, B. M.; Viano, A. M.; Yuan, Y.; Yang, Y.; Guda, T.; Appleford, M. R.; Ong, J. L.; Haggard, W. O.; Bumgardner, J. D., Design and characterization of a novel chitosan/nanocrystalline calcium phosphate composite scaffold for bone regeneration. *J Biomed Mater Res A* **2009,** *88*, 491-502.

14. Chesnutt, B. M.; Yuan, Y.; Buddington, K.; Haggard, W. O.; Bumgardner, J. D., Composite chitosan/nano-hydroxyapatite scaffolds induce osteocalcin production by osteoblasts in vitro and support bone formation in vivo. *Tissue Eng Part A* **2009,** *15*, 2571-2579.

15. Reves, B. T.; Bumgardner, J. D.; Cole, J. A.; Yang, Y.; Haggard, W. O., Lyophilization to improve drug delivery for chitosan-calcium phosphate bone scaffold construct: a preliminary investigation. *J Biomed Mater Res B Appl Biomater* **2009,** *90*, 1-10.

16. Di Martino, A.; Sittinger, M.; Risbud, M. V., Chitosan: A versatile biopolymer for orthopaedic tissue-engineering. *Biomaterials* **2005,** *26*, 5983-5990.

17. Kim, I. Y.; Seo, S. J.; Moon, H. S.; Yoo, M. K.; Park, I. Y.; Kim, B. C.; Cho, C. S., Chitosan and its derivatives for tissue engineering applications. *Biotechnol Adv* **2008,** *26*, 1-21.

18. Jayakumar, R.; Prabaharan, M.; Nair, S. V.; Tamura, H., Novel chitin and chitosan nanofibers in biomedical applications. *Biotechnol Adv* **2010,** *28*, 142-150.

19. Shi, C.; Zhu, Y.; Ran, X.; Wang, M.; Su, Y.; Cheng, T., Therapeutic potential of chitosan and its derivatives in regenerative medicine. *J Surg Res* **2006,** *133*, 185-192.

20. Venkatesan, J.; Kim, S. K., Chitosan composites for bone tissue engineering--an overview. *Mar Drugs* **2010,** *8*, 2252-2266.

21. Coelho, P. G.; Freire, J. N.; Granato, R.; Marin, C.; Bonfante, E. A.; Gil, J. N.; Chuang, S. K.; Suzuki, M., Bone mineral apposition rates at early implantation times around differently prepared titanium surfaces: a study in beagle dogs. *Int J Oral Maxillofac Implants* **2011,** *26*, 63-69.

22. Hermida, J. C.; Bergula, A.; Dimaano, F.; Hawkins, M.; Colwell, C. W., Jr.; D'Lima, D. D., An in vivo evaluation of bone response to three implant surfaces using a rabbit intramedullary rod model. *J Orthop Surg Res* **2010,** *5*, 57.

23. Thian, E. S.; Huang, J.; Ahmad, Z.; Edirisinghe, M. J.; Jayasinghe, S. N.; Ireland, D. C.; Brooks, R. A.; Rushton, N.; Best, S. M.; Bonfield, W., Influence of nanohydroxyapatite patterns deposited by electrohydrodynamic spraying on osteoblast response. *J Biomed Mater Res A* **2008,** *85*, 188-194.

24. Bagheri-Khoulenjani, S.; Taghizadeh, S. M.; Mirzadeh, H., An investigation on the short-term biodegradability of chitosan with various molecular weights and degrees of deacetylation. *Carbohydrate Polymers* **2009,** *78*, 773-778.

25. Madihally, S. V.; Matthew, H. W., Porous chitosan scaffolds for tissue engineering. *Biomaterials* **1999,** *20*, 1133-1142.

26. Seda Tigli, R.; Karakecili, A.; Gumusderelioglu, M., In vitro characterization of chitosan scaffolds: influence of composition and deacetylation degree. *J Mater Sci Mater Med* **2007,** *18*, 1665-1674.

27. Thein-Han, W. W.; Kitiyanant, Y., Chitosan scaffolds for in vitro buffalo embryonic stem-like cell culture: an approach to tissue engineering. *J Biomed Mater Res B Appl Biomater* **2007,** *80*, 92-101.

28. Lim, S. M.; Song, D. K.; Oh, S. H.; Lee-Yoon, D. S.; Bae, E. H.; Lee, J. H., In vitro and in vivo degradation behavior of acetylated chitosan porous beads. *J Biomater Sci Polym Ed* **2008,** *19*, 453-466.

29. Ren, D.; Yi, H.; Wang, W.; Ma, X., The enzymatic degradation and swelling properties of chitosan matrices with different degrees of N-acetylation. *Carbohydr Res* **2005,** *340*, 2403-2410.

30. Tomihata, K.; Ikada, Y., In vitro and in vivo degradation of films of chitin and its deacetylated derivatives. *Biomaterials* **1997,** *18*, 567-575.

31. Liu, W. G.; Sun, S. J.; Cao, Z. Q.; Xin, Z.; Yao, K. D.; Lu, W. W.; Luk, K. D. K., An investigation on the physicochemical properties of chitosan/DNA polyelectrolyte complexes. *Biomaterials* **2005,** *26*, 2705-2711.

32. Jiang, T.; Kumbar, S. G.; Nair, L. S.; Laurencin, C. T., Biologically active chitosan systems for tissue engineering and regenerative medicine. *Curr Top Med Chem* **2008,** *8*, 354-364.

33. Jones, A. C.; Arns, C. H.; Hutmacher, D. W.; Milthorpe, B. K.; Sheppard, A. P.; Knackstedt, M. A., The correlation of pore morphology, interconnectivity and physical properties of 3D ceramic scaffolds with bone ingrowth. *Biomaterials* **2009,** *30,* 1440-1451.

34. Varum, K. M.; Myhr, M. M.; Hjerde, R. J.; Smidsrod, O., In vitro degradation rates of partially N-acetylated chitosans in human serum. *Carbohydr Res* **1997,** *299,* 99-101.

35. Huang, Y.; Onyeri, S.; Siewe, M.; Moshfeghian, A.; Madihally, S. V., In vitro characterization of chitosan-gelatin scaffolds for tissue engineering. *Biomaterials* **2005,** *26,* 7616-7627.

36. Tangsadthakun, C.; Kanokpanont, S.; Sanchavanakit, N.; Pichyangkura, R.; Banaprasert, T.; Tabata, Y.; Damrongsakkul, S., The influence of molecular weight of chitosan on the physical and biological properties of collagen/chitosan scaffolds. *J Biomater Sci Polym Ed* **2007,** *18,* 147-163.

37. Peter, M.; Ganesh, N.; Selvamurugan, N.; Nair, S. V.; Furuike, T.; Tamura, H.; Jayakumar, R., Preparation and characterization of chitosan-gelatin/nanohydroxyapatite composite scaffolds for tissue engineering applications. *Carbohydrate Polymers* **2010,** *80,* 687-694.

38. Li, Z.; Yubao, L.; Aiping, Y.; Xuelin, P.; Xuejiang, W.; Xiang, Z., Preparation and in vitro investigation of chitosan/nano-hydroxyapatite composite used as bone substitute materials. *J Mater Sci Mater Med* **2005,** *16,* 213-219.

Chapter 4 Fabrication of Crosslinked Carboxymethylchitosan Microspheres and Their Incorporation Into Composite Scaffolds for Enhanced Bone Regeneration

INTRODUCTION

Although bone has a tremendous capacity to heal itself, approximately five to ten percent of bone fractures will result in delayed healing or non-union.[1] Bone grafting procedures are commonly used to treat these fractures, but both autograft and allografts are associated with a number of drawbacks.[2-5] For this reason, our laboratories have developed chitosan microspheres and scaffolds to augment fracture healing.[6-9] The microspheres are prepared using a precipitation method and are then adhered together into scaffolds using an acid wash. These scaffolds are designed to provide a matrix to which osteoblasts can attach and proliferate. Initially, the scaffolds will provide some mechanical stability to the fracture site. As new bone is formed, ideally the scaffolds will degrade to allow complete regeneration.[10-12] These bone scaffolds can also be used as local drug delivery vehicles to release growth factors such as bone morphogenetic protein-2 (BMP-2) that will aid in the healing process.[8,13-15]

Our scaffolds have demonstrated potential in augmenting fracture healing. However, the scaffolds have shown slow in vitro and in vivo degradation rates.[6,7,9] If the scaffolds do not degrade in a timely manner, new bone cannot fill the defect site and bone regeneration will be impaired.[16,17] We believe that our chitosan microbead scaffolds can be improved by increasing the degradation rate of the constructs. Similar to many other local BMP-2 delivery systems, our microspheres and scaffolds have previously demonstrated a significant burst release of BMP-2 in which much of the growth factor is released within the first few days.[8] BMP-2 is involved in all stages of bone healing and promotes recruitment of mesenchymal stem cells (MSCs) to the fracture site,

angiogenesis, and differentiation of MSCs into osteoblasts.[14,18-21] Recent studies have demonstrated that an extended elution of BMP-2 is more effective at augmenting fracture healing compared to a large burst effect alone.[22-24]

Chitosan is a versatile carbohydrate co-polymer of glucosamine and N-acetyl-D-glucosamine containing hydroxyl and amine groups that allow for numerous modification strategies.[25-27] One such strategy is the carboxymethylation of chitosan using monochloroacetic acid.[28-31] Carboxymethylchitosan (CMCS) is water-soluble and can be crosslinked to form hydrogels. CMCS-based biomaterials crosslinked using 1-ethyl-3-(3-dimethylaminopropyl) carbodiimide (EDC) have demonstrated extensive degradation capacity and good biocompatibility.[29-35] EDC is a zero-length crosslinker that forms amide bonds between carboxyl and amine groups.[36-39] The natural crosslinker genipin, which is derived from the Gardenia plant, has received attention recently due to its very good biocompatibility compared to synthetic crosslinkers such as glutaraldehyde.[40-42] Genipin is an amine-amine crosslinker, and genipin-crosslinked CMCS hydrogels have also demonstrated potential use in biomedical applications.[41,43-45] Most research using EDC and genipin to prepare CMCS hydrogels has been performed in solution or on highly porous constructs. Little research has been conducted on the feasibility of using these chemicals to crosslink dense CMCS beads.

In addition to improved degradation, CMCS beads may also have improved BMP-2 elution properties. The isoelectric point of BMP-2 is approximately 9.0, meaning that BMP-2 will have a net-positive charge at neutral pH.[46-48] The addition of a negatively-charged carboxyl group to chitosan may promote interaction between BMP-2 and the material resulting in a more extended elution. The objective of these experiments is to

fabricate EDC- and genipin-crosslinked CMCS microspheres and incorporate them into our chitosan scaffolds. We hypothesize that the addition of CMCS beads to our scaffolds will result in scaffolds with increased degradation and enhanced BMP-2 elution.

MATERIALS AND METHODS

Chitosan Microsphere Fabrication

Chitosan-nano-hydroxyapatite microspheres were prepared using a co-precipitation method as previously described.[7,8] A solution containing 7.00g of 61% DDA chitosan (Primex, Siglufjordur, Iceland), 0.10M $CaCl_2$, and 0.06M NaH_2PO_4 (Ca:P ratio = 1.67) was prepared in 200mL of 2 volume percent (vol. %) acetic acid. Using a syringe pump, the chitosan solution was added dropwise through 16G needles into a precipitation solution (pH=13) containing 20 weight percent (wt. %) sodium hydroxide (NaOH), 30 wt. % methanol, and 50 wt. % water (H_2O). Microspheres immediately formed and were allowed to wash in the precipitation solution for 24 hours to allow crystalline hydroxyapatite to form. The microspheres were then washed a few times with deionized (DI) water and stored in DI H_2O until carboxymethylation.

Carboxymethylation of Chitosan Microspheres

The chitosan microspheres were carboxymethylated using monochloroacetic acid based on methods described by Chen and Park.[28] A full batch of microspheres was added to 200mL of an 80:20 isopropyl alcohol/water (IPA/H_2O) mixture containing 30.00g of sodium hydroxide. An amount of 30.00g of monochloroacetic acid (Fisher Scientific) was dissolved in 40mL of isopropyl alcohol. After the beads had stirred for ten minutes in the IPA/H_2O mixture, the monochloroacetic acid solution was added dropwise. The beads were stirred briskly and the reaction was allowed to proceed at 40^{o} C. After four hours,

the reaction was stopped by adding 400 mL of 70% ethanol (EtOH). The beads were then washed in 70% EtOH and 95% EtOH. The carboxymethylchitosan (CMCS) beads were dried overnight in a vacuum oven at 50^{o}C.

Crosslinking of Carboxymethylchitosan Beads

Crosslinking was performed using carbodiimide chemistry to form amide bonds between the amine and carboxyl groups of the CMCS beads.[30] A solution containing 100mM 2-(N-morpholino)ethanesulfonic acid (MES), 20mM 1-ethyl-3-(3-dimethylaminopropyl) carbodiimide (EDC; Thermo Scientific Prod. # 22980), and 50mM N-hydroxysuccinimide (NHS; Thermo Scientific Prod. # 24500) was prepared in 300mL of DI H_2O. A full batch of CMCS beads was then added. The pH was adjusted to 6.5 using 1.0M hydrochloric acid (HCl). The beads were covered and the reaction proceeded at room temperature. After 90 minutes, the beads were removed from the EDC/NHS solution and were washed extensively with DI H_2O followed by 70% EtOH. The microspheres were then dried in a convection oven at 35^{o}C. These beads will be referred to as X-CMCS microspheres.

Crosslinking was also performed using the natural crosslinker genipin. A mixture containing 300mL DI H_20 and 50mL EtOH was prepared. An amount of 50mM MES and 5.7mM genipin (Wako Prod. #078-03021) were dissolved in the mixture. After waiting a few minutes to allow dissolution of the genipin, a full batch of CMCS beads was added. The pH was adjusted to and maintained at pH 7.4 using 6.0M HCl. The reaction was allowed to proceed at room temperature for 8 hours. The beads were then removed from the crosslinking solution and were washed extensively with DI H_2O. The microspheres

were then dried in a convection oven at 35^{o}C. These beads will be referred to as Gen-X CMCS microspheres.

Microsphere Characterization

ATR-FTIR

Fourier transform infrared analysis was performed using a Nicolet iZ10 spectroscope (Thermo Scientific) with attenuated total reflectance. Powders of raw 61% DDA chitosan flakes, 61% DDA chitosan microspheres, and uncrosslinked CMCS beads were obtained by cooling the samples in liquid nitrogen followed by grinding with a mortar and pestle. Transmission spectra were recorded in the range of 4000-500 cm^{-1} using thirty-two scans with 4 cm^{-1} resolution.

Ninhydrin Assay

Crosslinking was verified by determining the number of free amine groups in the microspheres using a ninhydrin assay.[49] A solution containing 1.15g of citric acid monohydrate and 40.0mg of stannous chloride dihydrate in 15mL of DI H_2O and 10mL of 1.0M NaOH was prepared (Solution A). A solution containing 1.00g of ninhydrin (Acros Organics) in 25mL of ethylene glycol monomethyl ether was also prepared (Solution B). Solutions A and B were mixed together and stirred for 45 minutes covered by aluminum foil to protect from light. Approximately, 5 mg of microspheres (n=4) were weighed and placed in Pyrex test tubes containing 100µL of DI H_2O. Standards containing 5, 4, 3, 2, 1, and 0 µmole/mL glycine were prepared in DI H_2O with a total volume of 100µL. An amount of 1mL of ninhydrin solution was added to all samples. The samples were placed in a water bath at 100^{o}C and monitored for development of purple color. After eight minutes, the samples were removed from the water bath and

5mL of 50% IPA was added to each sample. The samples were transferred to a 96-well plate after being vortexed, and the absorbance of 100uL of each sample was read in triplicate at 570nm.

Swelling Ratio

The swelling ratio of microspheres (n=3) was determined by placing pre-weighed microspheres in 3mL of 1x phosphate buffered saline (PBS) in 12-well plates. The samples were covered and placed in an incubator at 37^{o}C. After 24 hours, the samples were pat-dried to remove excess PBS and re-weighed. The swelling ratio of the microspheres was determined by the following:

(Final weight – initial weight) / (Initial weight) * 100%.

Degradation

The degradation profile of microspheres was determined in 1x PBS and lysozyme. Lysozyme is the main enzyme responsible for chitosan degradation in vivo.[50,51] Pre-weighed microspheres (n=4) were placed in 4mL of 1x PBS containing antibiotics/antimycotic (AB/AM; 1 unit/mL penicillin, 1μg/mL streptomycin, and 0.25μg/mL amphotericin B; MP Biomedicals Cat. No. 1674049) or 1x PBS containing AB/AM and 100μg/mL lysozyme (MP Biomedicals, Cat. # 100834). Samples were incubated at 37^{o}C, and the degradation solutions were refreshed every three days. After fifteen days or thirty days, the microspheres were removed from the degradation solution, dried, and re-weighed. The percent weight change was determined using the following equation:

(Initial weight – final weight) / (Initial weight) * 100%.

rhBMP-2 Elution

Approximately, 200 mg of beads (n=4) were weighed and placed in small glass scintillation vials. The beads were loaded overnight at room temperature with 4mL of a 5μg/mL rhBMP-2 (Medtronic, Inc.) solution in 1xPBS. On the following day, the BMP-2 loading solution was aspirated and 4mL of elution buffer (1x PBS containing AB/AM and 0.01% bovine serum albumin (BSA)) was added to each vial. Elution samples were obtained on days 1, 3, 6, 10, 15, 21, 28, 36, and 45 by removing a 1mL eluate. The remaining solution was aspirated, and 4mL of fresh elution buffer was added at each timepoint. Elution samples were stored in low retention microcentrifuge tubes at -80^{o}C. The amount of rhBMP-2 eluted was determined using an ELISA kit (PeproTech, Inc.) according to the manufacturer's instructions.

Scaffold Fabrication

Composite scaffolds containing crosslinked CMCS beads and 80% DDA chitosan (CS) beads were prepared. Firstly, 80% DDA microspheres were fabricated as previously described by dissolving 6.00g of chitosan in 200mL of 2 vol. % acetic acid. Following precipitation in the basic solution, the beads were washed in DI H_2O until the pH was less than 8.0. The 80% DDA CS beads were then allowed to air-dry at room temperature.

Porous scaffolds were prepared by fusing dried microspheres together. The microspheres were rinsed in 1 vol. % acetic acid for approximately ten seconds in a porcelain Buchner funnel (CoorsTek Prod. # 60243). Excess acid was removed using a vacuum. The microspheres were placed in 12mm diameter polystyrene tubes. After approximately one minute, the scaffolds were removed from the molds and allowed to

air-dry. When rehydrated, scaffolds can be cut to any height as desired using a razor blade.

The following three groups were prepared: 80% DDA CS-only scaffolds, composite X-CMCS/CS scaffolds, and composite Gen-X CMCS/CS scaffolds. The composite scaffolds contained a ratio of approximately 2:1 CS to CMCS beads. Before performing the acid wash, lines were drawn on the polystyrene tubes at 15mm and 45mm from the bottom of the tubes. CMCS beads were added to the first line, and 80% DDA CS beads were added until the second line was reached. The beads were then placed in the Buchner funnel for the acid wash.

Scaffold Characterization

Scaffold Compression, Degradation, and BMP-2 Elution

Compression testing of hydrated scaffolds (n=3) was performed as previously reported.[52] Scaffold degradation (n=4) was determined in 6mL of 100μg/mL lysozyme solution at thirty days in the same manner as microsphere degradation. The elution of rhBMP-2 from the scaffolds (n=4) was also determined in a manner similar to bead elution. The scaffolds were loaded with 6mL of 5μg/mL rhBMP-2 solution, and the rhBMP-2 was eluted into a volume of 6mL. As before, rhBMP-2 eluate concentrations were determined using ELISAs.

rhBMP-2 Activity Determination

In order to determine the bioactivity of the rhBMP-2 eluted from the scaffolds, an additional 1mL eluate was obtained at each timepoint. The activity of the released rhBMP-2 was determined by alkaline phosphatase (ALP) induction in W20-17 mouse stromal cells (ATCC® Number CRL-2623™) based on ASTM standard F2131.[53] In a 96-

well plate, 200µL of $5x10^4$ cells/mL suspension in complete media (Thermo Scientific HyClone® DMEM/High Glucose media containing 10% standard fetal bovine serum (FBS; Thermo Scientific HyClone®) and AB/AM) was added to each well. The cells were allowed to attach overnight in an incubator at 37°C with 5% CO_2 and 100% humidity. On the following day, the complete media was aspirated from the wells, and the wells were washed with 1x PBS. An amount of 180µL of fresh media without FBS and 20µL of rhBMP-2 sample were added to each well. Sample dilutions were prepared in elution buffer as needed. A standard curve was prepared by adding 20µL of the following rhBMP-2 solutions (in elution buffer) to 180µL of fresh media: 10000, 5000, 2500, 1250, 625, 313, 156, 78, 39, 20 and 0ng/mL. The plates were returned to the incubator.

After 24 hours, the amount of ALP produced by the cells was determined. Media was aspirated from the wells, and 80µL of microbiology-grade H_2O was added to each well. After the cells had lysed, two freeze-thaw cycles were performed. An amount of 20µL of 0.5M alkaline buffer (Sigma-Aldrich Prod. # A9266) and 100µL of 5mM 4-nitrophenyl (Sigma-Aldrich Prod. # P4744) solution were added to the wells. The plates were returned to the incubator for fifty minutes. An amount of 100µL of 0.3M NaOH was added to stop the reaction, and the absorbance of each well was determined at 405nm.

SAOS-2 Cell Proliferation

The cytocompatibility of the composite scaffolds was demonstrated using SAOS-2 osteosarcoma cells (ATCC® Number HTB-85™). The scaffolds (n=4) were placed in 24-well plates and soaked in 70% EtOH for two hours. The scaffolds were washed in 1x PBS three times and transferred to new plates. An amount of 1mL of media (Thermo

Scientific HyClone® McCoy's 5A media containing 15% FBS and AB/AM) was added to each well, and the scaffolds were placed in an incubator overnight.

On the following day, the media was aspirated. The scaffolds were then seeded with SAOS-2 cells in 1mL of media at a density of $2x10^5$ cells/well. After three hours, the scaffolds were transferred to empty wells and the number of cells attached (Day 0) was determined using the CellTiter-Glo® assay (Promega). A standard curve relating relative luminescence units to cell number was obtained by plating a known amount of cells. The remaining scaffolds were transferred to new wells with fresh media. Cell numbers were determined on Days 2 and 6 using CellTiter-Glo®. On Day 6, LIVE/DEAD® staining was also performed. Amounts of 20μL of calcein (Invitrogen Prod. # C3099) and 20μL of ethidium bromide (Invitrogen Prod. # L3224) were added to 10mL of 1xPBS. Then, 1mL of this solution was added to each scaffold, and cells were viewed using a fluorescent microscope equipped with BioQuant imaging software.

Scanning Electron Microscopy and Photograph Imaging

Scanning electron micrograph (SEM) images of microspheres and scaffolds were obtained using a Philips XL30 environmental microscope. Samples were coated with 30nm of Au/Pd before imaging to make them conductive. Photographs of beads and scaffolds were also obtained using a Nikon Coolpix 5400 digital camera.

Statistics

Data are presented as mean ± standard deviation. Statistics were performed using an appropriate ANOVA method with $p<0.05$ considered significant. Kruskal-Wallis analysis was used when data was not normal or unequal variances were detected. Pairwise comparisons were obtained using the Student-Neuman-Keuls (SNK) test.

RESULTS

CMCS microspheres were successfully prepared as seen in Figure 1. The Gen-X CMCS beads have a distinctive dark green color to them, and the X-CMCS beads are deep golden in color (see online for full color images). All of the microspheres are similar in size with a diameter of roughly 1mm, and the beads have a slight tear-drop shape. Both the Gen-X CMCS and X-CMCS beads have a more textured surface compared to the smoother 61% DDA CS beads. The CMCS beads were successfully incorporated into porous composite scaffolds (Figure 2).

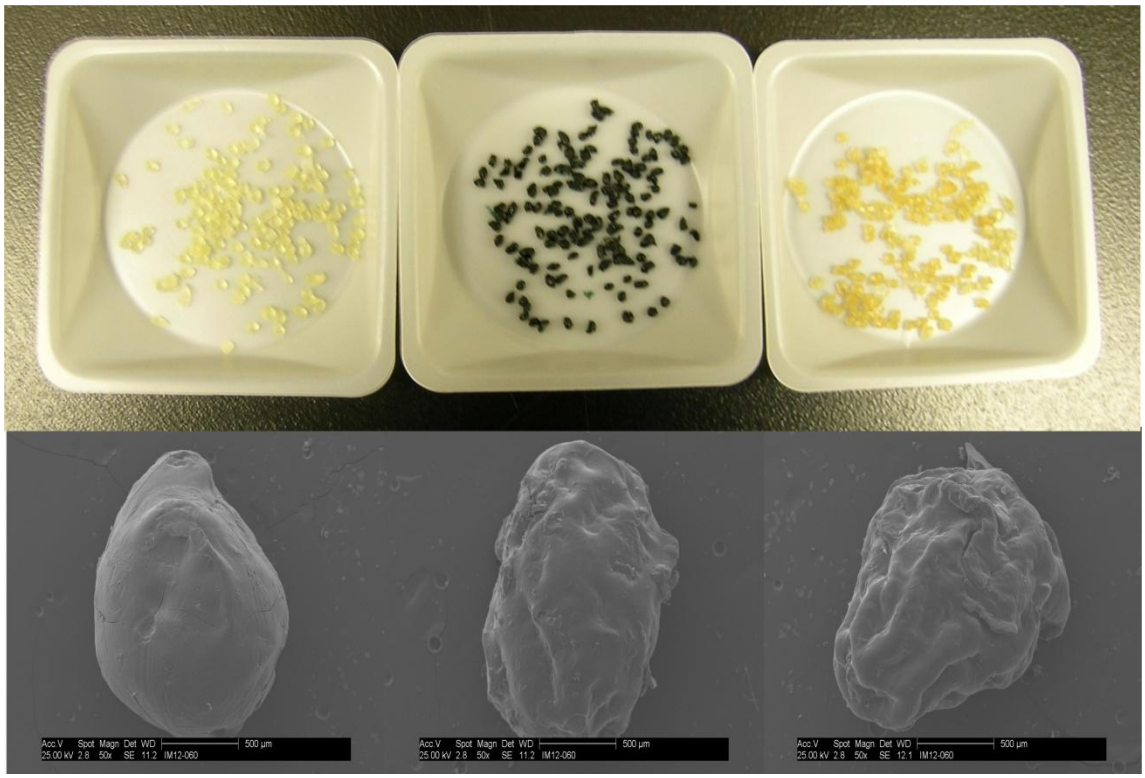

Figure 1. Digital photographs and SEM micrographs of microspheres. Top row (L-R): 61% DDA CS bead, Gen-X CMCS bead, and X-CMCS bead photographs; Bottom row (L-R): 61% DDA CS bead, Gen-X CMCS bead, and X-CMCS bead micrographs at 50x magnification (scale bar is 500µm).

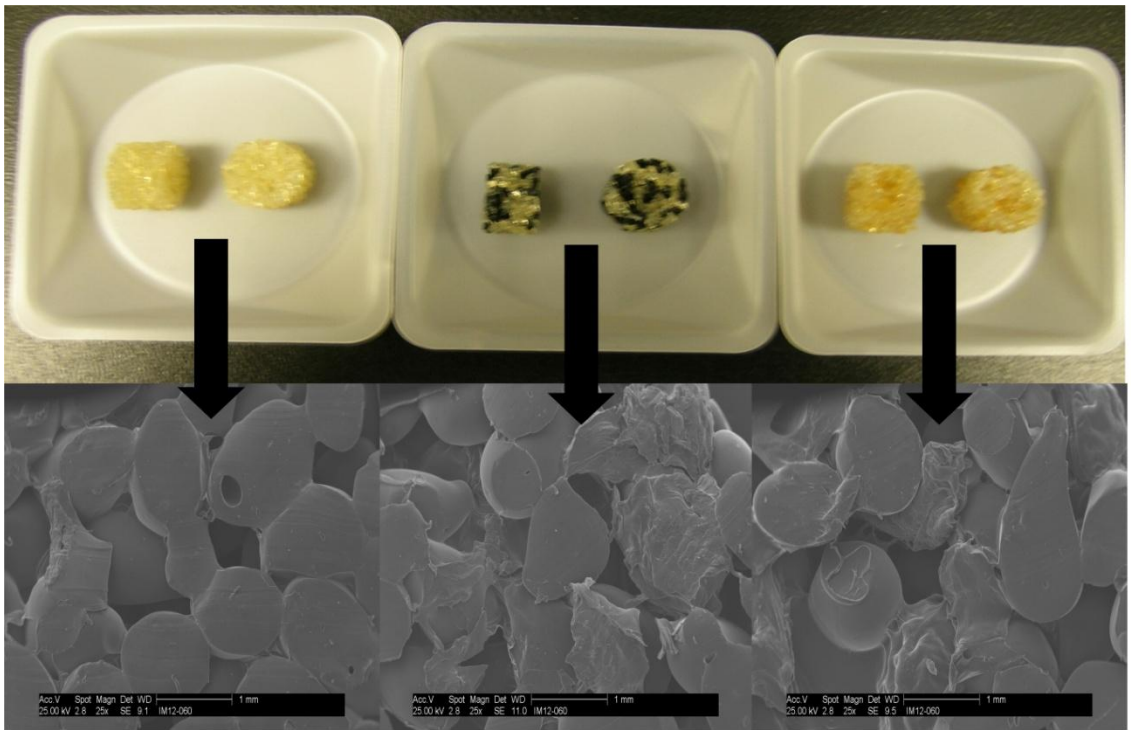

Figure 2. Digital photographs and SEM micrographs of scaffolds. Top row (L-R): 80% DDA CS-only scaffold, composite Gen-X CMCS/CS scaffold, and composite X-CMCS/CS scaffold photographs; Bottom row (L-R): 80% DDA CS-only scaffold, composite Gen-X CMCS/CS scaffold, and composite X-CMCS/CS scaffold micrographs at 25x magnification (scale bar is 1,000µm).

Microsphere Characterization

The FTIR spectra demonstrated that carboxymethylation of the chitosan beads had occurred (Figure 3). The 61% DDA powder and 61% DDA bead spectra display the characteristic peaks of chitosan.[28,54] The bands at 1591 cm^{-1} and 1416 cm^{-1} on the CMCS spectrum denote a carboxyl group and confirm that the carboxymethylation reaction was successful.[33,54,55]

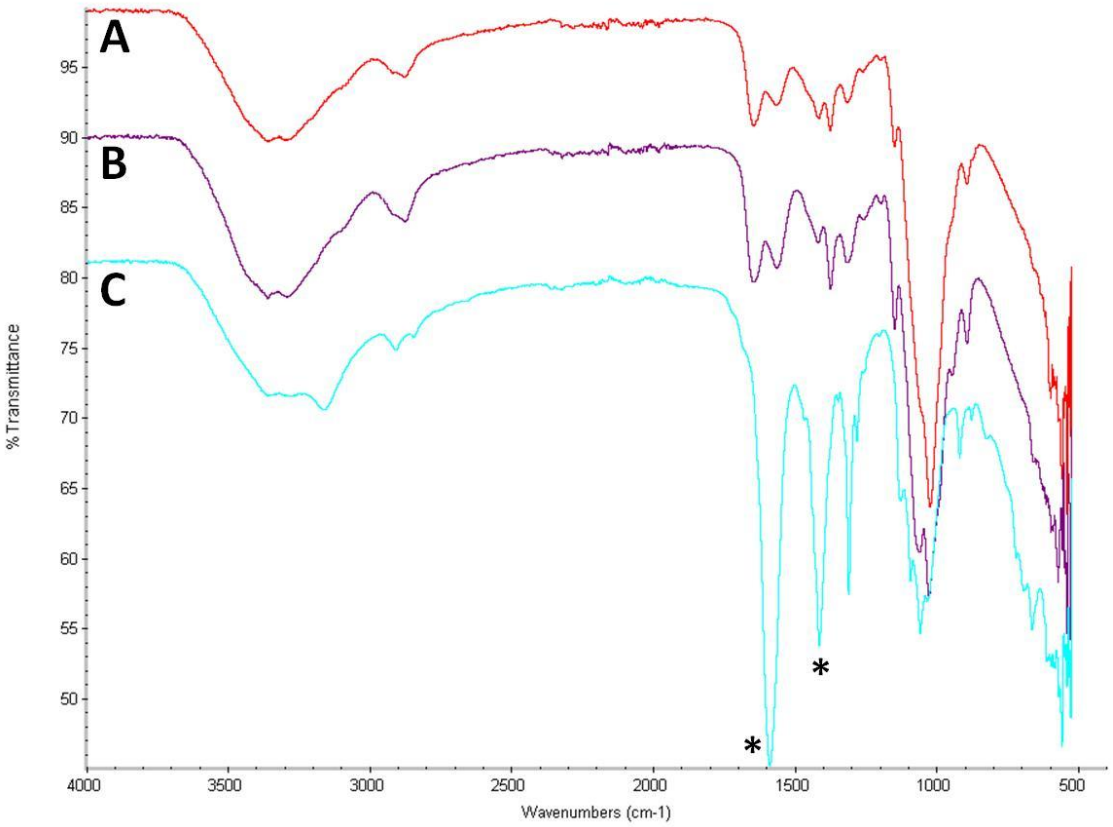

Figure 3. ATR-FTIR spectra of chitosan and CMCS. A) 61% DDA chitosan powder; B) 61% DDA chitosan beads; and C) CMCS beads. * represents peaks characteristic of carboxyl groups.

Crosslinking of the CMCS beads was confirmed by the ninhydrin assay. A reduction in the number of free amine groups was observed for the Gen-X CMCS ($p=0.015$) and X-CMCS ($p=0.003$) beads (Table 1). Although the number of free amine groups remaining after crosslinking was lower in the X-CMCS beads compared to the Gen-X CMCS beads, this difference was not significant ($p=0.061$).

Table 1. Free amine groups and swelling ratio of beads. * represents statistical difference from all other groups. # represents no statistical difference between groups.

Bead Type	**µmole amine/g beads**	**Swelling Ratio** (%)
61% DDA CS	44.4 ± 7.9*	176.3 ± 18.1*
Gen-X CMCS	32.0 ± 4.3$^{\#}$	398.1 ± 8.1*
X-CMCS	22.6 ± 2.5$^{\#}$	612.1 ± 3.2*

The CMCS beads demonstrated increased swelling properties in 1x PBS compared to the 61% DDA CS microspheres (Table 1). The swelling ratio of the Gen-X CMCS beads increased to around 400%; whereas, the swelling ratio of the X-CMCS increased to over 600%.

The microsphere groups demonstrated very different degradation properties (Table 2). The CS beads displayed slight degradation in lysozyme, but gained weight in PBS. The Gen-X CMCS beads displayed roughly 23% degradation for all conditions. The X-CMCS beads displayed approximately 10% weight loss after thirty days in PBS; whereas; the X-CMCS beads were almost completely degraded after thirty days in the lysozyme solution.

Table 2. Degradation of microspheres. Negative values indicate weight gain. Statistics performed using two-factor ANOVA with SNK post-hoc test for each buffer condition.* and & represent statistical difference from all other groups at timepoint. a, b, and c represent statistical difference between timepoints.

	1x PBS		**100µg/mL lysozyme**	
Bead Type	**Fifteen Days** (% Weight Change)	**Thirty Days** (% Weight Change)	**Fifteen Days** (% Weight Change)	**Thirty Days** (% Weight Change)
61% DDA CS	-1.8 ± 0.5 *	-2.4 ± 0.2*	4.1 ± 0.1$^{\&,b}$	8.4 ± 0.8$^{\&,b}$
Gen-X CMCS	23.3 ± 0.5*	22.6 ± 1.1*	23.3 ± 0.7$^{\&}$	23.6 ± 0.3$^{\&}$
X-CMCS	8.7 ± 1.1*^{,a}	10.1 ± 1.2*^{,a}	54.4 ± 2.4$^{\&,c}$	82.7± 1.2$^{\&,c}$

The 61% DDA CS and X-CMCS beads both displayed a moderate burst release of BMP-2 followed by extended elution (Figure 4). The Gen-X CMCS beads eluted very little BMP-2 over the course of the study.

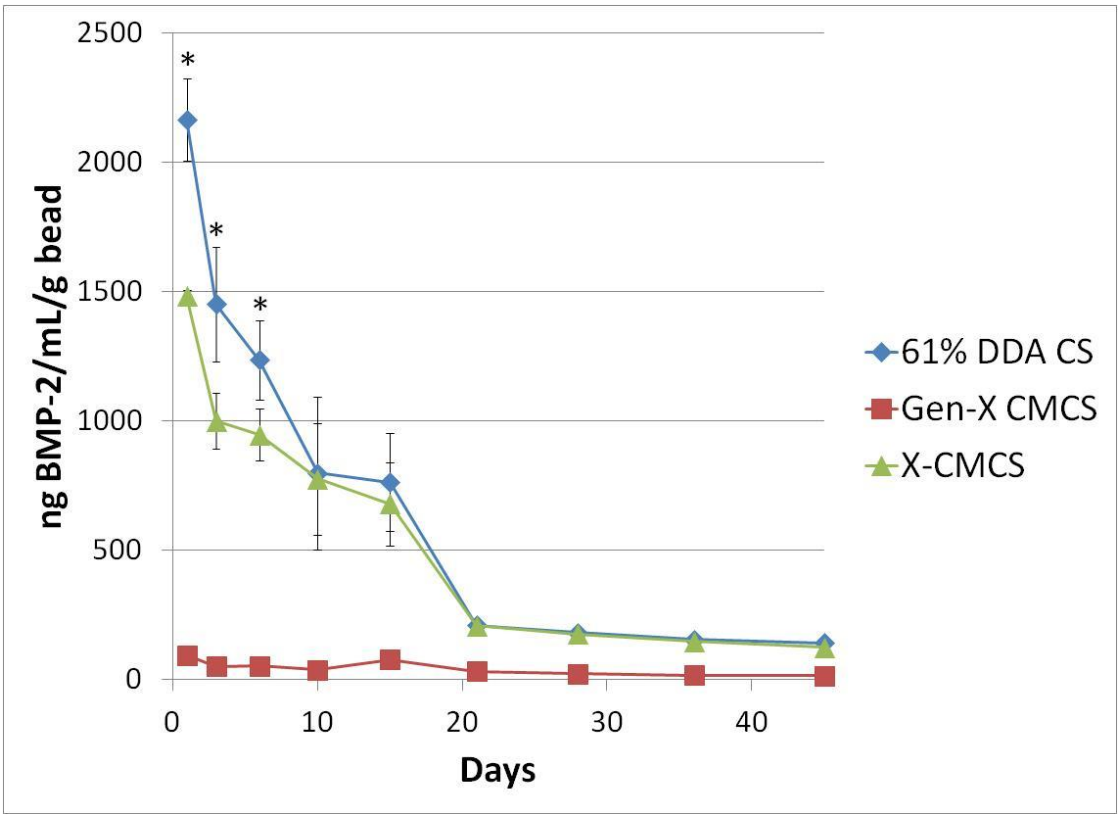

Figure 4. rhBMP-2 elution from microspheres. Gen-X CMCS microspheres were significantly different from both other groups at all timepoints. * represents statistical difference between 61% DDA chitosan and X-CMCS microspheres.

Scaffold Characterization

Although the compressive moduli of the composite scaffolds were slightly lower than that of the CS-only scaffold (Table 3), the differences were not significant ($p=0.050$).

Table 3. Scaffold compression and degradation. * represents statistical difference from all other groups. # represents no statistical difference between groups.

Scaffold Type	**Compressive Modulus** (MPa)	**Thirty Day Degradation** (% Weight Change)
80% DDA CS	$1.6 \pm 0.3^{\#}$	0.5 ± 0.4*
Gen-X CMCS/CS	$1.0 \pm 0.1^{\#}$	-2.7 ± 0.3*
X-CMCS/CS	$1.4 \pm 0.1^{\#}$	14.5 ± 6.6*

Scaffold degradation was increased by the addition of X-CMCS microspheres (Table 3). CS-only scaffolds displayed minimal degradation, and Gen-X CMCS/CS scaffolds gained weight during the study. After four weeks, the mass of the composite X-CMCS/CS scaffolds had decreased over fourteen percent.

The elution of rhBMP-2 from scaffolds was improved by the addition of X-CMCS beads (Figure 5). The X-CMCS/CS scaffolds released more rhBMP-2 at all timepoints compared to the CS-only and Gen-X CMCS/CS scaffolds. The CS-only scaffolds and Gen-X CMCS/CS scaffolds had very similar release profiles that were statistically different only on days 10 and 15.

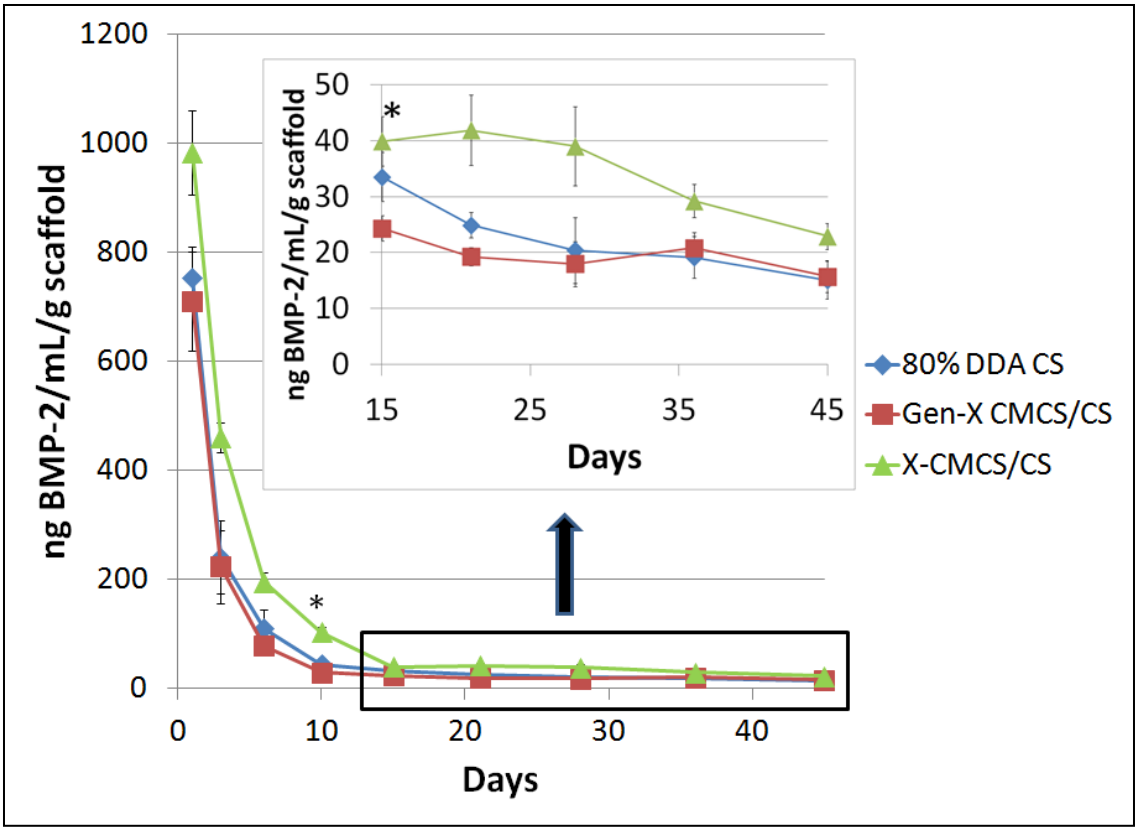

Figure 5. rhBMP-2 elution from scaffolds. X-CMCS/CS scaffolds released more BMP-2 on all days. * represent statistical difference between Gen-X CMCS/CS and CS-only scaffolds.

All of the rhBMP-2 eluates were determined to be bioactive as shown by their ability to induce alkaline phosphatase production in W20-17 mouse stromal cells (Figure 6). The shape of the release profiles obtained using the W20-17 assay to measure active BMP-2 was similar to those obtained using ELISAs. As before, composite X-CMCS/CS scaffolds released statistically significant higher levels of growth factor on all days.

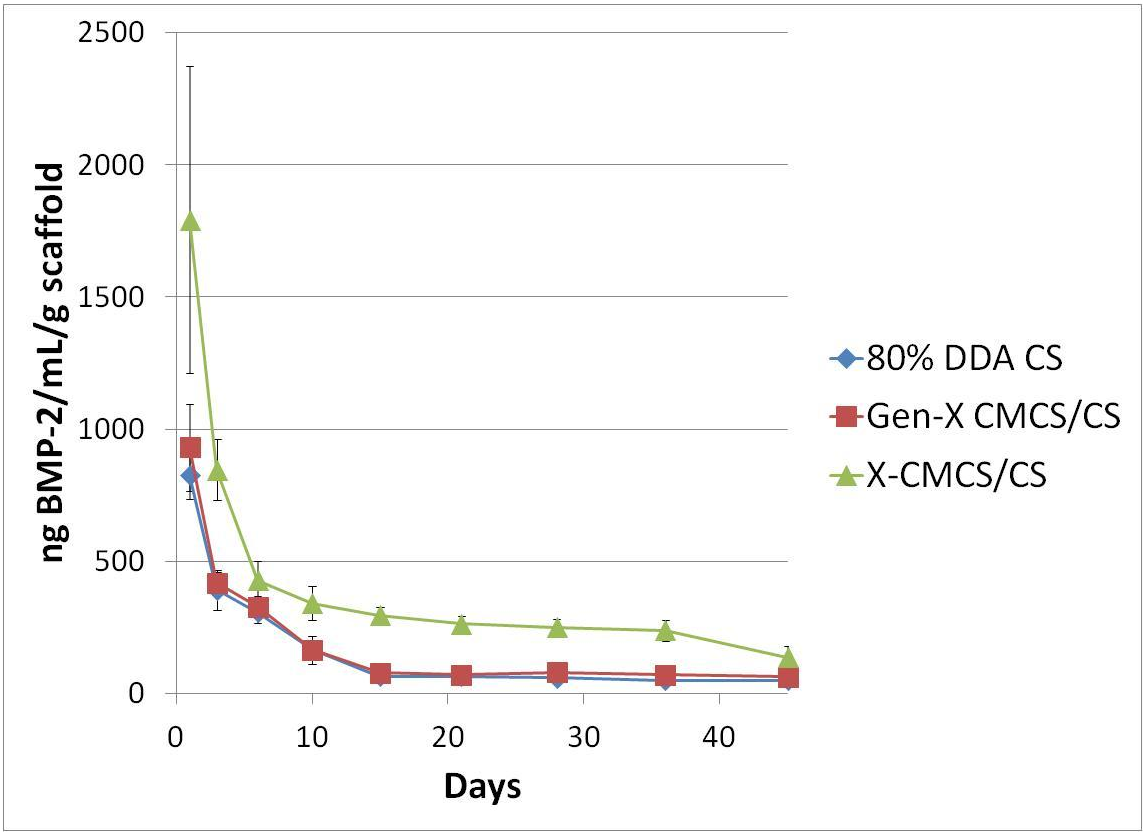

Figure 6. Amount of active rhBMP-2 in scaffold eluates as determined by W20-17 assay. X-CMCS/CS scaffolds released more active BMP-2 on all days. No statistical differences exist between Gen-X CMCS/CS and CS-only scaffolds.

The composite scaffolds promoted the attachment and proliferation of SAOS-2 cells in this study (Figure 7).

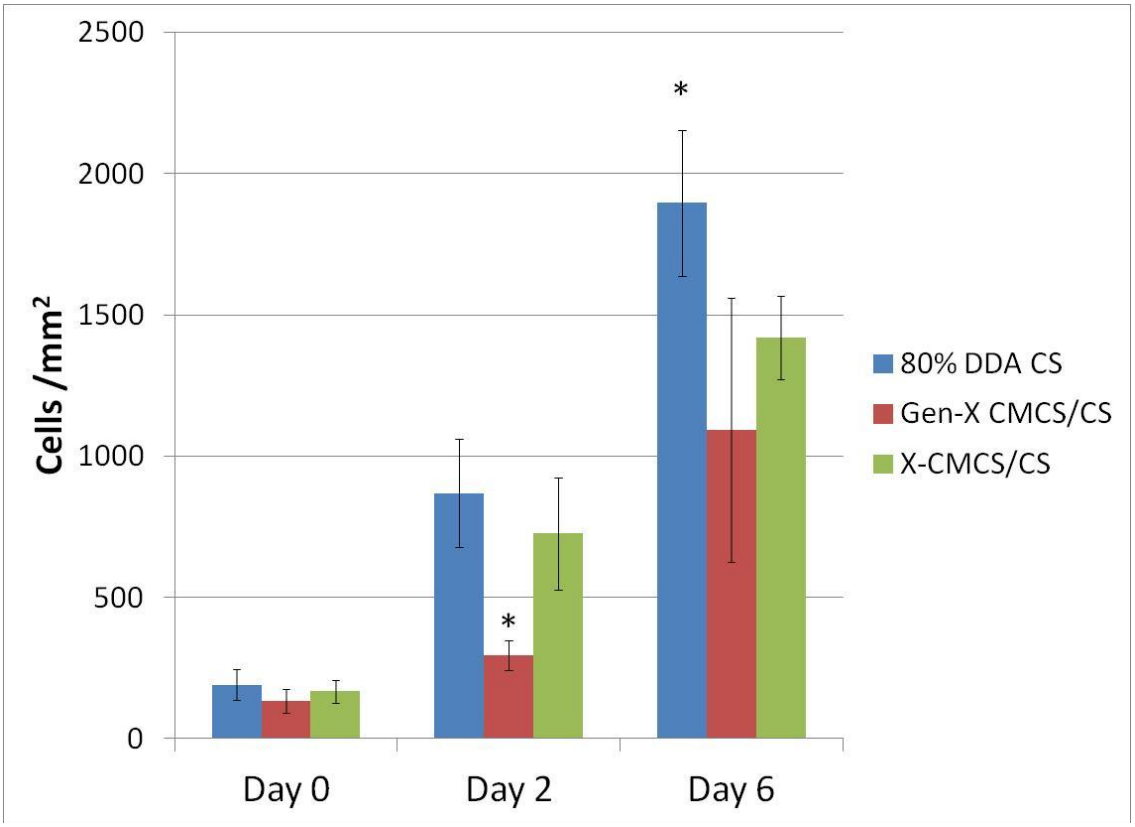

Figure 7. SAOS-2 attachment and proliferation on chitosan scaffolds. * represents statistical significance from other groups.

However, the Gen-X CMCS/CS scaffolds had fewer cells on Day 2 compared to the other groups, and the CS-only scaffolds had more cells on Day 6. Very few dead cells were observed on the scaffolds using Live/Dead staining (Figure 8). Cells spread very well on the X-CMCS/CS and CS scaffolds and displayed an elongated morphology; whereas, the SAOS-2 cells had a rounded morphology on the Gen-X CMCS/CS scaffolds and did not spread as well.

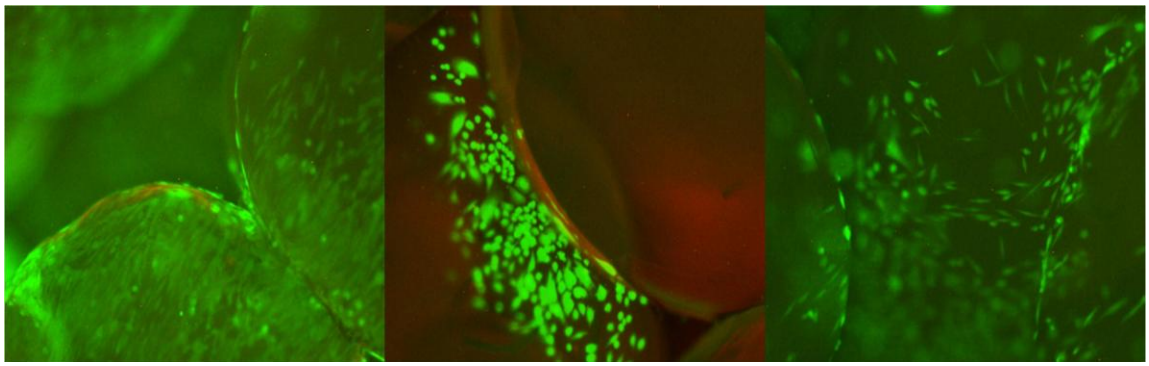

Figure 8. Live/Dead staining of SAOS-2 cells on scaffolds on Day 6. Original magnification of 4x. L-R: 80% DDA CS-only scaffold, Gen-X CMCS/CS scaffold, and X-CMCS/CS scaffold.

DISCUSSION

CMCS beads were fabricated by carboxymethylation of CS microspheres using monochloroacetic acid. The reaction conditions were selected based on previous optimization experiments.[28] Chen and Park previously demonstrated that an IPA:H_2O ratio of 80:20 and reaction temperature of 40^{o}C will result in a high degree of carboxymethylation.[28] Our data shows that this reaction scheme can be used to successfully perform carboxymethylation of dense microspheres.

Genipin-crosslinking of CMCS beads was successful but occurs somewhat slowly as evidenced by the eight hours required for sufficient crosslinking. Shorter reaction times resulted in beads in which the outside of the microspheres would crack when the beads were subjected to swelling evaluations in aqueous solutions. The reaction was performed at room temperature and at neutral pH, since these conditions result in high degrees of crosslinking.[41,56] The 5.7mM (0.13% w/v) genipin concentration used is similar to those previously employed to crosslink chitosan-based materials.[41,43,49,56]

Similar to other researchers, our experiments suggest that genipin-crosslinking can result in the outer layers of a material being thoroughly crosslinked while the interior

of the material experiences limited crosslinking.[42,49,56] This hypothesis is supported by the previously described cracking of insufficiently crosslinked microspheres and the degradation profile of the Gen-X CMCS beads. The roughly 23% weight loss displayed by all of the Gen-X CMCS microsphere groups was not enzyme or time-dependent. This weight loss was likely due to very fast dissolution of insufficiently crosslinked CMCS in the interior of the beads, but the remaining crosslinked material was highly stable and did not degrade. In fact, evidence suggests that genipin may sterically hinder lysozyme from accessing the glycosidic bonds of genipin-crosslinked chitosan.[40,41]

Crosslinking proceeded more quickly using EDC/NHS. X-CMCS degradation was found to be primarily enzymatic and not due to hydrolysis. The increase in enzymatic degradation (over 80% after thirty days) is likely related to the crystallinity of the X-CMCS beads. Abreu et al. reported that carboxymethylation of chitosan altered the arrangement of polymer chains resulting in lower crystallinity.[57] Furthermore, Guangyuan et al. demonstrated the loss of crystallinity that occurs after EDC crosslinking in CMCS films.[29] Presumably, the reduced crystallinity of the X-CMCS beads allows lysozyme easier access to the glycosidic bonds between the chitosan monomers. Similar to our results, Wang et al. observed a 70% reduction in the mass of carboxymethylchitosan scaffold tubes after eight weeks in a lysozyme solution, compared to only 4.3 ± 3.6% weight loss of chitosan scaffold tubes.[31]

Crosslinking method was found to have a large impact on BMP-2 release from the microspheres. The Gen-X CMCS beads released little BMP-2 over the course of the study; whereas, the X-CMCS and 61% DDA CS microspheres both demonstrated a tempered burst release followed by extended elution of BMP-2. Even at Day 45,

considerable amounts of BMP-2 were still being released from these groups. In a critical-size rat femoral defect, Brown et al. demonstrated that a burst release of BMP-2 followed by sustained elution is more effective than a burst release only or even sustained elution without a burst.[22] The X-CMCS and 61% DDA beads both demonstrated this efficacious release profile. Our data suggests that DDA can be used to modify the release of BMP-2 from chitosan. In this study, 80% DDA chitosan displayed a larger initial burst release of BMP-2 compared to 61% DDA chitosan, and we have previously observed a large burst release from 92.3% DDA chitosan microspheres.[8] Thus, chitosan with a lower DDA seems to promote a smaller burst release and more extended elution compared to higher DDAs. Although the X-CMCS beads were not able to further enhance the growth factor release, these microspheres are better suited than CS beads for applications such as bone regeneration in which both growth factor release and degradability is desired.

X-CMCS and Gen-X CMCS beads were successfully incorporated into composite chitosan scaffolds. The slight dissolution of chitosan beads in the 1% acetic acid wash due to protonation of the amine group makes the chitosan beads adherent and allows the microspheres to be fused into scaffolds. Due to the significant loss of amine groups caused by crosslinking, X-CMCS and Gen-X CMCS beads do not become adherent in the acid wash. As found in these evaluations, the crosslinked beads can only be fused into scaffolds when a sufficient amount of CS beads are present. The smallest ratio of CS:CMCS beads that could be used to fabricate scaffolds that stayed together was 2:1. 80% DDA microspheres without hydroxyapatite were chosen as the CS bead component due to their good mechanical properties and cytocompatibility as previously reported.[52]

The incorporation of X-CMCS beads into composite scaffolds improved the degradation and drug delivery properties of the scaffolds. The 14.5 ± 6.6% weight loss of the X-CMCS/CS scaffolds after thirty days is much higher than the 0.5 ± 0.4% weight loss of the CS-only scaffolds. This increased degradation is expected to promote better osteoblast penetration into the scaffolds resulting in more extensive bone regeneration. The X-CMCS/CS composite scaffolds released more rhBMP-2 at all timepoints and are expected to promote increased osteogenesis. Furthermore, the BMP-2 eluted was shown to be active by its ability to increase ALP production in W20-17 mouse stromal cells. If more X-CMCS beads could be incorporated into the composite scaffolds, the amount of degradation and BMP-2 eluted would likely increase even more.

The X-CMCS/CS composite scaffolds demonstrated good cytocompatibility with SAOS-2 cells in this study. EDC-crosslinked CMCS materials have previously shown the ability to support attachment and proliferation of a number of cell types including osteoblasts and MSCs.[29-31,33,34] Cai et al. demonstrated enhanced proliferation and increased ALP production of rat calvarial cells cultured on PDLLA films containing CMCS and crosslinked with EDC.[32] Although the Gen-X CMCS/CS scaffolds appeared to be cytocompatible, SAOS-2 proliferation was slower on this group and these cells displayed atypical morphology. Wang et al. recently published experiments suggesting that genipin exhibits a dose-dependent toxicity with human fetal osteoblast cells and that exposure of cells to genipin should be kept less than 0.5mM.[58] A concentration of 5.7mM genipin was used to crosslink the microspheres, and residual genipin could be responsible for the decreased proliferation and atypical morphology.

CONCLUSIONS

CMCS beads were produced by the carboxymethylation of chitosan microspheres using monochloroacetic acid. The crosslinking agent was found to have a large impact on the properties of the beads. Genipin-crosslinked microspheres displayed an undesirable degradation profile, and Gen-X CMCS beads released very little rhBMP-2. EDC-crosslinked beads demonstrated increased enzymatic degradation of 82.7 ± 1.2% after thirty days. The X-CMCS beads demonstrated a tempered burst release followed by an extended elution of growth factor. Composite scaffolds containing X-CMCS microspheres had improved degradation and drug release properties. These scaffolds were found to be cytocompatible with SAOS-2 cells and are expected to promote enhanced bone regeneration. Future studies will evaluate the ability of composite X-CMCS/CS scaffolds to augment fracture healing in vivo.

ACKNOWLEDGEMENTS

The authors gratefully acknowledge the donation of rhBMP-2 provided by Medtronic, Inc. The authors would also like to thank Lou Boykins and the Integrated Microscopy Center at the University of Memphis for use of the scanning electron microscope. The authors are grateful to Wright Medical Technology for use of their ATR-FTIR machine. The authors would also like to acknowledge the Biomaterials Association of Memphis for the many stimulating discussions of tissue engineering and bone regeneration.

REFERENCES

1. Dawson JI, Oreffo RO. Bridging the regeneration gap: stem cells, biomaterials and clinical translation in bone tissue engineering. Arch Biochem Biophys 2008;473(2):124-31.

2. Griffin M, Iqbal SA, Bayat A. Exploring the application of mesenchymal stem cells in bone repair and regeneration. J Bone Joint Surg Br 2011;93(4):427-34.

3. Khan Y, Yaszemski MJ, Mikos AG, Laurencin CT. Tissue engineering of bone: material and matrix considerations. J Bone Joint Surg Am 2008;90 Suppl 1:36-42.

4. Kretlow JD, Mikos AG. Review: mineralization of synthetic polymer scaffolds for bone tissue engineering. Tissue Eng 2007;13(5):927-38.

5. Nandi SK, Roy S, Mukherjee P, Kundu B, De DK, Basu D. Orthopaedic applications of bone graft & graft substitutes: a review. Indian J Med Res 2010;132:15-30.

6. Chesnutt BM, Viano AM, Yuan Y, Yang Y, Guda T, Appleford MR, Ong JL, Haggard WO, Bumgardner JD. Design and characterization of a novel chitosan/nanocrystalline calcium phosphate composite scaffold for bone regeneration. J Biomed Mater Res A 2009;88(2):491-502.

7. Chesnutt BM, Yuan Y, Buddington K, Haggard WO, Bumgardner JD. Composite chitosan/nano-hydroxyapatite scaffolds induce osteocalcin production by osteoblasts in vitro and support bone formation in vivo. Tissue Eng Part A 2009;15(9):2571-9.

8. Reves BT, Bumgardner JD, Cole JA, Yang Y, Haggard WO. Lyophilization to improve drug delivery for chitosan-calcium phosphate bone scaffold construct: a preliminary investigation. J Biomed Mater Res B Appl Biomater 2009;90(1):1-10.

9. Reves BT, Jennings JA, Bumgardner JD, Haggard WO. Osteoinductivity Assessment of BMP-2 Loaded Composite Chitosan-Nano-Hydroxyapatite Scaffolds in a Rat Muscle Pouch. Materials 2011;4(8):1360-1374.

10. Karageorgiou V, Kaplan D. Porosity of 3D biomaterial scaffolds and osteogenesis. Biomaterials 2005;26(27):5474-91.

11. Logeart-Avramoglou D, Anagnostou F, Bizios R, Petite H. Engineering bone: challenges and obstacles. J Cell Mol Med 2005;9(1):72-84.

12. Muzzarelli C, Muzzarelli RA. Natural and artificial chitosan-inorganic composites. J Inorg Biochem 2002;92(2):89-94.

13. Devescovi V, Leonardi E, Ciapetti G, Cenni E. Growth factors in bone repair. Chir Organi Mov 2008;92(3):161-8.

14. Lieberman JR, Daluiski A, Einhorn TA. The role of growth factors in the repair of bone. Biology and clinical applications. J Bone Joint Surg Am 2002;84-A(6):1032-44.

15. Schmidmaier G, Schwabe P, Strobel C, Wildemann B. Carrier systems and application of growth factors in orthopaedics. Injury 2008;39 Suppl 2:S37-43.

16. Alsberg E, Kong HJ, Hirano Y, Smith MK, Albeiruti A, Mooney DJ. Regulating bone formation via controlled scaffold degradation. J Dent Res 2003;82(11):903-8.

17. Oest ME, Dupont KM, Kong HJ, Mooney DJ, Guldberg RE. Quantitative assessment of scaffold and growth factor-mediated repair of critically sized bone defects. J Orthop Res 2007;25(7):941-50.

18. Ai-Aql ZS, Alagl AS, Graves DT, Gerstenfeld LC, Einhorn TA. Molecular mechanisms controlling bone formation during fracture healing and distraction osteogenesis. J Dent Res 2008;87(2):107-18.

19. Fiedler J, Roderer G, Gunther KP, Brenner RE. BMP-2, BMP-4, and PDGF-bb stimulate chemotactic migration of primary human mesenchymal progenitor cells. J Cell Biochem 2002;87(3):305-12.

20. Huang Z, Nelson ER, Smith RL, Goodman SB. The sequential expression profiles of growth factors from osteoprogenitors [correction of osteroprogenitors] to osteoblasts in vitro. Tissue Eng 2007;13(9):2311-20.

21. Zhang F, Qiu T, Wu X, Wan C, Shi W, Wang Y, Chen JG, Wan M, Clemens TL, Cao X. Sustained BMP signaling in osteoblasts stimulates bone formation by promoting angiogenesis and osteoblast differentiation. J Bone Miner Res 2009;24(7):1224-33.

22. Brown KV, Li B, Guda T, Perrien DS, Guelcher SA, Wenke JC. Improving bone formation in a rat femur segmental defect by controlling bone morphogenetic protein-2 release. Tissue Eng Part A 2011;17(13-14):1735-46.

23. Jeon O, Song SJ, Yang HS, Bhang SH, Kang SW, Sung MA, Lee JH, Kim BS. Long-term delivery enhances in vivo osteogenic efficacy of bone morphogenetic protein-2 compared to short-term delivery. Biochem Biophys Res Commun 2008;369(2):774-80.

24. Yang HS, La WG, Bhang SH, Jeon JY, Lee JH, Kim BS. Heparin-conjugated fibrin as an injectable system for sustained delivery of bone morphogenetic protein-2. Tissue Eng Part A 2010;16(4):1225-33.

25. Di Martino A, Sittinger M, Risbud MV. Chitosan: a versatile biopolymer for orthopaedic tissue-engineering. Biomaterials 2005;26(30):5983-90.

26. Kim IY, Seo SJ, Moon HS, Yoo MK, Park IY, Kim BC, Cho CS. Chitosan and its derivatives for tissue engineering applications. Biotechnol Adv 2008;26(1):1-21.

27. Shi C, Zhu Y, Ran X, Wang M, Su Y, Cheng T. Therapeutic potential of chitosan and its derivatives in regenerative medicine. J Surg Res 2006;133(2):185-92.

28. Chen XG, Park HJ. Chemical characteristics of O-carboxymethyl chitosans related to the preparation conditions. Carbohydrate Polymers 2003;53(4):355-359.

29. Lu GY, Sheng BY, Wang G, Wei YJ, Gong YD, Zhang XF. Controlling the Degradation of Covalently Cross-linked Carboxymethyl Chitosan Utilizing Bimodal Molecular Weight Distribution. Journal of Biomaterials Applications 2009;23(5):435-451.

30. Shi ZL, Neoh KG, Kang ET, Poh CK, Wang W. Surface Functionalization of Titanium with Carboxymethyl Chitosan and Immobilized Bone Morphogenetic Protein-2 for Enhanced Osseointegration. Biomacromolecules 2009;10(6):1603-1611.

31. Wang G, Lu GY, Ao Q, Gong YD, Zhang XF. Preparation of cross-linked carboxymethyl chitosan for repairing sciatic nerve injury in rats. Biotechnology Letters 2010;32(1):59-66.

32. Cai KY, Yao KD, Li Z, Yang ZM, Li XQ. Rat osteoblast functions on the o-carboxymethyl chitosan-modified poly(D,L-lactic acid) surface. Journal of Biomaterials Science-Polymer Edition 2001;12(12):1303-1315.

33. Budiraharjo R, Neoh KG, Kang ET. Hydroxyapatite-coated carboxymethyl chitosan scaffolds for promoting osteoblast and stem cell differentiation. J Colloid Interface Sci 2012;366(1):224-32.

34. Chen RN, Wang GM, Chen CH, Ho HO, Sheu MT. Development of N,O-(carboxymethyl)chitosan/collagen matrixes as a wound dressing. Biomacromolecules 2006;7(4):1058-1064.

35. Tseng HJ, Tsou TL, Wang HJ, Hsu SH. Characterization of chitosan-gelatin scaffolds for dermal tissue engineering. J Tissue Eng Regen Med 2011.

36. Adhirajan N, Shanmugasundaram N, Babu M. Gelatin microspheres cross-linked with EDC as a drug delivery system for doxycyline: development and characterization. J Microencapsul 2007;24(7):647-59.

37. Collins RF, Flint TD, Holzenburg A, Ford RC. Structural changes in photosystem II after treatment with the zero-length bifunctional cross-linker 1-ethyl-3-(3-dimethylaminopropyl)carbodi-imide: an electron microscopic study. Biochem J 1996;319 (Pt 2):585-9.

38. Duan X, Sheardown H. Crosslinking of collagen with dendrimers. J Biomed Mater Res A 2005;75(3):510-8.

39. Grabarek Z, Gergely J. Zero-length crosslinking procedure with the use of active esters. Anal Biochem 1990;185(1):131-5.

40. Mi FL, Tan YC, Liang HF, Sung HW. In vivo biocompatibility and degradability of a novel injectable-chitosan-based implant. Biomaterials 2002;23(1):181-91.

41. Mi FL, Shyu SS, Peng CK. Characterization of ring-opening polymerization of genipin and pH-dependent cross-linking reactions between chitosan and genipin. Journal of Polymer Science Part a-Polymer Chemistry 2005;43(10):1985-2000.

42. Mi FL, Tan YC, Liang HC, Huang RN, Sung HW. In vitro evaluation of a chitosan membrane cross-linked with genipin. J Biomater Sci Polym Ed 2001;12(8):835-50.

43. Chen SC, Wu YC, Mi FL, Lin YH, Yu LC, Sung HW. A novel pH-sensitive hydrogel composed of N,O-carboxymethyl chitosan and alginate cross-linked by genipin for protein drug delivery. J Control Release 2004;96(2):285-300.

44. Mi FL, Liang HF, Wu YC, Lin YS, Yang TF, Sung HW. pH-sensitive behavior of two-component hydrogels composed of N,O-carboxymethyl chitosan and alginate. Journal of Biomaterials Science-Polymer Edition 2005;16(11):1333-1345.

45. Yang LQ, Lan YQ, Guo H, Cheng LZ, Fan JZ, Cai X, Zhang LM, Chen RF, Zhou HS. Ophthalmic drug-loaded N,O-carboxymethyl chitosan hydrogels: synthesis, in vitro and in vivo evaluation. Acta Pharmacol Sin 2010;31(12):1625-34.

46. Geiger M, Li RH, Friess W. Collagen sponges for bone regeneration with rhBMP-2. Adv Drug Deliv Rev 2003;55(12):1613-29.

47. Macdonald ML, Samuel RE, Shah NJ, Padera RF, Beben YM, Hammond PT. Tissue integration of growth factor-eluting layer-by-layer polyelectrolyte multilayer coated implants. Biomaterials 2011;32(5):1446-53.

48. Patterson J, Siew R, Herring SW, Lin AS, Guldberg R, Stayton PS. Hyaluronic acid hydrogels with controlled degradation properties for oriented bone regeneration. Biomaterials 2010;31(26):6772-81.
49. Yuan Y, Chesnutt BM, Utturkar G, Haggard WO, Yang Y, Ong JL, Bumgardner JD. The effect of cross-linking of chitosan microspheres with genipin on protein release. Carbohydrate Polymers 2007;68(3):561-567.

50. Varum KM, Myhr MM, Hjerde RJ, Smidsrod O. In vitro degradation rates of partially N-acetylated chitosans in human serum. Carbohydr Res 1997;299(1-2):99-101.

51. Ren D, Yi H, Wang W, Ma X. The enzymatic degradation and swelling properties of chitosan matrices with different degrees of N-acetylation. Carbohydr Res 2005;340(15):2403-10.

52. Reves BT, Jennings JA, Bumgardner JD, Haggard WO. Preparation and functional assessment of composite chitosan-nano-hydroxyapatite scaffolds for bone regeneration. J. Funct. Biomater. 2012;3:114-130.

53. Thies RS, Bauduy M, Ashton BA, Kurtzberg L, Wozney JM, Rosen V. Recombinant human bone morphogenetic protein-2 induces osteoblastic differentiation in W-20-17 stromal cells. Endocrinology 1992;130(3):1318-24.

54. Ge HC, Luo DK. Preparation of carboxymethyl chitosan in aqueous solution under microwave irradiation. Carbohydr Res 2005;340(7):1351-6.

55. Oliveira JM, Costa SA, Leonor IB, Malafaya PB, Mano JF, Reis RL. Novel hydroxyapatite/carboxymethylchitosan composite scaffolds prepared through an innovative "autocatalytic" electroless coprecipitation route. J Biomed Mater Res A 2009;88(2):470-80.

56. Bi L, Cao Z, Hu Y, Song Y, Yu L, Yang B, Mu J, Huang Z, Han Y. Effects of different cross-linking conditions on the properties of genipin-cross-linked chitosan/collagen scaffolds for cartilage tissue engineering. J Mater Sci Mater Med 2011;22(1):51-62.

57. de Abreu FR, Campana SP. Characteristics and properties of carboxymethylchitosan. Carbohydrate Polymers 2009;75(2):214-221.

58. Wang C, Lau TT, Loh WL, Su K, Wang DA. Cytocompatibility study of a natural biomaterial crosslinker--Genipin with therapeutic model cells. J Biomed Mater Res B Appl Biomater 2011;97(1):58-65.

Chapter 5 Additional Characterization of Composite Scaffolds

1. Porosity Determination

The porosity of scaffolds was determined using a liquid displacement method based on Archimedes' principle [86]. The following three groups of scaffolds were prepared as described in Chapter 4: CS, composite Gen-X CMCS/CS, and composite X-CMCS/CS scaffolds. The height (H) and diameter (D) of the scaffolds was measured using calipers. The components of a density determination kit (Mettler Toledo, Switzerland) were assembled according to the manufacturers' instructions. Methanol was placed in a beaker, and the wire basket was submerged in the liquid. The balance was tared, and a scaffold was placed in the upper cup holder. The mass of the dry scaffold was recorded as A. The balance was tared again, and the scaffold was placed in the beaker of methanol. Air bubbles were removed from the scaffold by placing the beaker in a vacuum oven (Fisher Scientific, Isotemp® Model 285A) at 15 inches Hg gauge for five minutes. The density kit was reassembled, and the scaffold was placed in the submerged wire basket. This mass was recorded as P. The density of the scaffold was determined using the following equation:

$$\rho = \frac{A \times \rho_{methanol}}{P},$$

where $\rho_{methanol}$ is the density of methanol. The total volume of the cylindrical scaffold was calculated by the following:

$$V_{total} = \frac{\pi \times D^2 \times H}{4}.$$

The volume of the scaffold without pores was determined using the following equation:

$$V_{without\ pores} = \frac{A}{\rho}.$$

The porosity was then calculated by the following:

$$Porosity = \frac{V_{total} - V_{without\ pores}}{V_{total}} \times 100\%.$$

The composite scaffolds had higher porosities that the CS-only scaffolds (Table 1).

Table 1. Scaffold porosity. Statistics performed using one-way ANOVA with SNK post-hoc test. p-values less than 0.05 considered statistically significant. * represents statistical difference from all other groups.

Scaffold Type	Porosity (%)
80% DDA CS	35.5 ± 2.1*
Gen-X CMCS/CS	41.1 ± 2.2*
X-CMCS/CS	44.3 ± 1.5*

In addition, the X-CMCS/CS composites had a slightly higher porosity than the Gen-X CMCS/CS scaffolds. Presumably, the slightly different shape and size of the Gen-X CMCS and X-CMCS beads resulted in less-tight microsphere packing during scaffold fabrication which resulted in slightly higher porosity (Figure 1).

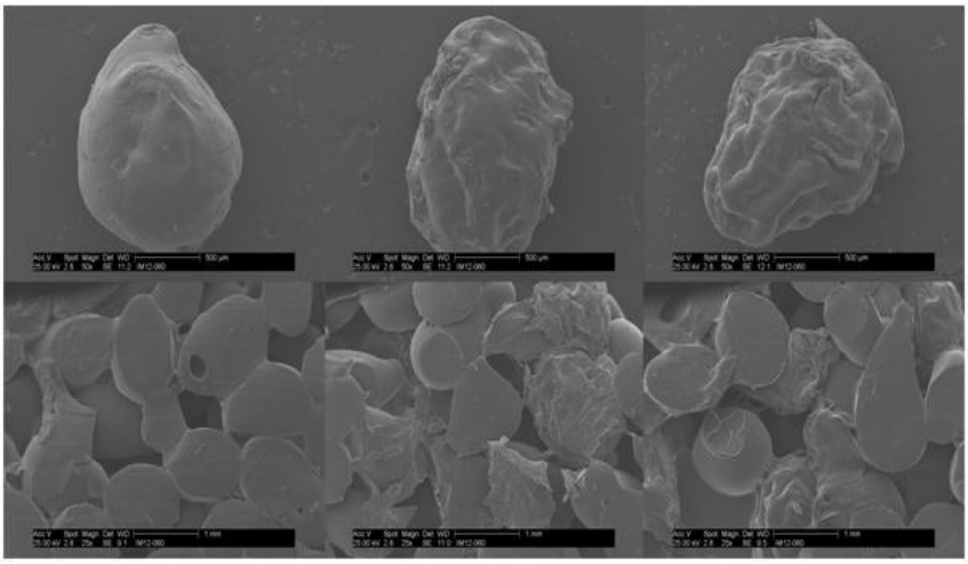

Figure 1. SEM micrographs of chitosan microspheres and scaffolds. Top row (L-R): 61% DDA CS bead, Gen-X CMCS bead, and X-CMCS bead micrographs at 50x magnification (scale bar is 500µm). Bottom row (L-R): 80% DDA CS-only scaffold, composite Gen-X CMCS/CS scaffold, and composite X-CMCS/CS scaffold micrographs at 25x magnification (scale bar is 1,000µm).

Porosity is a very important characteristic of tissue engineered scaffolds. Porosity must be adequate enough to promote good nutrient and waste exchange to and from the scaffold [1, 60, 87, 88]. It has been suggested that a minimum porosity of thirty percent is needed for bone scaffolds to promote osteogenesis [89]. Thus, the CS-only scaffolds barely meet the minimum requirement. The additional porosity obtained by the incorporation of the CMCS beads should be beneficial and is expected to promote increased fluid exchange and tissue ingrowth. In addition, the compressive moduli of the X-CMCS/CS and Gen-X CMCS/CS scaffolds (Table 2) did not decrease during compression testing ($p=0.061$). Since an increase in porosity can result in poorer mechanical properties, a compromise between mechanical stability and porosity is required [60]. Indeed, the composite scaffolds displayed increased porosity while maintaining good mechanical characteristics.

Table 2. Compressive moduli of scaffolds. Statistics performed using Kruskal-Wallis with p-value less than 0.05 considered statistically significant. # represents no statistical difference between groups.

Scaffold Type	**Compressive Modulus** (MPa)
80% DDA CS	$1.6 \pm 0.3^{\#}$
Gen-X CMCS/CS	$1.0 \pm 0.1^{\#}$
X-CMCS/CS	$1.4 \pm 0.1^{\#}$

Chapter 6 Conclusions

The rat muscle pouch osteoinductivity study in Chapter 2 demonstrated the need for increased scaffold degradation. Although the scaffolds demonstrated good biocompatibility, little to no degradation was observed in vivo after one month. Very little (less than 2% of the defect area) contained new bone. In contrast, the BMP-2 loaded collagen sponge used as a positive control had completely degraded after one month and extensive osteogenesis was observed. This in vivo model demonstrated the potential of our scaffolds for use in bone regeneration but reaffirmed the need for increased degradation.

The selection of the chitosan bead component of the composite scaffolds was described in Chapter 3. The effects of DDA, drying method, and hydroxyapatite content on biocompatibility, degradation, compressive properties, and swelling ratio were investigated. All of the scaffolds demonstrated minimal degradation. 80% DDA scaffolds had higher compressive moduli compared to 60% DDA scaffolds. Interestingly, scaffolds without hydroxyapatite were found to have better cytocompatibility with SAOS-2 cells compared to scaffolds containing hydroxyapatite. For this reason, air-dried 80% DDA microspheres without hydroxyapatite were chosen as the chitosan bead component of the composite scaffolds due to their excellent cytocompatibility and good mechanical properties (compressive modulus of 1.6 ± 0.3 MPa).

The fabrication of CMCS microspheres and the different properties obtained using genipin and EDC as crosslinking agents was described in Chapter 4. Gen-X CMCS microspheres had poor degradation properties and released very little BMP-2 during the elution study. In contrast, the X-CMCS microspheres degraded over eighty percent in one

month and demonstrated an extended BMP-2 elution profile. The incorporation of X-CMCS beads into composite scaffolds improved the properties of the constructs. The degradation of composite X-CMCS/CS scaffolds increased to 14.5 ± 6.6% compared to 0.5 ± 0.4% for CS-only scaffolds. The X-CMCS/CS scaffolds released more BMP-2 at all timepoints. These composite scaffolds also displayed good cytocompatibility with SAOS-2 cells, and their compressive modulus (1.4 ± 0.1 MPa) was not decreased by the inclusion of X-CMCS beads. Thus, our hypothesis was confirmed.

These experiments demonstrated the benefit of using a composite approach when designing biomaterial technologies for bone regeneration. Due to the numerous characteristics required of a bone tissue scaffold including cytocompatibility, degradability, and mechanical stability, very few materials can meet these demands alone. In many cases, a composite approach incorporating multiple materials into a construct may be beneficial. Indeed, our chitosan bone regeneration technology was improved by the addition of X-CMCS beads into the constructs to form composite scaffolds. The X-CMCS/CS composite scaffolds showed increased potential for augmentation of bone healing and improved outcomes for severe fractures.

Chapter 7 Recommendations for Future Work

The ability of the X-CMCS/CS scaffolds to promote bone regeneration should be assessed in an animal model in vivo. Preferably, the constructs should be evaluated in a critical-sized segmental bone defect. The X-CMCS/CS composites can potentially be further enhanced in a number of ways. The reaction conditions for both the carboxymethylation and EDC-crosslinking steps can be optimized to yield microspheres with the most desirable properties. Both of these reactions depend on a number of parameters and a high degree of tailorability should be possible. Methods for incorporating more X-CMCS beads into the composite scaffolds should be pursued. The current scaffold fabrication process limits the amount of X-CMCS beads that can be incorporated, and the benefits of X-CMCS addition were not fully realized. Use of the X-CMCS beads in other composite strategies should also be considered. For instance, a composite containing X-CMCS beads embedded in calcium phosphate cement could be useful as a bone graft substitute. The mechanical properties of the X-CMCS/CS scaffolds should be improved. Although the scaffolds have compressive moduli similar to those of trabecular bone when dry, the moduli of the hydrated scaffolds are lower than desired. Perhaps, some sort of fiber or particle reinforcement could be used to improve the mechanical properties of the scaffolds. For example, the inclusion of small polyester fibers into the beads could potentially increase their compressive strength and modulus.

References

1. Logeart-Avramoglou, D.; Anagnostou, F.; Bizios, R.; Petite, H., Engineering bone: challenges and obstacles. *J Cell Mol Med* **2005,** *9*, 72-84.

2. Dawson, J. I.; Oreffo, R. O., Bridging the regeneration gap: stem cells, biomaterials and clinical translation in bone tissue engineering. *Arch Biochem Biophys* **2008,** *473*, 124-131.

3. Simpson, A. H.; Mills, L.; Noble, B., The role of growth factors and related agents in accelerating fracture healing. *J Bone Joint Surg Br* **2006,** *88*, 701-705.

4. Geiger, M.; Li, R. H.; Friess, W., Collagen sponges for bone regeneration with rhBMP-2. *Adv Drug Deliv Rev* **2003,** *55*, 1613-1629.

5. Khan, Y.; Yaszemski, M. J.; Mikos, A. G.; Laurencin, C. T., Tissue engineering of bone: material and matrix considerations. *J Bone Joint Surg Am* **2008,** *90 Suppl 1*, 36-42.

6. Kretlow, J. D.; Mikos, A. G., Review: mineralization of synthetic polymer scaffolds for bone tissue engineering. *Tissue Eng* **2007,** *13*, 927-938.

7. Liu, Y.; Lu, Y.; Tian, X.; Cui, G.; Zhao, Y.; Yang, Q.; Yu, S.; Xing, G.; Zhang, B., Segmental bone regeneration using an rhBMP-2-loaded gelatin/nanohydroxyapatite/fibrin scaffold in a rabbit model. *Biomaterials* **2009,** *30*, 6276-6285.

8. Young, S.; Patel, Z. S.; Kretlow, J. D.; Murphy, M. B.; Mountziaris, P. M.; Baggett, L. S.; Ueda, H.; Tabata, Y.; Jansen, J. A.; Wong, M.; Mikos, A. G., Dose effect of dual delivery of vascular endothelial growth factor and bone morphogenetic protein-2 on bone regeneration in a rat critical-size defect model. *Tissue Eng Part A* **2009,** *15*, 2347-2362.

9. Jiang, T.; Kumbar, S. G.; Nair, L. S.; Laurencin, C. T., Biologically active chitosan systems for tissue engineering and regenerative medicine. *Curr Top Med Chem* **2008,** *8*, 354-364.

10. Patterson, T. E.; Kumagai, K.; Griffith, L.; Muschler, G. F., Cellular strategies for enhancement of fracture repair. *J Bone Joint Surg Am* **2008,** *90 Suppl 1*, 111-119.

11. Shi, C.; Zhu, Y.; Ran, X.; Wang, M.; Su, Y.; Cheng, T., Therapeutic potential of chitosan and its derivatives in regenerative medicine. *J Surg Res* **2006,** *133*, 185-192.

12. Chesnutt, B. M.; Viano, A. M.; Yuan, Y.; Yang, Y.; Guda, T.; Appleford, M. R.; Ong, J. L.; Haggard, W. O.; Bumgardner, J. D., Design and characterization of a novel chitosan/nanocrystalline calcium phosphate composite scaffold for bone regeneration. *J Biomed Mater Res A* **2009,** *88*, 491-502.

13. Chesnutt, B. M.; Yuan, Y.; Buddington, K.; Haggard, W. O.; Bumgardner, J. D., Composite chitosan/nano-hydroxyapatite scaffolds induce osteocalcin production by osteoblasts in vitro and support bone formation in vivo. *Tissue Eng Part A* **2009,** *15*, 2571-2579.

14. Reves, B. T.; Bumgardner, J. D.; Cole, J. A.; Yang, Y.; Haggard, W. O., Lyophilization to improve drug delivery for chitosan-calcium phosphate bone scaffold construct: a preliminary investigation. *J Biomed Mater Res B Appl Biomater* **2009,** *90*, 1-10.

15. Bernstein, J., *Musculoskeletal Medicine*. First ed.; American Acacademy of Orthopaedic Surgeons: 2003.

16. Lines, L. D., The management of ballistic trauma: an infection control perspective. *Br J Nurs* **2005,** *14*, 196-199.

17. Petersen, K.; Riddle, M. S.; Danko, J. R.; Blazes, D. L.; Hayden, R.; Tasker, S. A.; Dunne, J. R., Trauma-related infections in battlefield casualties from Iraq. *Ann Surg* **2007,** *245*, 803-811.

18. Carano, R. A.; Filvaroff, E. H., Angiogenesis and bone repair. *Drug Discov Today* **2003,** *8*, 980-989.

19. Kalfas, I. H., Principles of bone healing. *Neurosurg Focus* **2001,** *10*, E1.

20. Lieberman, J. R.; Daluiski, A.; Einhorn, T. A., The role of growth factors in the repair of bone. Biology and clinical applications. *J Bone Joint Surg Am* **2002,** *84-A*, 1032-1044.

21. Tsuji, K.; Bandyopadhyay, A.; Harfe, B. D.; Cox, K.; Kakar, S.; Gerstenfeld, L.; Einhorn, T.; Tabin, C. J.; Rosen, V., BMP2 activity, although dispensable for bone formation, is required for the initiation of fracture healing. *Nat Genet* **2006,** *38*, 1424-1429.

22. Ai-Aql, Z. S.; Alagl, A. S.; Graves, D. T.; Gerstenfeld, L. C.; Einhorn, T. A., Molecular mechanisms controlling bone formation during fracture healing and distraction osteogenesis. *Journal of Dental Research* **2008,** *87*, 107-118.

23. Fiedler, J.; Roderer, G.; Gunther, K. P.; Brenner, R. E., BMP-2, BMP-4, and PDGF-bb stimulate chemotactic migration of primary human mesenchymal progenitor cells. *Journal of Cellular Biochemistry* **2002,** *87*, 305-312.

24. Huang, Z. N.; Nelson, E. R.; Smith, R. L.; Goodman, S. B., The sequential expression profiles of growth factors from osteroprogenitors to osteoblasts In vitro. *Tissue Engineering* **2007,** *13*, 2311-2320.

25. Reddi, A. H., Bone morphogenetic proteins: from basic science to clinical applications. *J Bone Joint Surg Am* **2001,** *83-A Suppl 1*, S1-6.

26. Zhang, F. J.; Qiu, T.; Wu, X. W.; Wan, C.; Shi, W. B.; Wang, Y.; Chen, J. G.; Wan, M.; Clemens, T. L.; Cao, X., Sustained BMP Signaling in Osteoblasts Stimulates Bone Formation by Promoting Angiogenesis and Osteoblast Differentiation. *Journal of Bone and Mineral Research* **2009,** *24*, 1224-1233.

27. Bae, H.; Zhao, L.; Zhu, D.; Kanim, L. E.; Wang, J. C.; Delamarter, R. B., Variability across ten production lots of a single demineralized bone matrix product. *J Bone Joint Surg Am* **2010,** *92*, 427-435.

28. Kinney, R. C.; Ziran, B. H.; Hirshorn, K.; Schlatterer, D.; Ganey, T., Demineralized bone matrix for fracture healing: fact or fiction? *J Orthop Trauma* **2010,** *24 Suppl 1*, S52-55.

29. Dumas, J. E.; Davis, T.; Holt, G. E.; Yoshii, T.; Perrien, D. S.; Nyman, J. S.; Boyce, T.; Guelcher, S. A., Synthesis, characterization, and remodeling of weight-bearing allograft bone/polyurethane composites in the rabbit. *Acta Biomater* **2010,** *6*, 2394-2406.

30. Williams, J. M.; Adewunmi, A.; Schek, R. M.; Flanagan, C. L.; Krebsbach, P. H.; Feinberg, S. E.; Hollister, S. J.; Das, S., Bone tissue engineering using polycaprolactone scaffolds fabricated via selective laser sintering. *Biomaterials* **2005,** *26*, 4817-4827.

31. Chung, C.; Beecham, M.; Mauck, R. L.; Burdick, J. A., The influence of degradation characteristics of hyaluronic acid hydrogels on in vitro neocartilage formation by mesenchymal stem cells. *Biomaterials* **2009,** *30*, 4287-4296.

32. Huang, A. H.; Farrell, M. J.; Mauck, R. L., Mechanics and mechanobiology of mesenchymal stem cell-based engineered cartilage. *J Biomech* **2010,** *43*, 128-136.

33. Kuo, C. K.; Ma, P. X., Ionically crosslinked alginate hydrogels as scaffolds for tissue engineering: part 1. Structure, gelation rate and mechanical properties. *Biomaterials* **2001,** *22*, 511-521.

34. Mohajeri, S.; Hosseinkhani, H.; Ebrahimi, N. G.; Nikfarjam, L.; Soleimani, M.; Kajbafzadeh, A. M., Proliferation and differentiation of mesenchymal stem cell on collagen sponge reinforced with polypropylene/polyethylene terephthalate blend fibers. *Tissue Eng Part A* **2010,** *16*, 3821-3830.

35. Boccaccini, A. R.; Blaker, J. J., Bioactive composite materials for tissue engineering scaffolds. *Expert Rev Med Devices* **2005,** *2*, 303-317.

36. Dorozhkin, S. V., Bioceramics of calcium orthophosphates. *Biomaterials* **2010,** *31*, 1465-1485.

37. Schliephake, H., Application of bone growth factors--the potential of different carrier systems. *Oral Maxillofac Surg* **2010,** *14*, 17-22.

38. Suzuki, A.; Terai, H.; Toyoda, H.; Namikawa, T.; Yokota, Y.; Tsunoda, T.; Takaoka, K., A biodegradable delivery system for antibiotics and recombinant human bone morphogenetic protein-2: A potential treatment for infected bone defects. *J Orthop Res* **2006,** *24*, 327-332.

39. Devescovi, V.; Leonardi, E.; Ciapetti, G.; Cenni, E., Growth factors in bone repair. *Chir Organi Mov* **2008,** *92*, 161-168.

40. Asamura, S.; Mochizuki, Y.; Yamamoto, M.; Tabata, Y.; Isogai, N., Bone regeneration using a bone morphogenetic protein-2 saturated slow-release gelatin hydrogel sheet: evaluation in a canine orbital floor fracture model. *Ann Plast Surg* **2010,** *64*, 496-502.

41. Balmayor, E. R.; Feichtinger, G. A.; Azevedo, H. S.; van Griensven, M.; Reis, R. L., Starch-poly-epsilon-caprolactone microparticles reduce the needed amount of BMP-2. *Clin Orthop Relat Res* **2009,** *467*, 3138-3148.

42. Gharibjanian, N. A.; Chua, W. C.; Dhar, S.; Scholz, T.; Shibuya, T. Y.; Evans, G. R.; Calvert, J. W., Release kinetics of polymer-bound bone morphogenetic protein-2 and its effects on the osteogenic expression of MC3T3-E1 osteoprecursor cells. *Plast Reconstr Surg* **2009,** *123*, 1169-1177.

43. Uludag, H.; D'Augusta, D.; Palmer, R.; Timony, G.; Wozney, J., Characterization of rhBMP-2 pharmacokinetics implanted with biomaterial carriers in the rat ectopic model. *J Biomed Mater Res* **1999,** *46*, 193-202.

44. Gautschi, O. P.; Frey, S. P.; Zellweger, R., Bone morphogenetic proteins in clinical applications. *ANZ J Surg* **2007,** *77*, 626-631.

45. Jeon, O.; Song, S. J.; Yang, H. S.; Bhang, S. H.; Kang, S. W.; Sung, M. A.; Lee, J. H.; Kim, B. S., Long-term delivery enhances in vivo osteogenic efficacy of bone morphogenetic protein-2 compared to short-term delivery. *Biochem Biophys Res Commun* **2008,** *369*, 774-780.

46. Yang, H. S.; La, W. G.; Bhang, S. H.; Jeon, J. Y.; Lee, J. H.; Kim, B. S., Heparin-conjugated fibrin as an injectable system for sustained delivery of bone morphogenetic protein-2. *Tissue Eng Part A* **2010,** *16*, 1225-1233.

47. Huang, Z.; Ren, P. G.; Ma, T.; Smith, R. L.; Goodman, S. B., Modulating osteogenesis of mesenchymal stem cells by modifying growth factor availability. *Cytokine* **2010,** *51*, 305-310.

48. Tabata, Y., Significance of release technology in tissue engineering. *Drug Discov Today* **2005,** *10*, 1639-1646.

49. Zara, J. N.; Siu, R. K.; Zhang, X.; Shen, J.; Ngo, R.; Lee, M.; Li, W.; Chiang, M.; Chung, J.; Kwak, J.; Wu, B. M.; Ting, K.; Soo, C., High doses of bone morphogenetic protein 2 induce structurally abnormal bone and inflammation in vivo. *Tissue Eng Part A* **2011,** *17*, 1389-1399.

50. Liu, H. W.; Chen, C. H.; Tsai, C. L.; Hsiue, G. H., Targeted delivery system for juxtacrine signaling growth factor based on rhBMP-2-mediated carrier-protein conjugation. *Bone* **2006,** *39*, 825-836.

51. Park, Y. J.; Kim, K. H.; Lee, J. Y.; Ku, Y.; Lee, S. J.; Min, B. M.; Chung, C. P., Immobilization of bone morphogenetic protein-2 on a nanofibrous chitosan membrane for enhanced guided bone regeneration. *Biotechnol Appl Biochem* **2006,** *43*, 17-24.

52. Zhang, H.; Migneco, F.; Lin, C. Y.; Hollister, S. J., Chemically-conjugated bone morphogenetic protein-2 on three-dimensional polycaprolactone scaffolds stimulates osteogenic activity in bone marrow stromal cells. *Tissue Eng Part A* **2010,** *16*, 3441-3448.

53. Bumgardner, J. D.; Wiser, R.; Gerard, P. D.; Bergin, P.; Chestnutt, B.; Marin, M.; Ramsey, V.; Elder, S. H.; Gilbert, J. A., Chitosan: potential use as a bioactive coating for orthopaedic and craniofacial/dental implants. *J Biomater Sci Polym Ed* **2003,** *14*, 423-438.

54. Sinha, V. R.; Singla, A. K.; Wadhawan; Kaushik; Kumria; Bansal; Dhawan, Chitosan microspheres as a potential carrier for drugs. *Int J Pharm* **2004,** *274*, 1-33.

55. Di Martino, A.; Sittinger, M.; Risbud, M. V., Chitosan: a versatile biopolymer for orthopaedic tissue-engineering. *Biomaterials* **2005,** *26*, 5983-5990.

56. Kim, I. Y.; Seo, S. J.; Moon, H. S.; Yoo, M. K.; Park, I. Y.; Kim, B. C.; Cho, C. S., Chitosan and its derivatives for tissue engineering applications. *Biotechnol Adv* **2008,** *26*, 1-21.

57. Venkatesan, J.; Kim, S. K., Chitosan composites for bone tissue engineering--an overview. *Mar Drugs* **2010,** *8*, 2252-2266.

58. Costa-Pinto, A. R.; Reis, R. L.; Neves, N. M., Scaffolds based bone tissue engineering: the role of chitosan. *Tissue Eng Part B Rev* **2011,** *17*, 331-347.

59. Hench, L. L.; Best, S., *Biomaterials Science: An Introduction to Materials in Medicine*. Second ed.; Elsevier Academic Press: 2004.

60. Karageorgiou, V.; Kaplan, D., Porosity of 3D biomaterial scaffolds and osteogenesis. *Biomaterials* **2005,** *26*, 5474-5491.

61. Hermida, J. C.; Bergula, A.; Dimaano, F.; Hawkins, M.; Colwell, C. W., Jr.; D'Lima, D. D., An in vivo evaluation of bone response to three implant surfaces using a rabbit intramedullary rod model. *J Orthop Surg Res* **2010,** *5*, 57.

62. Thian, E. S.; Huang, J.; Ahmad, Z.; Edirisinghe, M. J.; Jayasinghe, S. N.; Ireland, D. C.; Brooks, R. A.; Rushton, N.; Best, S. M.; Bonfield, W., Influence of nanohydroxyapatite patterns deposited by electrohydrodynamic spraying on osteoblast response. *J Biomed Mater Res A* **2008,** *85*, 188-194.

63. Xiong, J.; Li, Y.; Hodgson, P. D.; Wen, C., In vitro osteoblast-like cell proliferation on nano-hydroxyapatite coatings with different morphologies on a titanium-niobium shape memory alloy. *J Biomed Mater Res A* **2010,** *95*, 766-773.

64. Kong, L.; Gao, Y.; Cao, W.; Gong, Y.; Zhao, N.; Zhang, X., Preparation and characterization of nano-hydroxyapatite/chitosan composite scaffolds. *J Biomed Mater Res A* **2005,** *75*, 275-282.

65. Xu, Q.; Lu, H.; Zhang, J.; Lu, G.; Deng, Z.; Mo, A., Tissue engineering scaffold material of porous nanohydroxyapatite/polyamide 66. *Int J Nanomedicine* **2010,** *5*, 331-335.

66. Zhang, Y.; Ni, M.; Zhang, M.; Ratner, B., Calcium phosphate-chitosan composite scaffolds for bone tissue engineering. *Tissue Eng* **2003,** *9*, 337-345.

67. Alsberg, E.; Kong, H. J.; Hirano, Y.; Smith, M. K.; Albeiruti, A.; Mooney, D. J., Regulating bone formation via controlled scaffold degradation. *Journal of Dental Research* **2003,** *82*, 903-908.

68. Oest, M. E.; Dupont, K. M.; Kong, H. J.; Mooney, D. J.; Guldberg, R. E., Quantitative assessment of scaffold and growth factor-mediated repair of critically sized bone defects. *J Orthop Res* **2007,** *25*, 941-950.

69. Chen, X. G.; Park, H. J., Chemical characteristics of O-carboxymethyl chitosans related to the preparation conditions. *Carbohydrate Polymers* **2003,** *53*, 355-359.

70. Lu, G.; Sheng, B.; Wang, G.; Wei, Y.; Gong, Y.; Zhang, X.; Zhang, L., Controlling the degradation of covalently cross-linked carboxymethyl chitosan utilizing bimodal molecular weight distribution. *J Biomater Appl* **2009,** *23*, 435-451.

71. Shi, Z.; Neoh, K. G.; Kang, E. T.; Poh, C. K.; Wang, W., Surface functionalization of titanium with carboxymethyl chitosan and immobilized bone morphogenetic protein-2 for enhanced osseointegration. *Biomacromolecules* **2009,** *10*, 1603-1611.

72. Wang, G.; Lu, G.; Ao, Q.; Gong, Y.; Zhang, X., Preparation of cross-linked carboxymethyl chitosan for repairing sciatic nerve injury in rats. *Biotechnol Lett* **2010,** *32*, 59-66.

73. Adhirajan, N.; Shanmugasundaram, N.; Babu, M., Gelatin microspheres cross-linked with EDC as a drug delivery system for doxycyline: development and characterization. *J Microencapsul* **2007,** *24*, 647-659.

74. Duan, X.; Sheardown, H., Crosslinking of collagen with dendrimers. *J Biomed Mater Res A* **2005,** *75*, 510-518.

75. Grabarek, Z.; Gergely, J., Zero-length crosslinking procedure with the use of active esters. *Anal Biochem* **1990,** *185*, 131-135.

76. Chen, S. C.; Wu, Y. C.; Mi, F. L.; Lin, Y. H.; Yu, L. C.; Sung, H. W., A novel pH-sensitive hydrogel composed of N,O-carboxymethyl chitosan and alginate cross-linked by genipin for protein drug delivery. *J Control Release* **2004,** *96*, 285-300.

77. Mi, F. L.; Shyu, S. S.; Peng, C. K., Characterization of ring-opening polymerization of genipin and pH-dependent cross-linking reactions between chitosan and genipin. *Journal of Polymer Science Part a-Polymer Chemistry* **2005,** *43*, 1985-2000.

78. Mi, F. L.; Tan, Y. C.; Liang, H. C.; Huang, R. N.; Sung, H. W., In vitro evaluation of a chitosan membrane cross-linked with genipin. *J Biomater Sci Polym Ed* **2001,** *12*, 835-850.

79. Mi, F. L.; Tan, Y. C.; Liang, H. F.; Sung, H. W., In vivo biocompatibility and degradability of a novel injectable-chitosan-based implant. *Biomaterials* **2002,** *23*, 181-191.

80. Yang, L. Q.; Lan, Y. Q.; Guo, H.; Cheng, L. Z.; Fan, J. Z.; Cai, X. A.; Zhang, L. M.; Chen, R. F.; Zhou, H. S., Ophthalmic drug-loaded N,O-carboxymethyl chitosan hydrogels: synthesis, in vitro and in vivo evaluation. *Acta Pharmacologica Sinica* **2010,** *31*, 1625-1634.

81. Budiraharjo, R.; Neoh, K. G.; Kang, E. T., Hydroxyapatite-coated carboxymethyl chitosan scaffolds for promoting osteoblast and stem cell differentiation. *J Colloid Interface Sci* **2012,** *366*, 224-232.

82. Cai, K.; Yao, K.; Li, Z.; Yang, Z.; Li, X., Rat osteoblast functions on the o-carboxymethyl chitosan-modified poly(D,L-lactic acid) surface. *J Biomater Sci Polym Ed* **2001,** *12*, 1303-1315.

83. Chen, R. N.; Wang, G. M.; Chen, C. H.; Ho, H. O.; Sheu, M. T., Development of N,O-(carboxymethyl)chitosan/collagen matrixes as a wound dressing. *Biomacromolecules* **2006,** *7*, 1058-1064.

84. Macdonald, M. L.; Samuel, R. E.; Shah, N. J.; Padera, R. F.; Beben, Y. M.; Hammond, P. T., Tissue integration of growth factor-eluting layer-by-layer polyelectrolyte multilayer coated implants. *Biomaterials* **2011,** *32*, 1446-1453.

85. Patterson, J.; Siew, R.; Herring, S. W.; Lin, A. S.; Guldberg, R.; Stayton, P. S., Hyaluronic acid hydrogels with controlled degradation properties for oriented bone regeneration. *Biomaterials* **2010,** *31*, 6772-6781.

86. Zugravu, M. V. Design and biophysicochemical properties of chitosan-collagen-calcium phosphate microparticles and scaffolds for bone tissue regeneration. Thesis, Univerisity of Memphis, Memphis, TN, 2012.

87. Jones, A. C.; Arns, C. H.; Hutmacher, D. W.; Milthorpe, B. K.; Sheppard, A. P.; Knackstedt, M. A., The correlation of pore morphology, interconnectivity and physical properties of 3D ceramic scaffolds with bone ingrowth. *Biomaterials* **2009,** *30*, 1440-1451.

88. Karande, T. S.; Ong, J. L.; Agrawal, C. M., Diffusion in musculoskeletal tissue engineering scaffolds: design issues related to porosity, permeability, architecture, and nutrient mixing. *Ann Biomed Eng* **2004,** *32*, 1728-1743.

89. Borden, M.; Attawia, M.; Khan, Y.; Laurencin, C. T., Tissue engineered microsphere-based matrices for bone repair: design and evaluation. *Biomaterials* **2002,** *23*, 551-559.